

**SYNTHESIS, CHARACTERIZATION AND
BIOMEDICAL APPLICATIONS OF SILICA BASED
METAL NANOCOMPOSITES**

A report on Laboratory Dissertation
Submitted for the Partial Fulfillment of the

DEGREE OF MASTER OF TECHNOLOGY

in

NANOTECHNOLOGY

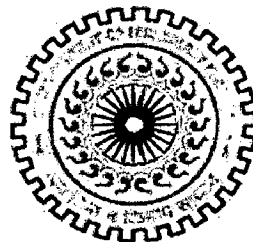
POOJA DEVI

WORK DONE AT

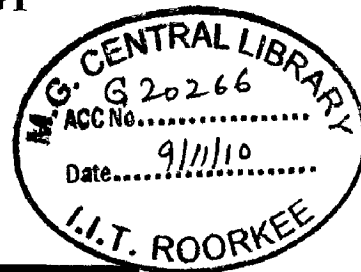


**OPTICAL BIO-MICROSYSTEM LABORATORY
CONCORDIA UNIVERSITY, MONTREAL
QUEBEC-H3G 1M8 (CANADA)**

&



**CENTRE OF NANOTECHNOLOGY
INDIAN INSTITUTE OF TECHNOLOGY ROORKEE
ROORKEE-247 667 (INDIA)**



CONTENTS

Candidate's declaration.....	v
Acknowledgements.....	vi
Preface.....	vii
Abbreviations.....	viii
Contents.....	ii
Chapter I: Synthesis and Characterization of Au- Poly (dimethylsiloxane) Nanocomposites based sensing Platform for the Detection of Human Serum Albumin	
Abstract.....	2
Section 1: Introduction and Literature Review.....	3
1.1 : Nanocomposites: General Description	
1.2 : Metal-Poly (dimethylsiloxane) Nanocomposites	
1.3 : LSPR based Sensing Platform	
1.4 : Au-PDMS Nanocomposites	
1.5 : Synthesis of Au/Ag-PDMS Nanocomposite	
1.6 : Applications of Au/Ag-PDMS Nanocomposite	
1.7 : Aim and Scope of the Present Work	
Section 2: Experimental Details.....	14
2.1: Materials Used	
2.2: Experimental Procedure	
2.3: Characterization of Samples	
Section 3: Results and Discussion.....	22

3.1: UV-Visible Spectroscopy	
3.2: Application of Au-PDMS Nanocomposites: Biodetection of human serum albumin	
3.3: FESEM images and EDXA data	
3.4: AFM imaging	
3.5: XPS analysis	
Section 4: Conclusions.....	41
Section 5: References.....	42
Chapter II: Synthesis, Characterization and Application of Silica – Silver Nanocomposite	
Abstract.....	46
Section 1: Introduction and Literature Review.....	47
1.1: Metal-Silica Nanocomposite: General Description	
1.2: Silver-Silica Nanoshells	
1.3: Synthesis of Dielectric Silica Core	
1.4: Methods for Synthesis of Silver Coated Silica Nanoparticles	
1.5: Applications of Silver nanoparticles Coated Silica Spheres	
1.6: Aim and Scope of the Present Work	
Section 2: Experimental Details.....	61
2.1: Materials Used	
2.2: Experimental Procedure	
2.3: Characterization of Samples	
Section 3: Results and Discussion.....	66
3.1: FT-IR Analysis	
3.2: Powder X-ray Diffraction	

3.3: FE-SEM images and EDXA data

3.4: Diffuse Reflectance Spectral Analysis

3.5: Antimicrobial Activity Studies

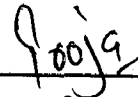
Section 4: Conclusions.....83

Section 5: References.....84

Publications.....87

CANDIDATE'S DECLARATION

I hereby certify that the work presented in the dissertation entitled, "***SYNTHESIS, CHARACTERIZATION AND BIOMEDICAL APPLICATIONS OF SILICA BASED METAL NANOCOMPOSITES***", has been carried out by me during the period from August 2009 to June 2010, under the joint supervision of ***Dr. Muthukumaran Packirisamy, Chair Person and Professor, Mechanical Engineering Department, Concordia University, Montreal, Canada and Dr. P. Jeevanandam, Assistant Professor, Department of Chemistry, Indian Institute of Technology Roorkee, Roorkee, India.***

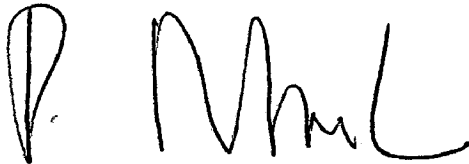


Signature of the Candidate

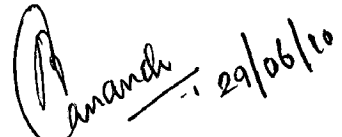
Date:29/6/10.....

(Signature of the Supervisors)

Date:29/06/10.....



***(Dr. Muthukumaran Packirisamy)
Chair Person and Professor
Department of Mechanical Engineering,
Concordia University, Montreal
MONTREAL-H3G1M8 (CANADA)***



***(Dr. P. Jeevanandam)
Assistant Professor
Department of Chemistry,
Indian Institute of Technology Roorkee
ROORKEE - 247667 (INDIA)***

ACKNOWLEDGEMENTS

Firstly, I would like to thank my supervisor and co-supervisor, Dr. P. Jeevanandam and Professor Muthukumaran Packirisamy, for giving me the opportunity and independence to pursue such an interesting thesis topic. Thank you for giving me the space to grow and learn in this domain. With due respect to their valuable scientific advices, and encouragement during my M.Tech Programme, I express my deepest gratitude to both of my mentors.

I would also like to extend my sincere thanks to Dr. Simona Badilescu, Research Associate, Concordia University for providing further insight into the theoretical and experimental aspect of this research. Thank you for your continuous support in helping me to achieve my research goals. I express my sincere regards to Professor Anil Kumar, Head of the Centre of Nanotechnology, IIT Roorkee and all other faculty members.

I acknowledge the help I received in several ways from Liselyn Adams (International programme co-ordinator), Hang Wang, Lena, Arvind Chandrasekaran, Alla, Srikant, Manu Sharma, Supriya and many others.

Financial support of the Canadian Government through Graduate Study Common Wealth Exchange Programme (GSEP) during my stay and work period at Canada and Ministry of Human Resources, Government of India is gratefully acknowledged. I am thankful to IITR and Concordia University for all the support and infrastructural facilities.

Lastly, I would like to thank my father, Mr. Shivdutt Sharma, my mother, Mrs. Rajbala, and my dear uncle Anil for their unconditional love, encouragement and support. You have always inspired me to strive for more, and I owe the success of this thesis to you.


POOJA DEVI

PREFACE

The work embodied in this thesis entitled “**Synthesis, Characterization and Biomedical Applications of Silica based Metal Nanocomposites**” consists of two chapters. The synthesis of Au-poly (dimethylsiloxane) nanocomposites by in situ synthesis and galvanic replacement approach, characterization and functionalization for biosensing application using human serum albumin as a model system are described in Chapter I. In Chapter II, the synthesis, characterization and antimicrobial activity of silica-silver nanocomposites are reported. Each chapter includes sections on literature survey, experimental details followed by results and discussion.

The nanocomposites were characterized by UV-Visible spectroscopy, Atomic Force Microscopy (AFM), Field Emission Scanning Electron Microscopy (FE-SEM), X-Ray Photoelectron Spectroscopy (XPS), Energy Dispersive X-Ray Analysis (EDXA) and Fourier Transform Infrared Spectroscopy (FT-IR). The Au-PDMS nanocomposite films were functionalized by dextran hydrogel matrix and used for the detection of human serum albumin (HSA) by monitoring the shift in position of localized surface Plasmon resonance (LSPR) band as a function of change in refractive index during the binding events. The silica-silver nanocomposites were explored for their antimicrobial activity against *Escherichia coli* and *Bacillus subtilis* using double dilution method to determine the minimal inhibitory concentration (MIC).

ABBREVIATIONS

S. No.	Abbreviation	Full Form
1	PDMS	Poly (dimethylsiloxane)
2	LSPR	Localized Surface Plasmon Resonance
3	PVD	Physical Vapor Deposition
4.	APTMS	Aminopropyltrimethoxysilane
5.	PMMA	Polymethylmethacrylate
6.	PTFE	Polytetrafluoroethylene
7.	DBTA	dibenzoyl tartaric acid
8.	PVA	Polyvinylalchol
9.	FITC	Fluorescein isothiocyanate
10.	ELISA	Enzyme Linked Immunosorbent assay
11.	PLED	Photo Light Emitting Diodes
12.	SERS	Surface Enhanced Raman Scattering
13.	EDC	1-Ethyl-3-(3-dimethylaminopropyl)carbodiimide
14.	NHS	N-Hydroxysuccinimide
15.	HSA	Human Serum Albumin
16.	Anti-HSA	Anti-Human Serum Albumin
17.	MPTMS	Mercaptopropyltrimethoxysilane
18.	PVP	Polyvinylpyrollidione
19.	LCST	Low Critical Solution Temperature
20.	ANSCCC	Ag nanoparticle coated silica colloidal crystal film

Chapter-1

**Synthesis and Characterization of Au-Poly (dimethylsiloxane)
Nanocomposites based Sensing Platform for the Detection of Human
Serum Albumin**

ABSTRACT

In the present project, Au-PDMS nanocomposites have been fabricated by means of an easy, cost effective, and rapid *in situ* synthesis approach with the purpose of localizing most of the gold nanoparticles in monodispersed form on the surface of PDMS so as to use this platform for biosensing. Also, a novel method based on galvanic replacement has been used to fabricate Au-PDMS nanocomposites using Ag-PDMS nanocomposite as a template, which otherwise has been reported in solution. Reduction of metal ions (Au^{3+} and Ag^+) by one of the components of the polymer i.e. the curing agent, lead to formation of the corresponding atoms, thus, avoiding the use of external reducing and capping agents. The synthesized nanoparticles could be localized at the surface by increasing the ratio of curing agent to pre-polymer. The Au-PDMS nanocomposites fabricated by galvanic replacement approach take advantage of both, the curing agent's inherent reducing property, and the reduction potential difference in Au and Ag when using Ag-PDMS as a template for Au-PDMS fabrication. The nanocomposites were characterized by UV-Visible spectroscopy, field emission scanning electron microscopy (FE-SEM), energy dispersive X-ray analysis (EDXA), atomic force microscopy (AFM), and X-ray photoelectron spectroscopy (XPS). The effect of varying the concentration of metal salt, incubation time and reaction conditions on the shape, size and dispersion of gold nanoparticles on the PDMS surface was investigated. The concentration of metal salt and incubation time was found to affect the size and dispersion of nanoparticles formed on the PDMS surface fabricated by *in situ* synthesis approach. For, the Au-PDMS composite, fabricated by the galvanic replacement approach, temperature was found to play a key role in controlling the replacement reaction and hence the final nanostructure formed on the surface. The Au-PDMS nanocomposite sensing platform was employed for the detection of HSA, as a model for biosensing application.

1.1: Nanocomposites: General Description

A nanocomposite is as a multi-phase solid material where one of the phases has at least one of dimensions less than 100 nanometers (nm), or structures having nano-scale repeat distances between the different phases that make up the material (1). In the broadest sense, this definition can include porous media, colloids, gels and co-polymers, but is more usually taken to mean the solid combination of a bulk matrix and nano-dimensional phase(s) differing in properties due to dissimilarities in structure and chemistry. The mechanical, electrical, thermal, optical, electrochemical, catalytic properties of the nanocomposites differ markedly from that of the component materials. They offer novel properties which are the synergetic combination of the two individual components. Nanocomposites are basically a subset of composites that take advantage of unique material properties on the small scale.

1.2: Metal-Poly (dimethylsiloxane) Nanocomposites

Among various types of nanocomposite materials, nanocomposites of inorganic materials in polymer matrices have attracted a great deal of attention because of their wide applications as biosensors, optical devices, micromechanical devices, and advanced catalytic membranes. Among various polymers available for micro fluidic devices fabrication, poly (dimethylsiloxane) (PDMS) is used widely. It has received the most attention due to its ease of preparation, low cost, good transparency down to 280 nm, and non-toxicity to biomolecules. Due to these properties, PDMS can be used directly for cell culturing (2, 3). Because of the wide utilization of metal nanoparticles in biosensing as well as in catalysis, biological labeling, etc., their association with PDMS, in the form of nanocomposite materials, opens new possibilities in micro fluidic biosensing. In addition, PDMS has a low glass transition temperature (T_g), excellent flexibility, high thermal and oxidative stability, good hemo- and biocompatibility (4), properties that make it a very attractive polymer host for the fabrication of nanocomposites (5). After cross linking, it becomes an elastomeric material with a low Young's modulus of ~ 750 kP which enables it to form reversible seals and it can be moulded into functional devices. Metal - PDMS nanocomposites are important functional materials with interesting potential applications as

sensors, filters, low refractive index materials, and thermochromic materials (6, 7). Noble metal nanoparticles such as gold and silver when dispersed in polymers integrate the use of controlled micro fluidic system in order to reduce the amount of reagents and localized surface plasmon resonance (LSPR) phenomenon of nanoparticles for the detection.

1.3: LSPR based Sensing Platform

LSPR can be considered as a type of optical enhancement, facilitated by the action of nanoparticles (8). The shape of the nanoparticle extinction and the scattering spectra, and in particular the peak wavelength (λ_{\max}) of the LSPR is dependent upon the composition, size, shape, interparticle spacing of the nanoparticles, and the dielectric properties of their local environment (i.e. substrate, solvent, and surface-confined molecules) (9, 10). This phenomenon enables noble-metal nanoparticles to serve as extremely intense labels for immunoassays, biochemical sensors and surface-enhanced spectroscopies (11-20). They act as transducers that convert small changes in the local refractive index into spectral shifts in the intense nanoparticle extinction and scattering spectra and hence used for biosensing as a function of change in refractive index during binding events.

1.4: Au-PDMS Nanocomposites

Research on noble metal nanostructures like Au and Ag has been an active area for decades, because of their interesting properties and their importance to a variety of applications such as photonics, surface enhanced Raman scattering (SERS), optoelectronics, catalysis and chemical and biological sensing (11-20). By controlling the size, shape, dielectric constant, and composition, their properties can be tailored. Particularly, for Au and Ag, the resonance frequency of surface plasmon (SPR) can be tuned by adjusting the size and morphology, and by changing the refractive index by incorporation in another material such as polymers (e.g. PDMS, PMMA, PTFE, and PVA etc.), silica, etc. The incorporation of Au nanoparticles not only enhances the surface modification capability of PDMS for biosensing application but also increases the mechanical strength, catalysis and gas separation capability. It is well known that gold nanoparticle is also a good substrate to be functionalized with antigen, enzymes and other biomolecules (32). Also, Au-PDMS composites offer certain advantages over Ag-PDMS

nanocomposites such as the greater stability of Au, relative to Ag, biocompatibility, and availability of well established functionalization approaches of Au (21).

1.5: Synthesis of Au/Ag-PDMS Nanocomposite

For the fabrication of Au/Ag-PDMS nanocomposites, introducing nanoparticles in polymer matrix is not the only requirement. The nanoparticles should be in the monodispersed form i.e. individually dispersed, should have uniform shape, and chemical composition. For biosensing applications, the nanoparticles should be localized in monodispersed form on the surface of the polymer. The synthesis of inorganic/organic nanocomposites having metal nanoparticles as an inorganic component is a subject of high interest in science and technology because of their rich commercial applications and easy scalability. So, various methods have been reported in literature for the synthesis of metal nanoparticles embedded PDMS films, and they can be classified as follows:

- a) Blending Premade Nanoparticles in the Polymer
- b) Surface Functionalization
- c) Micro Contact Printing
- d) Physico-Chemical Methods
 - Physical Vapor Deposition (PVD)
 - Cryochemical Method
 - Radiolysis
 - Photoreduction
 - Plasma Chemical Process
- e) Sol-Gel Method
- f) In Situ Synthesis
- g) Galvanic Replacement Approach

The literature methods are summarized in the Tables given below:-

a) **Blending Premade Nanoparticles in the Polymer**

S. No.	Polymer	Capping Agent	Size of nanoparticles (nm)	Reference
1.	Poly (9, 9'-dioctylfluorene)	-	5.0-10.0	(22)
2.	Polystyrene	- SH	2.5-7.5	(23)
3.	PDMS	Tetradecanethiol	3.2±0.4	(24)

b) **Surface Functionalization Method:**

S. No.	Polymer	Functionalizing Agent/Reducing Agent	Size of nanoparticles (nm)	Reference
1.	PDMS	APTMS	11.0	(25)
2.	PDMS	Chitosan	10.5-12.0	(26)

c) **Micro Contact Printing Method:**

S. No.	Polymer	Capping Agent	Transfer Method	Size of nanoparticles (nm)	Reference
1.	PDMS	Alkanethiol	Langmuir-Schaefer	11.0	(25)
2.	PDMS	Dodecanethiol	Langmuir-Schaefer	~ 5.0	(27, 28)

d) **Physico-Chemical Methods:**

S. No.	Method	Polymer	Nanoparticles	Size of nanoparticles (nm)	Reference
1.	PVD	PDMS	Ag	10.0-50.0	(29)
2.	Cryochemical	PMMA	Au, Pd	~ 15.0	(30)
3.	Radiolysis	PMMA	Au	~ 10.8	
4.	Photoreduction	PMMA	Au	~ 20.0	
5.	Plasma Chemical	PTFE	Ag	20-200	(30)

e) **Sol-Gel Method:**

S. No.	Precursors	Nonsurfactant Template	Size of nanoparticles (nm)	Reference
1.	TEOS and Gold sol	DBTA	2.0-8.0	(43)

f) **In Situ Synthesis Method:**

This method utilizes the inherent reducing properties of one of the components of a polymer. The polymer matrix acts as a capping agent, and hence no external reducing and capping agent are required. Various polymer-metal nanocomposites synthesized by this method are summarized below:

S. No.	Polymer	Size of nanoparticles (nm)	Reference
1.	Polyvinylferrocene	-	(31)
2.	PVA	Hexagonal plate ~ 10-70	(32)
3.	PDMS	7.0	(33, 34)
4.	PDMS based Micro fluidic devices	-	(35, 36)

g) **Galvanic Replacement Approach:**

In addition to the above well studied methods, Au-PDMS nanocomposites could be fabricated by taking advantage of the difference in the reduction potentials of Au and Ag. Fabrication of Au-PDMS composite using Ag-PDMS nanocomposite as a template is based on the principle of galvanic replacement reaction. Xia et al. has developed a method to prepare hollow nanostructures with controlled pore volume and wall thickness, using the galvanic replacement reaction carried out in aqueous solutions (37-39). The galvanic replacement reaction is based on the reduction potential difference between silver and gold ($\text{AuCl}_4^-/\text{Au}$ is 0.99V, which is higher than $\text{Ag}^+/\text{Ag} = 0.8\text{V}$) that allows the oxidation of Ag nanostructures by the

solution of a gold salt. The gold that results in the replacement reaction grows on the silver template adopting its morphology and forms a thin shell around it. Hollow structures are formed by the further oxidative dissolution of the core. In some cases, under appropriate conditions, the gold could alloy with the un-reacted silver (40). The galvanic replacement procedure was extended to other noble metals (Pt and Pd) using a silver template and the corresponding salts (52). It has been demonstrated that the size and shape of the initial Ag nanoparticles determine the morphology of the structures generated by the galvanic replacement reaction. Recently, the galvanic replacement reaction was studied in a highly viscous ionic liquid environment and the transformation of quasi-spherical Ag nanoparticles into dendritic flat Au-Ag nanostructures has been demonstrated (41). Ag@Au core-shell nanostructures were also prepared using a hexagonal shaped Ag template and performing the galvanic replacement reaction between Ag and HAuCl_4 in the presence of polyvinylpyrrolidone (PVP) (42).

1.6: Applications of Au/Ag-PDMS Nanocomposite

Noble metal nanoparticles exhibit unique optical, thermal, chemical, and catalytic properties. Nanoparticles when incorporated in polymers, harvest the synergetic benefit of both the components with the appearance of other new properties. The properties of Au/Ag-PDMS nanocomposites have fascinated the scientific as well as the industrial community because of their capability to mold easily into functional devices such as microfluidic devices for biosensing, chemo sensing, etc.,. Their potential application areas are summarized below:

- a) Medicine
- b) Catalysis
- c) Electronics
- d) Sensor
- e) Environmental

The current and projected applications of Au/Ag-PDMS nanocomposites in the above mentioned fields are described below by considering representative examples.

a) Biomedical Applications

PDMS itself exhibits wide biomedical applications such as biosensing, optical detection, cell culturing, electrophoresis etc. The incorporation of metal nanoparticles further helps on its application because of the synergetic effect of metal nanoparticles along with the polymers. Some of the applications are described below with representative examples.

(i) **Antimicrobial Substrate**

Silver is well known to exhibit good antibacterial and anti-inflammatory properties, yet is relatively nontoxic to mammalian cells, and some medical devices such as wound dressing and urinary catheters have adopted silver to inhibit the incidence of infections and to improve healing rate. In the past few years, silver nanoparticles (AgNPs) have been reported to be a more robust form of silver which could provide substantial and sustained contact with the bacterial cells and is not easily quenched by other salts and proteins due to its high surface to volume ratio. Therefore, the presence of silver nanoparticle makes the PDMS films attractive for biomedical applications and antibacterial coatings due to its inherent antimicrobial properties.

- PDMS-AgNPs composite have been shown to inhibit *E. coli* growth in comparison to native PDMS (44).
- The antibacterial activity of Ag-PDMS has been studied against *Bacillus. Subtilis* and *E. coli* bacterial strains and bacteriostatic as well as bactericidal effects were observed (35).

(ii) **Cell Culture**

The spatial control of mammalian cell adhesion, spreading, and growth plays a crucial role in the development of many research fields ranging from tissue engineering, medical diagnostics, drug screening, and biosensing to fundamental studies of cell biology. Two strategies have been exploited to capture cells in the designated areas on cell culture substrates: one is the usage of physical barriers, and the other is the construction of identification - based cell addressable regions in which physical adsorption and surface chemistry are widely used. Compared to physical adsorption, surface chemistry has been regarded as a more powerful tool in this field. And it has been perfectly developed to be a collection of techniques containing self-assembly,

layer by- layer assembly, plasma treatment, and so on. Gold substrate has been acting as one of the important noble metals for a long time in the application of self-assembly technique for spatial control of cells. So, gold nanoparticle embedded PDMS films are being widely used for cell culture. Also, Ag-PDMS has been shown to form self assembly of of H-Arg-Gly-Asp-Cys-OH (RGDC) tetrapeptide to grow cells selectively and spatially (44).

(iii) Electrophoretic Separation

PDMS based micro fluidic devices have been widely used for the electrophoretic separation of biomolecules, but, the hydrophobic nature of PDMS limits their use because of non-specific adsorption of analytes. The incorporation of metal nanoparticles, specifically, Au modifies the surface properties of PDMS. Also, Au is well known for its chemistry to bind biomolecules. Thus, Au-PDMS nanocomposite provides solution to overcome limitations of PDMS for electrophoretic purpose. In a study, suppression in protein adsorption has been observed with BSA blocking on the in situ synthesized PDMS–gold nanoparticles composite films. This was evidenced by the electrophoretic separation of FITC-labeled myoglobin (33).

(iv) Biosensing

A biosensor makes use of all naturally occurring biomolecular interactions for the detection of analytes (biomolecules). Among various biosensing platforms, metal nanoparticles are gaining wide attention because of their novel optical properties. When they are integrated with micro fluidic devices (made up of transparent polymers such as PDMS), then, not only the reduction in amount of reagent is observed but also the detection capability of microfluidic devices increases which otherwise is found to be poor because of non-specific adsorption of biomolecules to PDMS surface. Some of the examples, where PDMS-Au nanocomposites are used for biosensing are given below:

- As explained later in the catalytic section, the Au-PDMS nanocomposites have been reported for the detection of glucose (31, 36).
- Recently, a Au-PDMS nanocomposite has been fabricated and shown for the colorimetric detection of cardiac troponin I with the reduction of reagents required for the analysis in comparison to ELISA (34).

(b) In Catalysis

Noble metal nanoparticles have been reported as good catalysts. Their incorporation into the polymer opens new ways to build micro reactor for catalytic reactions.

- Recently, Au-PDMS composites, surface functionalized and immobilized by an enzyme GO_x (glucose oxidase), have been reported for the catalytic oxidation as well as detection of glucose in micro fluidic micro reactor. The glucose is enzymatically oxidized with the dissolved oxygen in the buffer solution with the subsequent production of hydrogen peroxide, which is detected at the working electrode (36).
- In another study, glucose oxidase enzyme immobilized on Au-polyvinylferrocene nanocomposite has been shown to catalyze and detect glucose by directly monitoring the H_2O_2 level (31).

(c) In Electronics

The potential use of polymer light-emitting diodes (PLED) is ultimately limited by their low quantum efficiency as well as by their poor stability due to oxygen. Various approaches have been attempted to prevent photo oxidation and to enhance device stability. One of them is the encapsulation of device with metal or glass caps, but this process is costly and incompatible. Recently, incorporation of nanoshells in polymer is proposed to avoid oxidation but the proposed polymer/metal nanoshell nanocomposite systems cannot be used in PLEDs because the nanoshells are larger than the typical emitting-layer thickness of PLEDs. The solution to the above problems is provided by the incorporation of metal nanoparticles (Au) into the polymer.

- Blue PLED with enhanced luminescence stability and quantum efficiency has been reported by incorporating 5-10 nm gold nanoparticles in poly (9, 9'-dioctylfluorene) (PDOF) polymer, where gold nanoparticles act as the quenchers of the triplet states of PDOF that lead to the polymer oxidation (22).

(d) In Sensor

Metal nanoparticles show a phenomenon of enhancement of localized field on interaction with incident light. This enhancement of electromagnetic field forms the basis for the development of a simple and sensitive biosensor. Their integration with polymer and micro fluidic platform further lowers down the amount of analytes to be detected.

(i) Chemosensor Application: Detection of Toluene

Au-PDMS nanocomposites were found to be sensitive to increasing concentration of toluene vapor and the effect was observed to be reversible. These polymer nanocomposite based chemosensor can be used as E-nose to detect various harmful chemicals as well as biological warfare agents (45).

(ii) As SERS substrate

As described above, metal nanoparticles enhance the localized electromagnetic field, and so they can be used as one of the best SERS substrates for sensing applications.

- In a study, clear Raman spectrum was observed for the detection of rohdamine dye, when using Au-PDMS nanocomposite as a sensing platform which otherwise was not observable in the absence of Au (26).
- The detection of *p*-aminobenzoic acid (*p*-ABA) using Ag-PDSM nanocomposites was shown to take advantage of SERS phenomenon because of silver nanoparticles (29).

(e) In Environmental Remediation

The increased presence and persistence of aromatic pollutants in natural water has become a problem of major importance in environmental sciences. These chemicals are often present in our water resources as a result of the natural degradation of organic matter and their use in agricultural and pharmaceutical processes. Many of these compounds, such as phenolics, naphthalene derivatives, and aromatic acids, are rapidly trapped by humic substances and suspended organic matter, which increases their presence and toxicological effects on the environment. Novel metal-polymer nanocomposites exhibit unique optical and sorption

properties that make them promising alternatives to more traditional substrates for the detection of these aromatic pollutants in water

- Recently, Ag-PDMS nanocomposites have been shown as good substrates for the detection of 4-aminobenzoic acid, phenolphthalein, benzoic acid, 1,5-diaminonaphthalene, 1,7-dihydroxynaphthalene, 1,5-dihydroxynaphthalene, and 4-nitrophenol in water (46).

1.7: Aim and Scope of the Present Work

The literature survey reveals that due to a very rich variety of applications of photonics integrated with microfluidics, there is lot of interest in finding new ways to fabricate Au/Ag-PDMS nanocomposites. In the present project, efforts have been made to fabricate Au/Ag-PDMS nanocomposites using an easy, cost effective *in situ* synthesis approach with the purpose of localizing most of nanoparticles on the surface in monodispersed form for biosensing applications. Also, an approach called galvanic replacement was brought into context at the polymer/solution interface to fabricate Au-PDMS nanocomposites, using silver template in aqueous solution. The intermediate stages of galvanic replacement were captured by controlling the rate of replacement reaction by changing the reaction conditions. The samples were characterized by UV-Visible spectroscopy, field emission scanning electron microscopy (FE-SEM), energy dispersive X-ray analysis (EDXA), atomic force microscopy (AFM), and X-ray photoelectron spectroscopy (XPS).

Section-2:

Experimental Details

2.1: Materials Used

The materials and the chemicals that were used for the synthesis and functionalization of Au-poly (dimethylsiloxane) nanocomposites are given in Table 2.1. All the chemicals were used as received, without further purification. Certain chemicals like 1-Ethyl-3-(3-dimethylaminopropyl) carbodiimide (EDC), Anti-Human Serum Albumin (Anti-HSA) and HSA

Table 2.1: Chemicals used for the synthesis and functionalization of Au-PDMS and Ag-PDMS nanocomposites

S.No.	Chemicals	Grade	Assay	Company
1	Sylgard [®] 184 Silicone Elastomer Kit	L.R.	-	Dow Corning Corporation
2	HAuCl ₄ .3H ₂ O	A.R	99.99%	Alfa Aesar
3	AgNO ₃	A.R	99.99%	Sigma Aldrich
4	CM Dextranomer	A.R	-	Fluka Analytical
5	Nano Think [™] Acid 11 (Mercaptoundecanoic acid in ethanol)	L.R	-	Aldrich
6	1-Ethyl-3-(3-dimethylaminopropyl)carbodiimide (EDC)	L.R	-	Sigma Aldrich
7	N-Hydroxysuccinimide (NHS)	L.R	98%	Aldrich [®]
8	Skimmed Dry Milk Powder	-	-	Carnation [®]
9	Anti-Human Serum Antibody (produced in rabbit)	A.R	-	Sigma [®]
10	Human Serum Albumin (HSA)	A.R	96-99%	Sigma [®]
11	Phosphate Buffer Saline (PBS)	-	-	Sigma [®]
12	Ethanol	L.R	96%	Loyala Labs
13	Isopropanol	L.R	99.9%	Life Brand
14	Tween-20	L.R	-	Sigma Aldrich

were stored in deep freezing temperatures to avoid decomposition and denaturation. Polyclonal antibody Anti-HSA and antigen HSA were reconstituted by phosphate buffer saline (PBS) and thawed before use. All glass ware used for the solution synthesis were first rinsed with aqua-regia, and then thoroughly washed with Millipore D.I water and oven dried before use. The glass wares used for the PDMS fabrication were cleaned by acetone and isopropanol.

2.2: Experimental Procedure:

Au/Ag-PDMS nanocomposite films with maximum nanoparticles localized on the surface were fabricated using *in situ* synthesis (33, 34) and the galvanic replacement approach (37-39). Various parameters including the concentration of the curing agent and the metal salt, incubation time, and the temperature were optimized. The Au-PDMS composites fabricated by the *in situ* synthesis approach were then used to study the bimolecular interaction. For biosensing, the films were functionalized by dextran hydrogel; -COOH group of dextran was activated using EDC/NHS chemistry which was then coupled to ligand PAb (Anti-HSA) for detecting HSA as described later in section 2.2.2 in detail.

2.2.1: Au-PDMS and Ag-PDMS Nanocomposite Fabrication

(1) PDMS Casting

In general for PDMS casting, the curing agent: pre-polymer mass ratio used is 1:10 ($\eta = 0.1$) but in the present project, a high mass ratio of $\eta = 0.25$ was used. PDMS was synthesized by mixing the PDMS pre-polymer and curing agent in a mass ratio of 4:1 ($\eta = 0.25$) for a total volume of 25 ml. The contents were well mixed to a milky color consistently to avoid the presence of un-reacted curing agent that could cause detrimental bonding results. The mixture was then poured in a glass mould, evacuated for 15-20 min to remove the air bubbles completely. Some of the remaining bubbles were busted by the backfilling of air into the vacuum chamber. Then, the degassed assembly was placed in the oven for curing at 60⁰C for 24 hours. Upon completion of the curing cycle, rectangular samples of size 6.5 × 1 × 0.2 cm³ were cut from the cured polymer. Proper care was taken to avoid any contamination as PDMS is hydrophobic and is prone to contaminant adsorption.

(2) Incubation of PDMS in Au and Ag salt solutions

Various concentration (0.1 to 0.5 wt %) of gold and silver salt solutions were prepared by adding the gold salt $\text{HAuCl}_4 \cdot 3\text{H}_2\text{O}$ (M. Wt. 393.83g) and silver salt AgNO_3 (M. Wt. 169.87g) in DI water, respectively. Rectangular PDMS samples of size $6.5 \times 1 \times 0.2 \text{ cm}^3$ were incubated in $\text{HAuCl}_4 \cdot 3\text{H}_2\text{O}$ and AgNO_3 solutions for varying times and concentrations (G1-G5) as described below for Au-PDMS composite fabrication in Table 2.2:-

Table 2.2: (a) PDMS incubated in different concentration salt solution for 18h (b) In 0.5 wt% salt solution for different time scales

Sample Set	Concentration of $\text{HAuCl}_4 \cdot 3\text{H}_2\text{O}$ (wt %)	Incubation time (h)
G-1	0.1	18
G-2	0.2	18
G-3	0.3	18
G-4	0.4	18
G-5	0.5	18

(a)

Sample Set	Concentration of $\text{HAuCl}_4 \cdot 3\text{H}_2\text{O}$ (wt %)	Incubation time (h)
G-5	0.5	3
G-5	0.5	6
G-5	0.5	12
G-5	0.5	24
G-5	0.5	48

(b)

Similarly, sample sets (S-1, S-2, S-3, S-4, and S-5) were prepared for Ag-PDMS composite fabrication by varying the salt concentration from 5mM to 25mM (AgNO_3) and the incubation time from 0 to 48 h, as in case of Au-PDMS nanocomposites fabrication.

2.2.2: Functionalization of Au-PDMS and Ag-PDMS samples for the detection of HSA

Well known surface engineering methods are available for Au and Ag nanoparticles, but functionalization by dextran offers certain advantages over others.

2.2.2.1: Preparation of Solutions

(1) Carboxymethyl-dextran Solution (CM5)

CM-Dextran is a polyanionic derivative of dextran with an average molecular weight of approximately 10,000. It is supplied in form of a white powder and is freely soluble in water and

the salt solution. It acts as stabilizer of proteins and other sensitive biopolymers as well as carrier for biosensor surfaces (47). The concentration of solution prepared was 50 µg/ml in DI water.

(2) EDC/NHS Solution

1-ethyl-3-(3-dimethylaminopropyl) carbodiimide (EDC) hydrochloride solution of molarity 0.4 M was prepared by adding 3.84 g in 50 ml DI water and stored in the -20°F freezer. Similarly, 0.1M of N-Hydroxysuccinimide (NHS) was prepared by adding 0.57g to 50 ml DI water. Equal volume of both of the solution was mixed just before use to activate the -COOH groups of dextran.

(3) Blocking Agent (5% skimmed milk)

A skimmed milk solution (5%) was prepared in phosphate buffer saline and was used to block unoccupied sites on PDMS surface after the initial adsorption of antibodies to avoid non-specific adsorption of the antigen. This means that the antigen would only be adsorbed on the antibody and not on the nanoparticles or PDMS surface, as all the sites are occupied by the proteins of skimmed milk.

(4) Anti-HSA solution

Human serum albumin is a soluble, monomeric protein which comprises about one half of the blood serum protein and has a molecular mass of 67 kDa with a half life of approximately 20 days. The reference range for albumin concentrations in blood is 30 to 50 g/L. The PAb obtained from Sigma[®] was produced in rabbit using whole serum as the antigen and purified by affinity chromatography. The product so obtained was stored at -20°C and kept at 2°C one day before the use. A stock solution with a dilution of 10⁻¹ was prepared by adding 1mg (1000µl) of PAb to 10ml of PBS using a micropipette. PBS was prepared by adding the dry powder pouch of PBS purchased from Sigma[®] in 1 liter de-ionized water to yield 0.01M phosphate buffer saline.

(5) HSA solution

Albumin functions primarily as a carrier protein for steroids, fatty acids, and thyroid hormones and plays a role in stabilizing the extracellular fluid volume (48). The albumin obtained from Sigma[®] was stored in a freezer at a temperature of -20°C. Before using it, it was removed from the freezer and kept in normal fridge at 2-8°C. A stock solution of HSA (10⁻¹

dilution) was prepared by adding 1000 μg of albumin protein to 10 ml of PBS using 20 μl micropipette, which was further diluted by PBS for 10^{-2} and 10^{-3} dilutions.

2.2.2.2: Functionalization Procedure

Dextran hydrogel has the advantage to keep the biomolecular structure intact by keeping them hydrated. The functionalization of gold and silver nanoparticles in composite sensing platform was carried out as follows: a solution of carboxymethylated dextran in DI water was used to cover the surface of the sample and was left overnight at room temperature. The sample was washed with DI water, dried, and then treated with a mixture of equal volumes of N-ethyl-N'-(3-dimethylaminopropyl)-carbodiimide hydrochloride and N-hydroxysuccinimide and left for 10 min at room temperature to activate the carboxyl groups of CM5 dextran. The polyclonal antibody, Anti-Human Serum Albumin produced in rabbit (Sigma Aldrich), was dissolved in PBS as mentioned earlier and 250 μL of the polyclonal antibody solution was placed on the functionalized gold surface and left overnight. The surface of the sample was then blocked with a solution of 5% skimmed milk powder and then washed several times with a solution of 0.05% Tween[®] in PBS. Finally, 300 μL of HSA (Sigma Aldrich[®]) in different dilutions (10^{-1} to 10^{-3}) was used to cover the surface of the samples and then incubated overnight. The UV-Visible spectrum was recorded for each step of functionalization.

2.2.3: Fabrication of Au-PDMS Composite by Galvanic Replacement Approach:

To fabricate the Au-PDMS composite by galvanic replacement method, the films Ag-PDMS fabricated with optimum conditions as in step 2.2.1 were incubated in 0.5mM Au solution at different temperatures and for different time scales as indicated in Table 2.3. In order to capture the intermediate stages in the galvanic replacement at the polymer/solution interface, the evolution of the UV-Visible spectra was monitored at low temperature for the incubation time from couple of seconds to several hours as mentioned in Table 2.4-

Table 2.3: Conditions for the fabrication of Au-PDMS composite by galvanic replacement

S.No.	Sample	Description	HAuCl ₄ .3H ₂ O concentration (mM)	Reaction Condition (Temperature)
(1)	B	Ag-PDMS in HAuCl ₄ .3H ₂ O solution	0.5	20°C
(2)			0.5	0°C
(3)			0.5	60°C

Table 2.4: Varying the incubation time at 0°C to capture the intermediate stages of galvanic replacement reaction at the solution/polymer interface

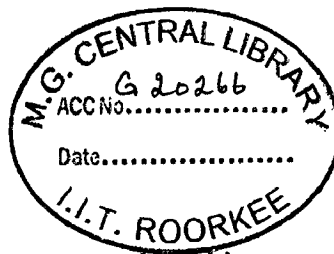
S. No.	Sample	Description	Incubation Time	Concentration (mM)
1	A	PDMS in AgNO ₃	22 h	15
2	B	Ag-PDMS in HAuCl ₄	Few seconds	0.5
3	C	Ag-PDMS in HAuCl ₄	Few minutes	0.5
4	D	Ag-PDMS in HAuCl ₄	10 h	0.5

2.3: Characterization of the samples:-

Characterization of nanostructures requires high precision and accuracy. The Au-PDMS and Ag-PDMS samples were characterized by various analytical techniques in order to determine the distribution, size, morphology, chemical composition properties of nanoparticles formed on PDMS surface. The optical characteristics of the composite films were also investigated. The various techniques used are described below in brief:-

2.3.1: Field Emission - Scanning Electron Microscopy

FE-SEM analysis was done to observe the morphology and size of the nanoparticles in the composite. The instrument used was S-4700 (Hitachi High Technologies America Inc) at McGill University. For PDMS-metal nanoparticle composite imaging, an electron beam with voltage 2 kV and beam current 10 μ A was used. In this technique, a beam of high energy



interacts with the sample and the secondary electrons generated in this process generate the image (49, 50). Because of the non-conductive nature of PDMS polymer, Au/Pd coating was done to make it conductive. Samples were prepared by coating a thin Au/Pd film ($\sim 5\text{\AA}$) at 10mA for one min using Au/Pd sputtering machine (HummerVI, marketed by Anatech Ltd), operating in Plate DC mode at a pressure of 60-70 millitorr.

2.3.2: Energy Dispersive X-Ray Analysis (EDXA)

The EDXA is an integrated part of FE-SEM used to get qualitative as well as quantitative information about chemical nature of the structures on the surface of specimen. For EDXA analysis of the specimen, a high beam of electron is used to get X-rays emitted from the element. An EDXA spectrum not only identifies the element corresponding to each of its peak, but also the type of X-ray to which it corresponds. A beam of acceleration voltage 20 kV was used for the EDXA analysis of the composites, fabricated using galvanic replacement reaction, by VP-SEM at McGill University.

2.3.3: Atomic Force Microscopy (AFM)

Atomic force microscope (AFM) is a very high-resolution scanning probe microscopy, with demonstrated resolution of fractions of a nanometer, more than 1000 times better than the optical diffraction limit (51). This is one of the best techniques for surface characterization of non-conducting polymers which otherwise is very difficult with the SEM. It gives atomic scale resolution. Imaging of Au-PDMS and Ag-PDMS nanocomposites were done by Multimode AFM (Veeco Company) at Concordia University. The imaging was done in tapping mode and the deflection was detected by a beam deflection detection method which can detect the deflection of cantilever ($< 1\text{\AA}$). Samples were cut in small size, glued to sample holder and mounted on a disc of diameter 15 mM. After mounting, the laser was aligned to have maximum root mean square (RMS) value and then, other parameters such as set point, X and Y offsets, integral gain, proportional gain, and scan rate were optimized to get the best image. Imaging was done in a scale of $5\mu\text{m}$ and $10\mu\text{m/s}$ and analysis using NanoScopeIIIa[®] software.

2.3.4: X-Ray Photoelectron Spectroscopy (XPS)

XPS or ESCA (Electron Spectroscopy for Chemical Analysis) is a highly surface sensitive technique, in which X-ray interacts with the sample to a depth of few nm and the interaction volume is very small. It has been a key tool in surface analysis, mainly because of two major features: quantitative analysis and information on the chemical nature and state of the detected elements. The XPS scans of the samples were carried out by ESCALAB 3 MKII X-ray photoelectron spectroscopy (XPS) system (Kratos) at Ecole Polytechnique de Montreal Institute.

2.3.5: UV-Vis Spectroscopy

UV-Visible spectroscopy was used to characterize the optical properties of materials. Noble metal nanoparticles show the phenomenon of localized surface plasmon resonance and exhibit the strong absorption band in UV-Visible region. UV-Visible spectroscopy was performed on a double beam Lambda 650 spectrophotometer marketed by Perkin Elmer[®]. Baseline was generated by keeping PDMS in center of both of the glass cuvettes and then the spectra for the samples were recorded.

3.1: UV-VISIBLE SPECTROSCOPY:**3.1.1: Optical Characteristics of Au-PDMS Nanocomposites Fabricated by *In Situ*****Synthesis Approach**

UV-Visible spectroscopy measurements were performed for all the Au/Ag-PDMS samples to characterize their optical properties. The optical properties were investigated as a function of:-

- Incubation Time
- Metal salt concentration
- Dielectric constant of the surrounding medium

In the last section, the spectral results of biosensing to detect HSA with Au-PDMS sensing platform, fabricated by *in situ* synthesis approach, are also explained.

3.1.1(a): Influence of Incubation Time

The kinetics of the reduction of chloroauric acid to Au was studied by incubating the cured PDMS for different times. Figure 3.1.1.1 shows the Au localized surface plasmon resonance band corresponding to different times of incubation (0 to 48 hours).

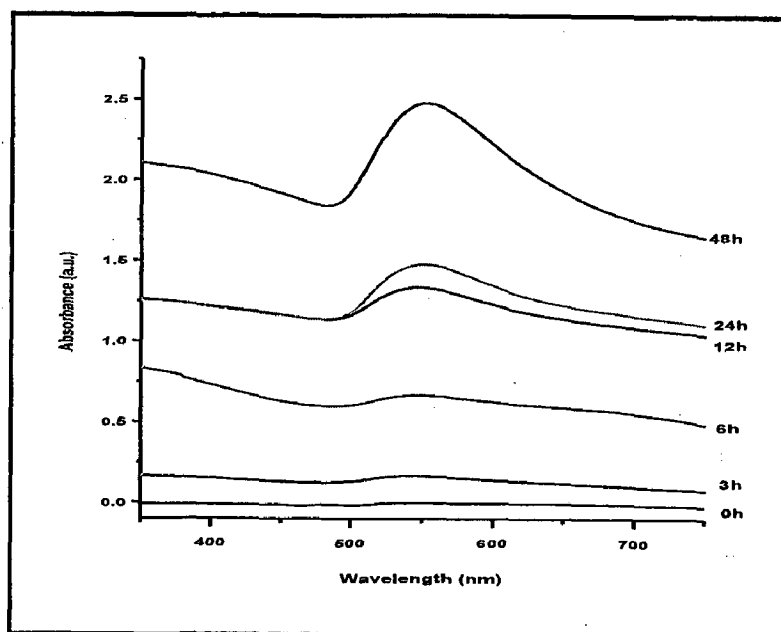


Figure 3.1.1.1: UV-Visible spectra of gold-PDMS prepared by incubation in gold salt solution of concentration 0.5 wt% (G-5) for different time periods.

It can be seen from Figure 3.1.1.1 that the absorbance of the Au LSPR band at around 550-560 nm increases with the incubation time. Also, with increase in the incubation time, the aggregation of nanoparticles increases on the surface which was confirmed through SEM imaging. This is because for longer incubation time, the time of contact between ions in solution and PDMS increases and hence aggregation increases. For the intended biosensing application, a high concentration of the curing agent was used in order to concentrate the Au nanoparticles on the surface layer of the composite. The incubation time variation study was done to fabricate the composite with nanoparticles in monodispersed form on surface in order to obtain a good sensing platform for the detection of antigen. So, the samples obtained by incubation for 18 h were selected and studied further for the effect of concentration of the Au salt.

3.1.1(b): Influence of $\text{HAuCl}_4 \cdot 3\text{H}_2\text{O}$ Concentration

In order to investigate the effect of Au salt concentration, PDMS samples were incubated in aqueous $\text{HAuCl}_4 \cdot 3\text{H}_2\text{O}$ solution of varying concentration (0.1 to 0.5 wt %) mentioned in Table 2.2 (a). The relationship between absorption intensity and concentration of the Au salt solution is shown in Figure 3.1.1.2 and results are summarized in Table 3.1 (a).

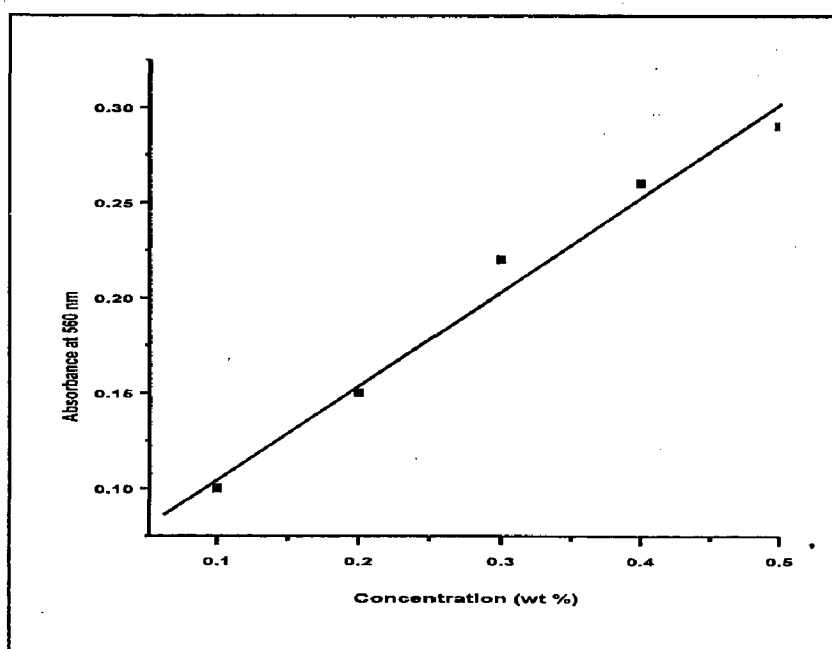


Figure 3.1.1.2: Plot of the absorbance as a function of concentration of gold salt

With increase in concentration of the gold salt solution, the absorbance increases since the no. of gold nanoparticles on the surface increases. This is because more gold ions become available for the reduction and the gold atoms are localized on the surface layer. In the spectra corresponding to the most diluted solution (0.1%), the Au LSPR band is well-defined and narrow. For more concentrated solutions, because of the aggregates that are formed in the surface layer, the wavelength shifts to higher wavelengths and the band broadens. The graph (Figure 3.1.1.2) allows a quick assessment of the amount of gold on the surface layer, when a solution of given gold salt concentration is used. The samples obtained by incubation in 0.1% solution for 18h were used for the biosensing experiment. This is because of the monodispersity and less aggregation observed in these samples, as evidenced by UV-Vis and other analytical techniques.

Table 3.1 (a): UV-Visible spectral data for Au-PDMS nanocomposite as a function of concentration of Au salt

S.No.	Sample	Concentration of $\text{HAuCl}_4 \cdot 3\text{H}_2\text{O}$ (wt %)	λ_{max} (nm)	Absorbance
1.	G-1	0.1	554	0.1
2.	G-1	0.2	562	0.15
3.	G-1	0.3	566	0.22
4.	G-1	0.4	568	0.26
5.	G-1	0.5	563	0.29

3.1.1(c): Influence of Dielectric Constant of the Surrounding Medium

To investigate the sensitivity of the sensing platform (samples fabricated by incubating PDMS in 0.1% Au salt solution for 18h) to the changes in refractive index of the medium, they were kept in different solvents with varying refractive index values and their altered optical properties were examined by the changes in the position of λ_{max} as shown below in Figure 3.1.1.3. The data is summarized in Table 3.1 (b). The analysis of Figure 3.1.1.3 reveals that the position of the absorption maxima of nanocomposite is dependent on the dielectric constant of surrounding medium. A red shift of 5 nm was observed when the surrounding medium was

ethanol rather than air and but not much shift was observed on changing the medium from water to ethanol. It was found to be ~ 0.12 nm for a Δn of 0.03 in case of water / ethanol system. Only a few media were employed to study the effect of surrounding medium, and this is because of the swelling problem of PDMS in most of the solvents.

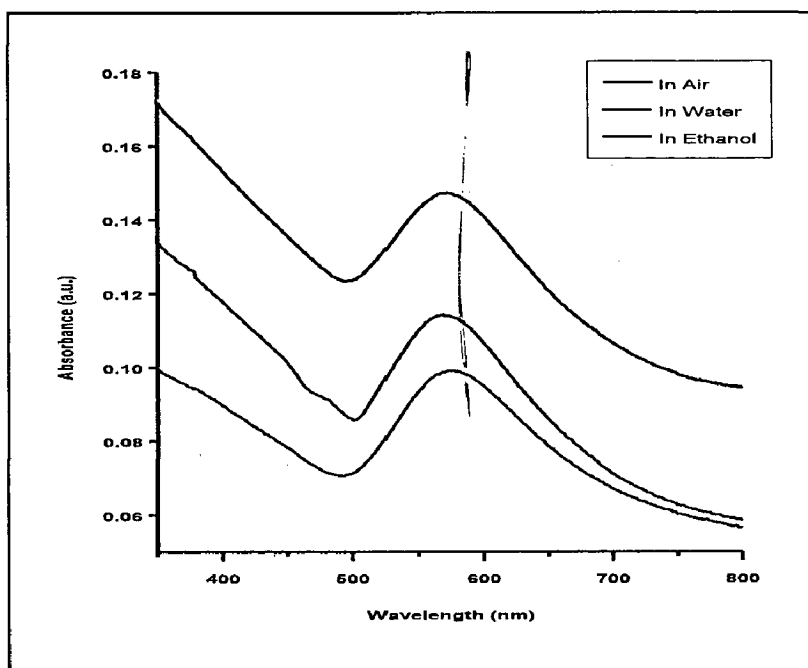


Figure 3.1.1.3: UV-Visible spectra of Au-PDMS (G-1) in different media with varying refractive index

Table 3.1 (b): Absorption maxima (λ_{\max}) of Au-PDMS nanocomposites (G-1) in media of varying dielectric constants.

S.No.	Surrounding Medium	Refractive Index (n)	λ_{\max} (nm)	$\Delta\lambda$ (nm)
1.	Air	1.0	569	-
2	Water	1.33	574	5
3	Ethanol	1.36	574	5

3.1.2: Optical Characteristics of Gold-PDMS Nanocomposites Fabricated by Galvanic Replacement Approach

In order to fabricate the Au-PDMS nanocomposite by means of galvanic replacement between Au and silver having different reduction potentials ($\text{AuCl}_4^-/\text{Au}$ is 0.99V, which is higher than $\text{Ag}^+/\text{Ag} = 0.8\text{V}$), firstly, Ag-PDMS nanocomposite was fabricated in manner similar to Au-PDMS nanocomposite fabrication. The optical characteristic of Ag-PDMS nanocomposite and the corresponding Au-PDMS nanocomposite fabricated by incubating Ag-PDMS nanocomposite in gold solution is described below:

3.1.2 (a): Sample A (Ag-PDMS):

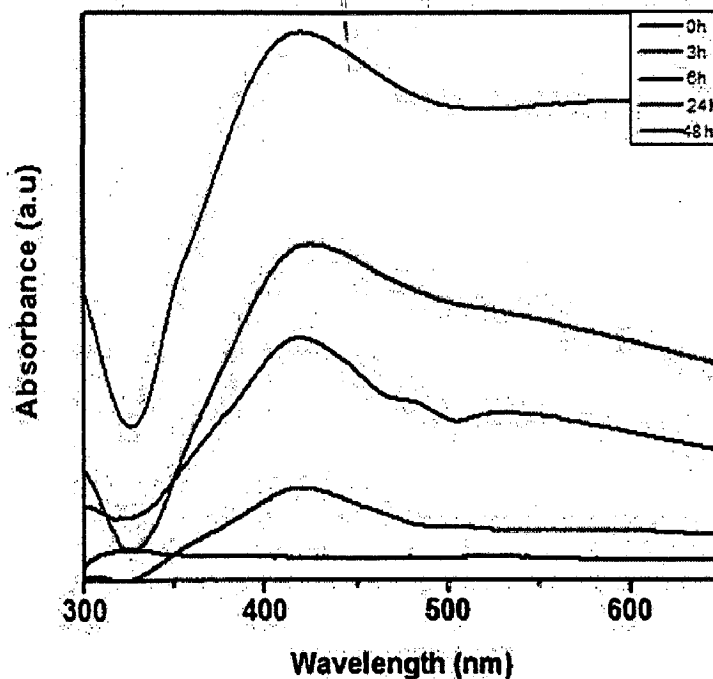


Figure 3.1.2.1: UV-Visible spectrum of Ag-PDMS nanocomposite prepared by incubating the PDMS film in a silver nitrate solution (15 mM) for times ranging from 0 to 48 hours.

Analysis of Figure 3.1.2.1 reveals that with an increase in incubation time, the absorbance increases corresponding to LSPR of silver nanoparticles (~430 nm) along with an increase in broadness of band, similar to Au-PDMS case described earlier. This is because of increase in aggregation as explained before for the optical spectra of the Au-PDMS composite. The relation between absorbance intensity and the concentration of silver salt is linear. Also, the color of PDMS sample changes from transparent to light brown (an indication of silver nanoparticle

formation). After optimizing all the parameters, the Ag-PDMS composite, obtained by incubation in 15mM silver for ~22 h, were further used to study the galvanic replacement at the polymer-solution interface to fabricate the Au-PDMS nanocomposite.

3.1.2 (b): Influence of Incubation time of Ag-PDMS in H₂AuCl₄.3H₂O Solution

Initially, when Ag-PDMS samples were incubated in gold solution to get an alloy, the final product obtained was gold-PDMS with a LSPR band at ~ 560 nm. In an attempt to capture some of the intermediate states of the replacement reaction, the Ag-PDMS samples were kept in the gold salt solution for different times (few seconds to 10 hours) until silver fully get galvanically replaced. The UV-Visible spectra corresponding to the different stages of the galvanic replacement reactions carried out at room temperature are shown in Figure 3.1.2.2.

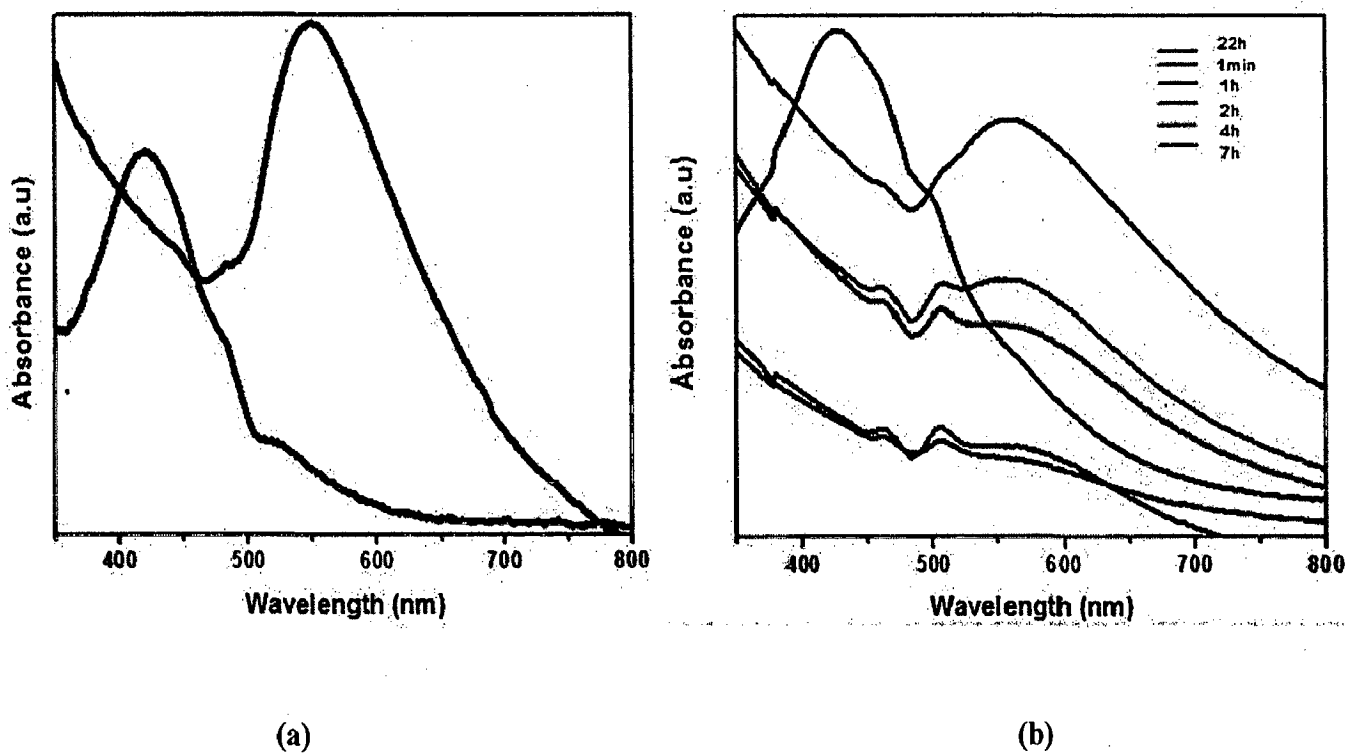
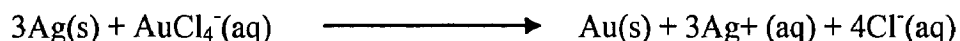


Figure 3.1.2.2: (a) UV-Visible spectra corresponding to initial (black curve) and final stage (red curve) of Ag/Au replacement reaction and (b) Spectra corresponding to the evolution with time of the Ag/Au replacement reaction

The Ag/Au galvanic replacement reaction in water and organic solvents is usually described by the stoichiometric oxidation of Ag atoms by the $(\text{AuCl}_4)^-$ ions (35, 36):



The band at 540 nm in Figure 3a corresponds to Au, the end product of the replacement reaction under these conditions. Weak bands at 462 and around 503 nm can be seen in the spectrum in Figure 3.1.2.2 (b) corresponding to a sample dipped into the solution for a very short time (couple of seconds ~ 1 min). The spectra show that, immediately upon dipping, there is already some replacement, as a shoulder around 520 nm can be seen together with the two bands at 462 and 503 nm; these two bands belong to the PDMS curing agent, confirmed by recording spectrum of the curing agent alone, but it is not clear at this point, why the bands due to the curing agent cannot be seen in the spectra of Ag-PDMS and in the end product of the replacement reaction. Their position is the same in all the spectra corresponding to different time of incubation, while the intensity of the Au LSPR band increases with time. After 7 hours, the Ag/Au replacement is almost completed and a broad band at 560 nm shows the exclusive presence of gold nanoparticles. No tuning of the Au LSPR band with the time of incubation, that is, with increasing Au concentration can be achieved, as observed very well in the case of replacement reactions carried out in water at high temperatures (35). This result can be accounted for by the fact that the replacement reaction proceeds at different rates on different particles because of their diversity in size and shape. At a given time, the replacement can be in an early stage, or a more advanced one, depending on the size and shape of the underlying silver nanoparticles.

3.1.2 (c): Influence of reaction condition

The spectral results above correspond to the replacement reaction at room temperature. In order to capture the intermediate stage in Ag/Au replacement at polymer interface, the reaction condition was changed to low temperature ~ 0°C. The observed spectral results are shown in Figure 3.1.2.3 below:-

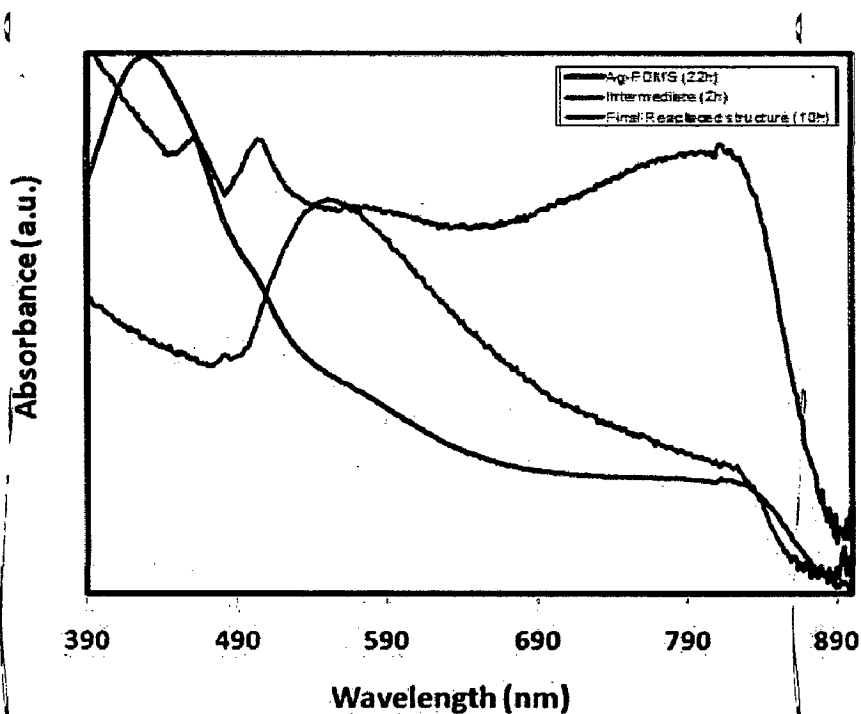


Figure 3.1.2.3: Spectra corresponding to the evolution of the galvanic replacement reaction at low temperature

The analysis of spectra corresponding to the low temperature replacement reaction reveals two broad Ag and Au LSPR bands (initial and end states), together with a broad absorption at higher wavelengths (around 800 nm) attributed to the intermediate state that could belong to a core-shell nanoparticle and/or the anisotropic particles seen in the SEM images, described later. The Au/Ag particles shown in SEM image Figure 3.2.2.3 are core-shell particles of a great size and shape diversity illustrated by the broad Ag and Au LSPR bands. Experiments were performed at 40°C as well but the replacement reaction was completed after approximately 15 min and no intermediate states could be observed. So, it could be concluded that the rate of galvanic replacement reaction at the polymer-solution interface depends on the reaction condition. Also, the presence of curing agent facilitates the reaction by lowering the activation energy for the reduction process of gold ions into gold atoms.

3.2: Application of Au-PDMS Nanocomposite (G-1): Biodetection of human serum albumin

The solution of the antibody in PBS was incubated on the nanocomposite samples, functionalized as described in the experimental section, and UV-Visible spectral measurements were taken in a phosphate buffered saline solution. Afterwards, the corresponding antigen was incubated on the covalently immobilized antibody and the spectra were recorded again. The biospecific interaction of the immobilized antibody with its antigen counterpart is evaluated by

measuring the shift of Au LSPR band to longer wavelengths. In order to determine the detection limit, experiments were conducted with different concentrations of the antigen (1.5×10^{-3} to 1.5×10^{-5} M). In all the experiments, approximately 2.5×10^{-2} mg of antibody was used to cover the surface of the sample. The red shifts obtained for the three concentrations of antigen were 5, 4 and 3 nm, respectively as shown in Figure 3.2.1.4 with corresponding data in Table 3.1 (c). The detection limit of antigen was found to be 10 μ g/ml.

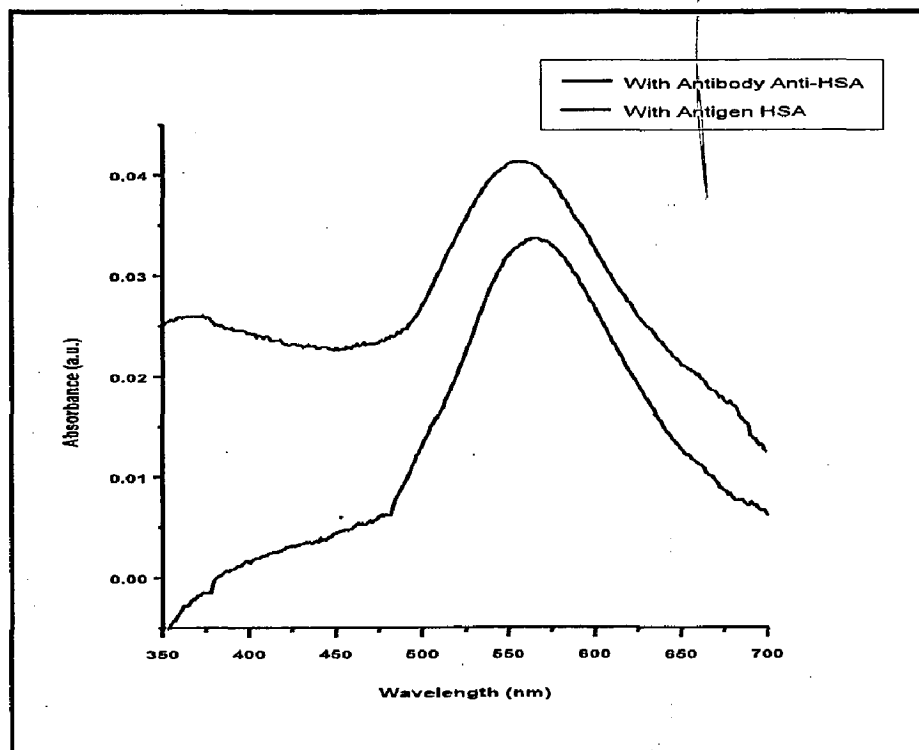


Figure 3.2.1.4: Position of Au LSPR band with the immobilized antibody (black curve) and after the interaction with the antigen (red curve) corresponding to the antigen concentration of 1.5×10^{-3} M.

Table 3.1 (c): UV-Visible spectral data for different concentration of HSA (antigen) detected by immobilized Anti-HSA polyclonal antibody on Au-PDMS surface.

S. No.	Antigen Conc. (dilution factor)	λ_{\max} with Antibody (nm)	λ_{\max} with Antigen (nm)	$\Delta\lambda = \lambda_{\text{Ag}} - \lambda_{\text{Ab}}$ (nm)
1	10^{-1}	556	561	5
2	10^{-2}	563	567	4
3	10^{-3}	560	562	2

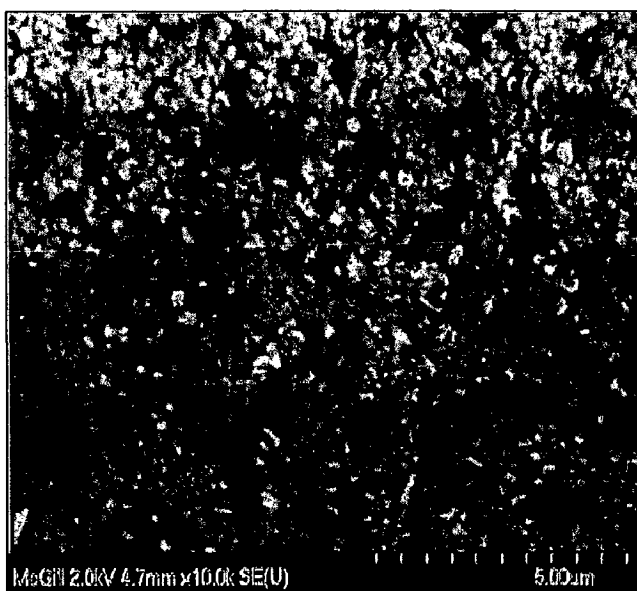
3.3: FE-SEM Images and EDXA:

The FE-SEM images were recorded for all samples fabricated by both *in situ* synthesis and galvanic replacement approach, so as to determine the size, morphology and dispersion of nanoparticles formed on the PDMS surface.

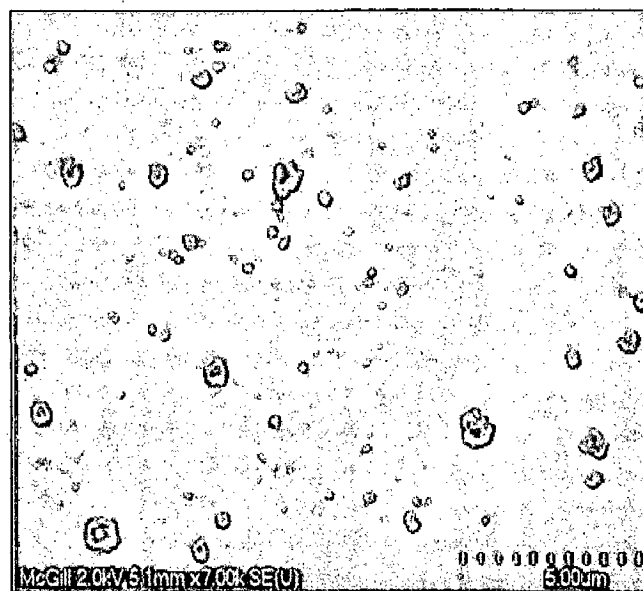
3.3.1: Au-PDMS nanocomposite fabricated by in situ synthesis approach

3.3.1.1: Samples G-5 and G-1

FEG-SEM images



(a)



(b)

Figure 3.3.1.1 (a): FE- SEM images of the PDMS incubated in aqueous $\text{HAuCl}_4 \cdot 3\text{H}_2\text{O}$ (a) 0.5% for 48h and (b) 0.1% for 18h

3.3.1.1: Analysis of FE-SEM images

For different concentration and incubation time, agglomerates to dispersed nanoparticles were observed. Because of non-conductivity of the polymer, the individual particles were very difficult to be visualized at a scale of 50-100 nm. From the image 3.3.1.1 (a), it is clear that with an increase in concentration of metal salt and incubation time, aggregation and concentration of nanoparticles increases in agreement with the optical spectral results. On the other hand, on reducing the metal salt concentration to 0.1% and incubation time to 18h, a very good dispersion of nanoparticles was observed as shown in Figure 3.3.1.1 (b). The monodispersed nanoparticles of size 100-200 nm with less aggregate of size ~ 500 nm were observed. Also, the surface coverage of nanoparticle observed in Figure 3.3.1.1(b) is good enough to be used in biosensing. The SEM results above are not showing the individual nanoparticle clearly, and so AFM imaging was done to understand better the effect of solution concentration and incubation time.

3.3.2: FE-SEM images of Au-PDMS nanocomposite fabricated by Galvanic Replacement

3.3.2.1: Sample A (Ag-PDMS):

FE-SEM image:

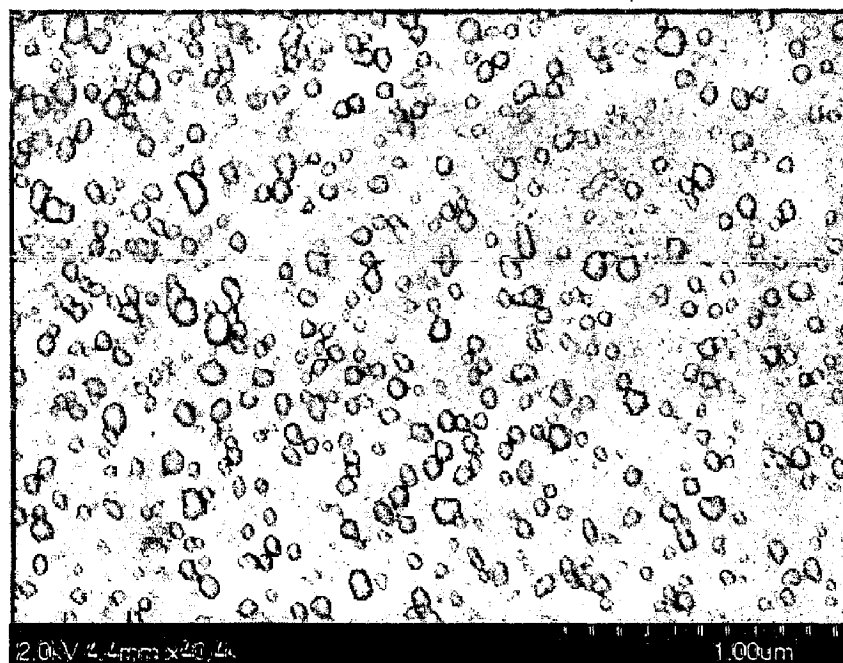


Figure 3.3.2.1: FE-SEM image of Ag-PDMS after incubation in 15 mM AgNO₃ aqueous solution for 22 h

EDXA data:

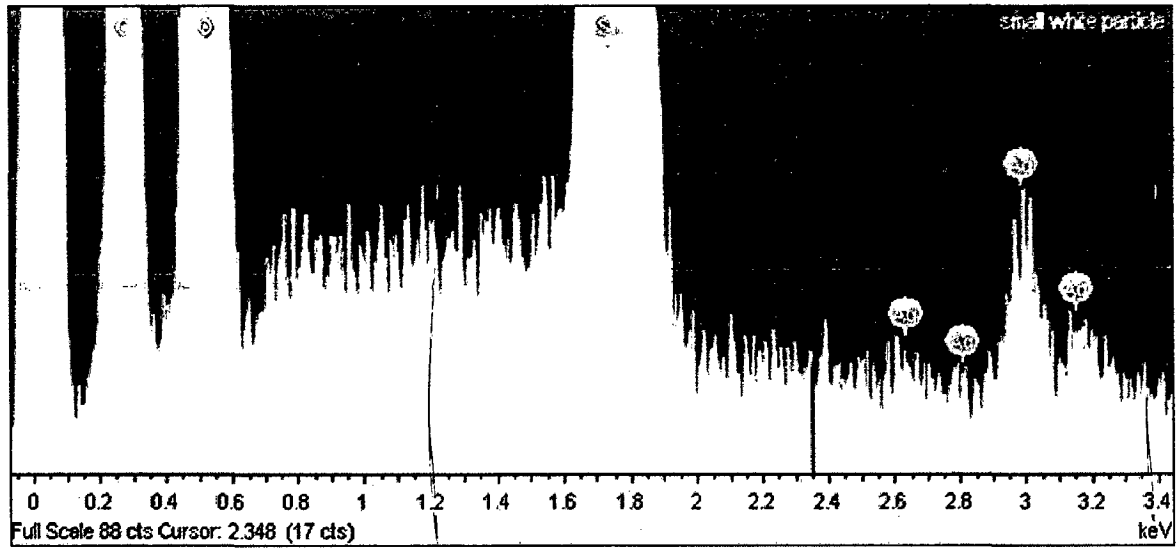


Figure 3.3.2.2: EDXA plot of sample-A

3.3.2.2: Sample B:

FE-SEM image:

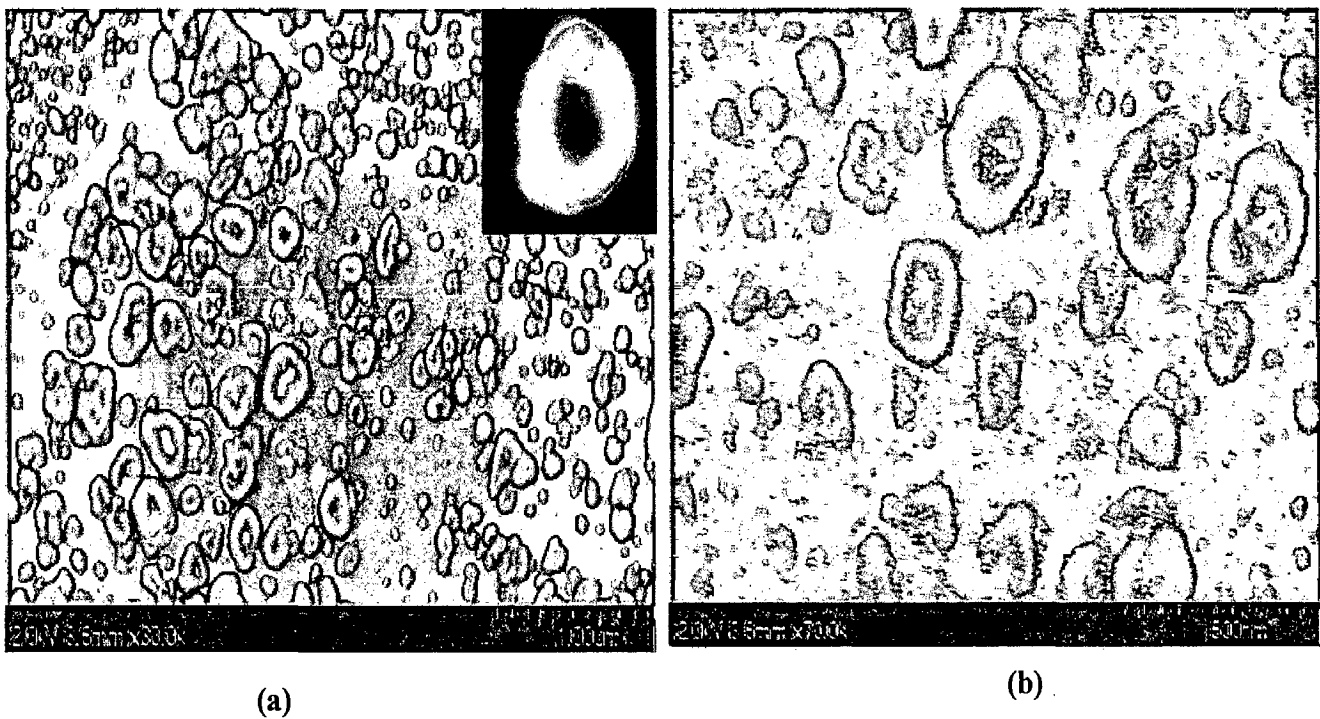


Figure 3.3.2.3: FE-SEM images of sample B at (a) lower magnification and (b) corresponding high magnification

EDXA data:

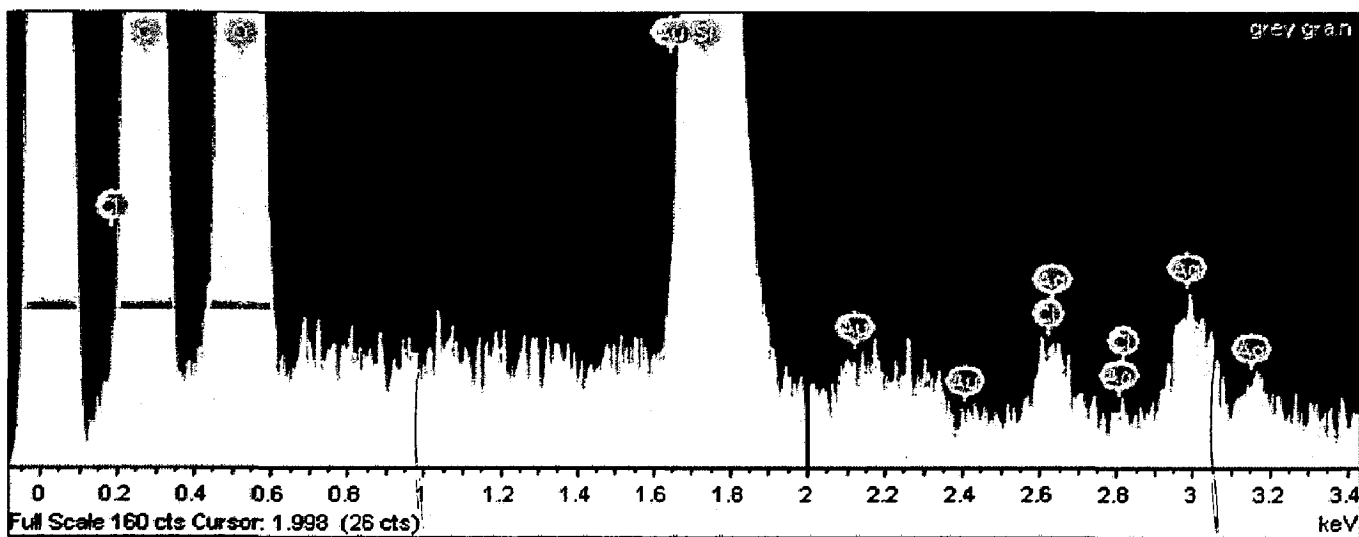


Figure 3.2.2.4: EDXA plot of sample-B

3.3.2.3: Sample D:

FE-SEM image:

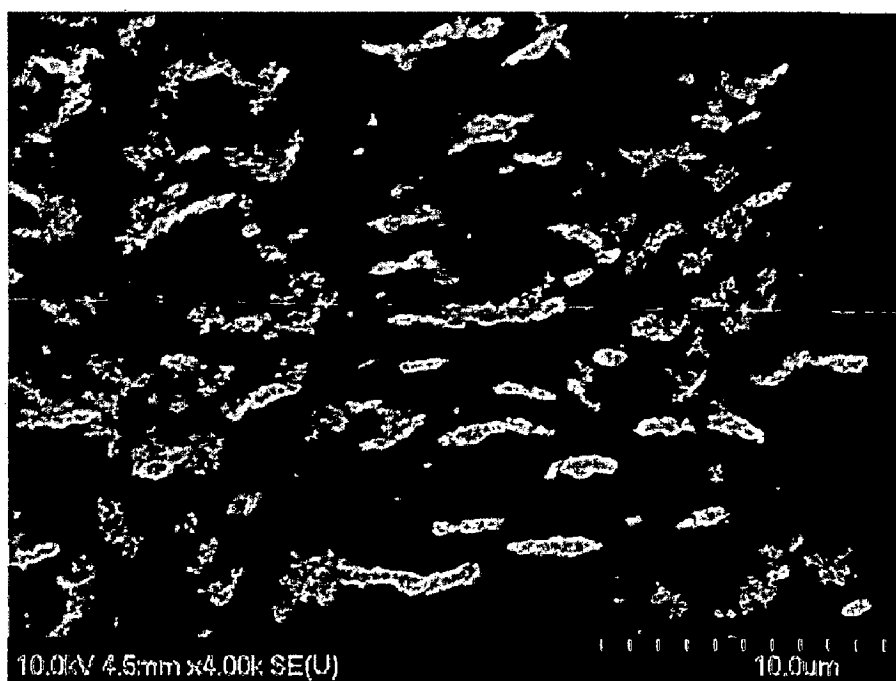


Figure 3.3.2.5: FE-SEM image of sample D

EDXA data

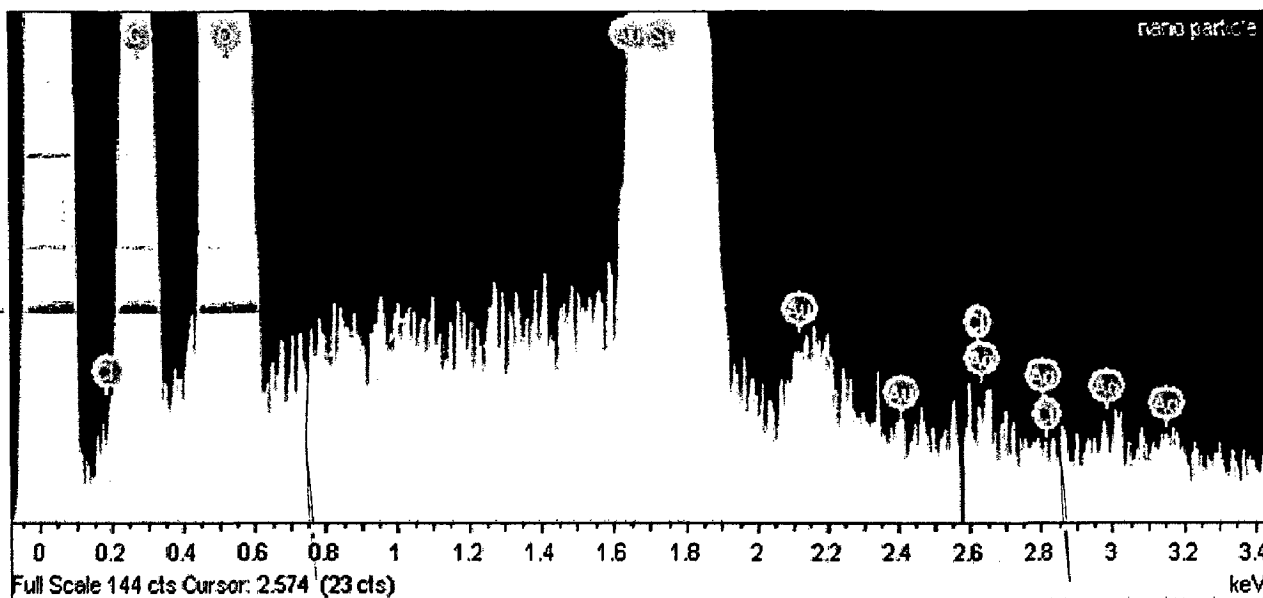


Figure 3.3.2.6: EDXA plot of sample-D

3.3.2: Analysis of FE-SEM images

Figure 3.3.2.1 is showing the monodispersed silver nanoparticles on PDMS surface along with some aggregation at few places, fabricated by incubating PDMS in 15 mM AgNO_3 solution for 22 h. The corresponding EDXA analysis confirms the formation of silver nanoparticles. These samples were used later for the galvanic replacement.

Figure 3.3.2.2 represents the very beginning stage of the replacement reaction, showing some interesting structures. It shows the close-up images of core-shell particles that have a quasi-spherical shape (see inset, Figure 3.3.2.2), in agreement with the EDXA results showing the presence of both gold and silver. However, as it can be seen in the figure, particles having other shapes, some of them anisotropic, are present in the sample as well which attributes to broadness and non-tuning of LSPR band, as explained before in optical spectral results in section 3.1.

The image in Figure 3.3.2.3 corresponds to the final replaced structure after a time period of 10 h, showing aggregated structures, mostly with elongated shapes. The backbones of the aggregates are formed from several rows of spherical particles at which branched structures are attached. This result could be explained as, at low temperature, the Ag-PDMS nanocomposite is

'frozen' and, in spite of the lower diffusion rate of Au^{3+} , a high concentration of core-shell particles will form, as seen in Figure 3.3.2.2. At this point, due to the proximity, the particle-particle interactions become stronger than the interaction of the particle with the polymer. When the quite fragile core-shell structures collapse, due to the high affinity between the gold particles, they aggregate and elongated domains are formed as seen in Figure 3.3.2.3. EDXA results also show the increase in amount of gold along with the presence of silver. The presence of silver was not found in optical spectrum of this sample, so, this silver presence could be due to formation of AgCl precipitate which is difficult to remove from PDMS surface by simply washing. The morphology of obtained Au-PDMS composite is significantly different from that of Au-PDMS prepared directly from HAuCl_4 by *in situ* synthesis.

3.4: AFM imaging:

The AFM imaging was done for samples G-1, G-5 and A-1 to get better information about the size, morphology and distribution of nanoparticles formed on the PDMS surface.

3.4.1: Sample G-5:

AFM image:

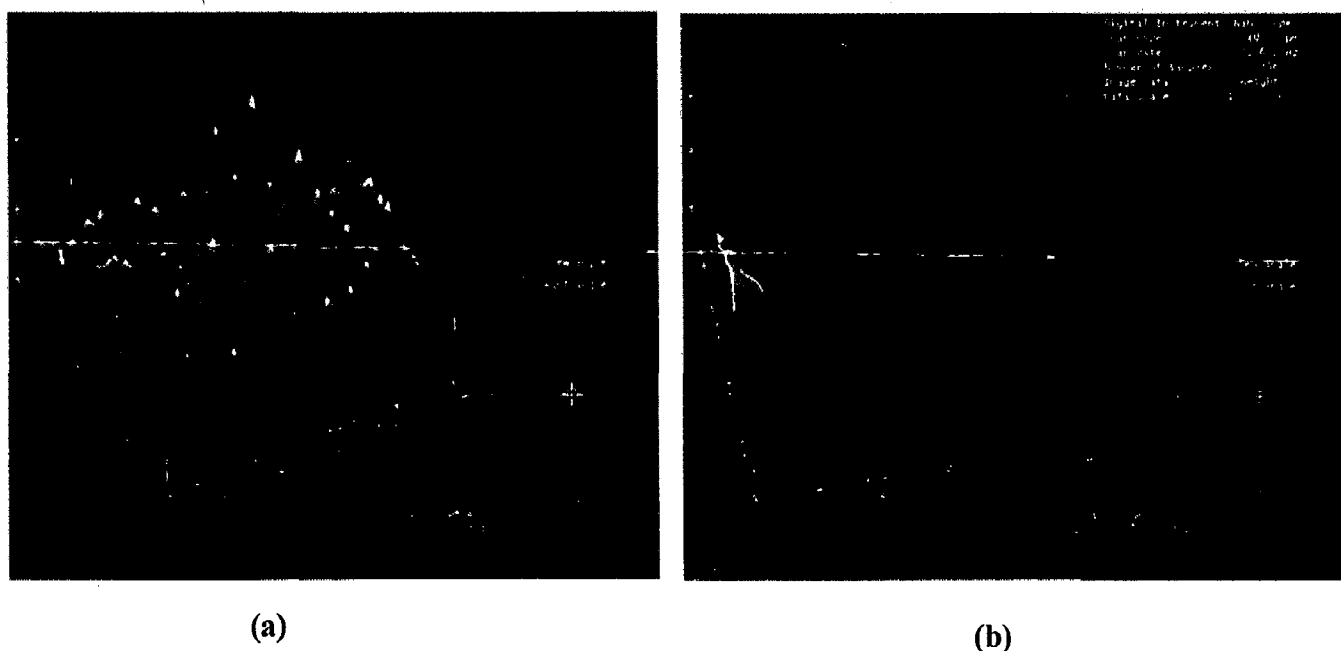


Figure 3.4.1: AFM image (3D) of sample G-5 for (a) 18h and (b) 48h incubation.

3.4.2: Sample G-1:

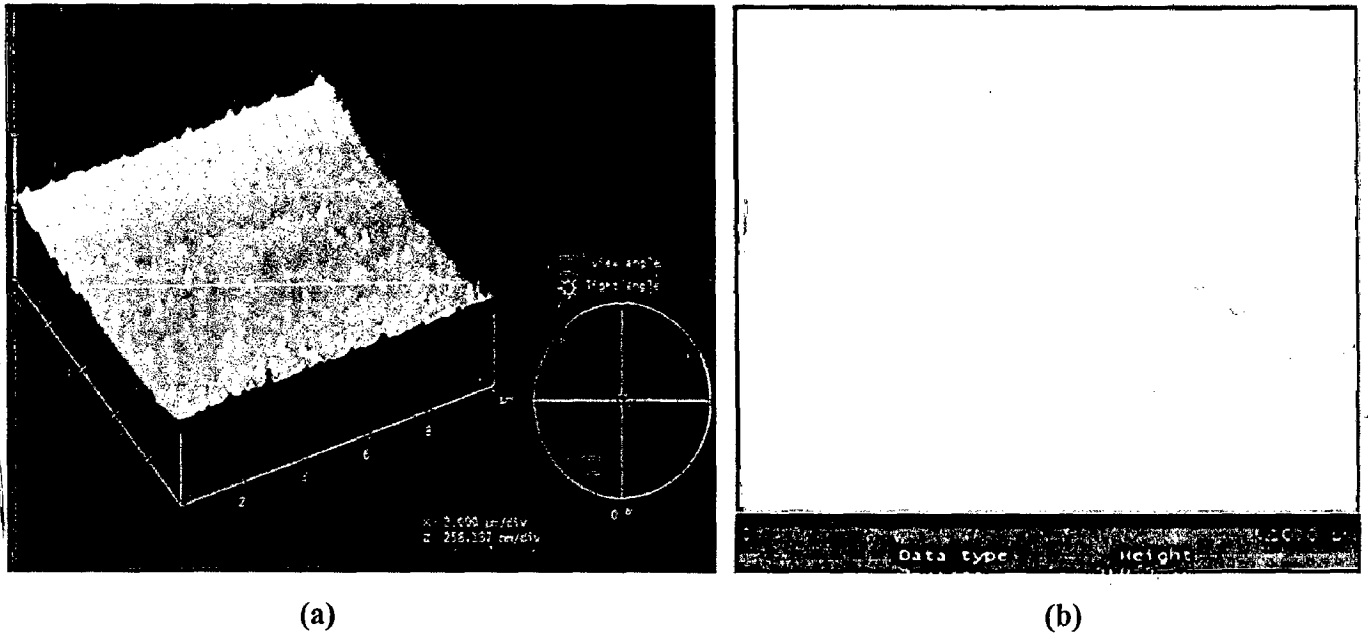


Figure 3.4.2: AFM image of sample G-1; (a) 3D and (b) 2D

3.4.3: Sample A:

AFM image (3D):

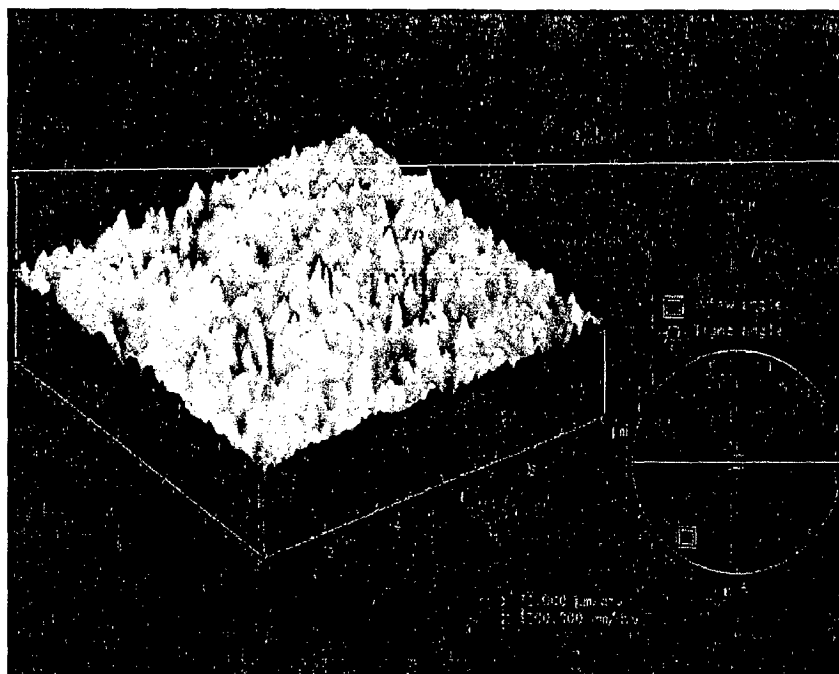


Figure 3.4.3: AFM image of sample A

AFM image (2D):

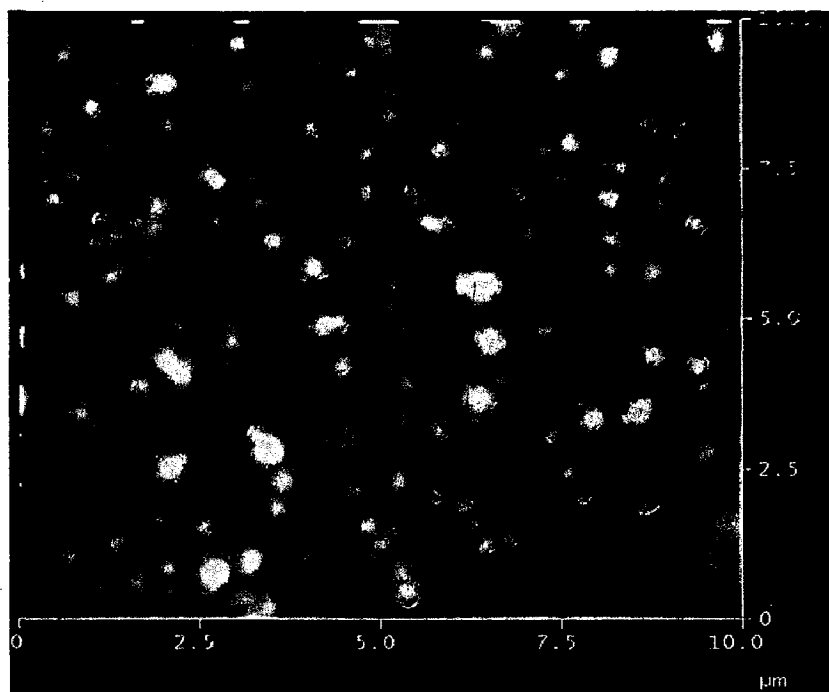


Figure 3.4.4: 2D AFM image of sample A

3.4.1: Analysis of AFM Images

The AFM images for sample G-5 (Figure 3.4.1) clearly reveal that with increase in incubation time, aggregation increases. Also, a comparison of the Figure 3.4.1 (a) and 3.4.2 (a) corresponding to sample G-5 and G-1, respectively shows that with increase in concentration of the metal salt ($\text{HAuCl}_4 \cdot 3\text{H}_2\text{O}$), the no. of particles on the surface increases along with some aggregation. Figure 3.4.2 shows the monodispersed gold nanoparticles present on PDMS surface which otherwise were difficult to be visualized by SEM. The size of nanoparticles calculated by using NanoScope IIIa[®] software was found to be 100-200 nm.

Figures 3.4.3 and 3.4.4 show the distribution of silver nanoparticles on the PDMS surface fabricated by incubating PDMS in 15mM AgNO_3 solution for 22 h. Nearly monodispersed silver nanoparticles distributed on its surface can be seen. These samples were further used to fabricate Au-PDMS nanocomposite by means of galvanic replacement reaction.

3.5: X-Ray Photoelectron Spectroscopy

Although EDXA analysis reveals the presence of gold and silver on surface for different stages of galvanic replacement in order to get correct quantitative information, XPS analysis was done. This technique is very surface sensitive and reveals qualitative as well as quantitative information about the elements present in the top few layers (~ 2 nm). The XPS spectra of all the samples and the corresponding data are represented in Figure 3.5 and Table 3.1 (d), respectively.

3.4.1: XPS Spectra:

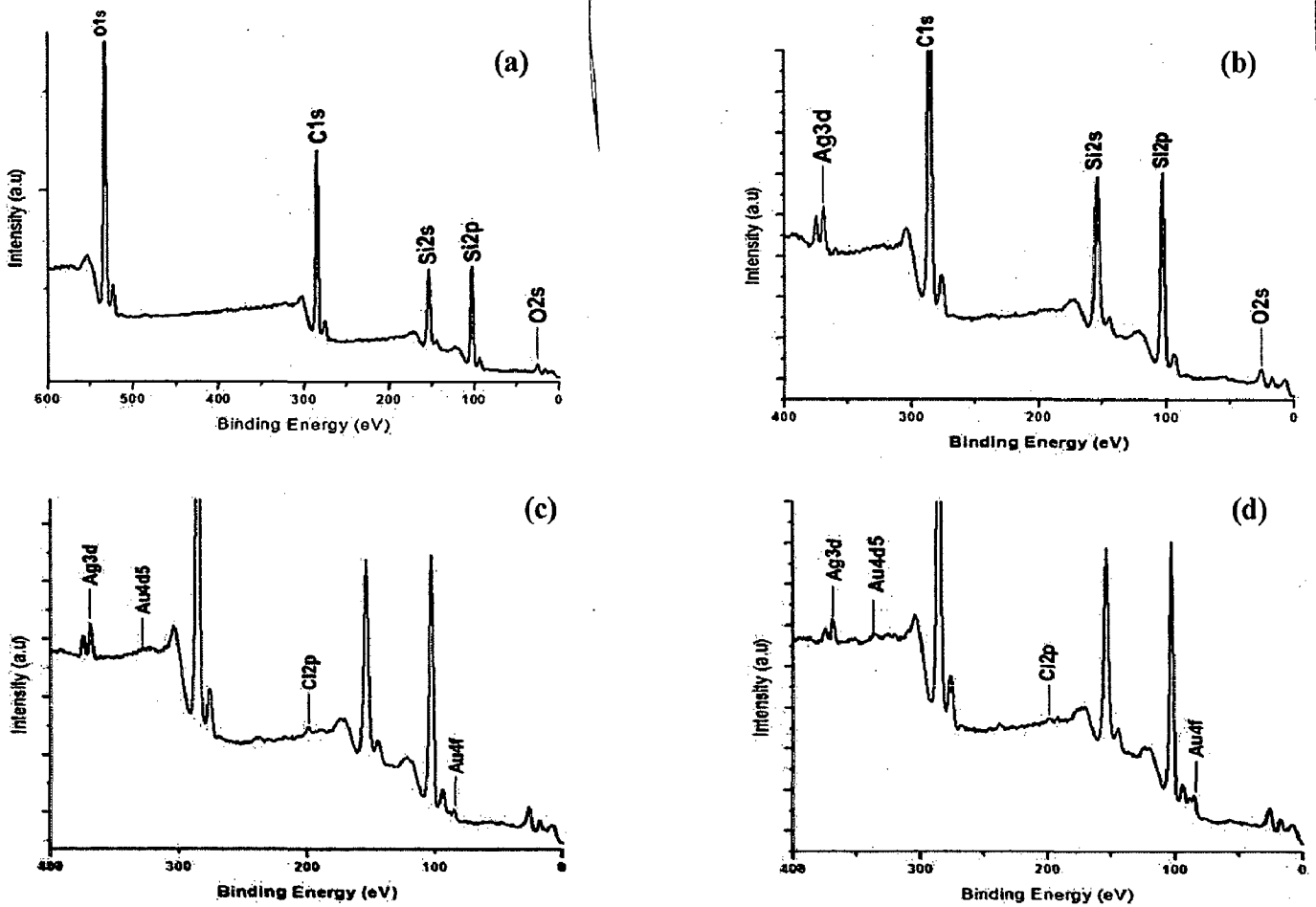


Figure 3.5: XPS spectra of samples (a) PDMS (b) Sample-A (c) Sample-B and (d) Sample-D corresponding to different stages of Au/Ag galvanic replacement at the polymer solution interface.

Table 3.1 (d): XPS data corresponding to spectra (a), (b), (c) and (d)

S.No.	Sample	Elemental ID	Binding Energy (eV)	Height CPS	Sensitivity Factor	Atomic Percentage (%)
1.	PDMS	Si2p	103.05	41258.12	0.27	22.25
		C1s	285.28	76309.67	0.25	47.83
		O1s	533.11	109421.07	0.66	29.92
2.	Sample-A	Si2p	103.22	38795.39	0.27	22.11
		C1s	285.83	72742.92	0.25	47.68
		O1s	533.30	102850.76	0.66	29.70
		Ag3d	369.17	8781.50	5.2	0.52
3.	Sample-B	Si2p	103.01	50115.90	0.27	22.05
		C1s	199.33	93443.80	0.25	47.20
		O1s	285.22	137722.34	0.66	30.26
		Ag3d	368.80	6543.61	0.25	0.27
		Au4f	84.13	1202.60	4.95	0.03
		Cl2p	199.33	1230.61	0.26	0.19
4.	Sample-D	Si2p	102.97	51411.59	0.27	22.4
		C1s	285.20	94922.04	0.25	47.57
		O1s	533.03	136975.44	0.66	29.77
		Ag3d	368.70	4743.72	5.2	0.19
		Au4f	85.21	2665.25	4.95	0.07
		Cl2p	199.33	-	0.26	-

3.5.1: Analysis of XPS data

The changes in the chemical composition as shown in Figure 3.5 and in Table 3.1 (d) are in good agreement with the EDXA results. Indeed, Figure 3.3.2.3 corresponding to the intermediate state shows the presence of both Ag and Au in the XPS spectra of sample. The increase in atomic percentage of Au in the XPS spectrum (Figure 3.5 (d)), is in agreement with optical results, where only Au LSPR band appears at around 560 nm. It is interesting to note that some Ag is still present in the end product of the replacement, as shown by XPS data; however, no Ag band can be seen in the optical spectra. The origin of silver could be explained probably, from AgCl, the insoluble product of the replacement which cannot be removed because of its low solubility at room temperature. Table 3.1 (d) is in agreement with the evolution of spectra for all the above four different samples corresponding to different stages of Ag/Au replacement reaction at the polymer interface.

Au-poly (dimethylsiloxane) nanocomposites were fabricated by *in situ* synthesis and galvanic replacement approach. Monodispersed gold nanoparticles localized only on PDMS surface were fabricated using inherent reducing and capping properties of PDMS while linear Au structures were obtained on PDMS surface fabricated by the second approach. The nanocomposites were characterized by field emission scanning electron microscopy (FE-SEM), energy dispersive X-ray analysis (EDXA), X-ray photoelectron spectroscopy (XPS), atomic force microscopy (AFM), and UV-Visible spectroscopy. The concentration of gold salt ($\text{HAuCl}_4 \cdot 3\text{H}_2\text{O}$), curing agent, and incubation time affects the size, shape and localization of Au nanoparticles on PDMS surface in *in situ* synthesis method. The temperature was found to play a key role in controlling the rate of galvanic replacement reaction at Ag-PDMS polymer/solution interface and hence the final Au nanostructures obtained. Initiating with Ag-PDMS as a template fabricated using same *in situ* synthesis method; the different intermediate stages of galvanic replacement reaction were captured by controlling rate of reaction as a function of temperature. Also, it was observed that with the increase in concentration of gold salt and the incubation time, the aggregation and size of gold nanoparticles on the PDMS surface increases. The Au-PDMS nanocomposite sensing platform fabricated by *in situ* synthesis method was found to be suitable for biosensing application and it was demonstrated using human serum albumin as a model system. A shift of ~5 to 3 nm was observed using Anti-human serum albumin polyclonal antibody as a ligand, immobilized on Au-PDMS surface through dextran - EDC-NHS chemistry, to detect human serum albumin for a concentration range of $\sim 1.5 \times 10^{-3}$ to 1.5×10^{-5} M. The antigen detection limit was found to be 10 $\mu\text{g/ml}$. The Au-PDMS nanocomposite fabricated by galvanic replacement approach resulted in formation of linear chains of gold nanoparticles, so, were not studied further for biosensing application.

1. P.M. Ajayan, L.S. Schadler and P.V. Braun, Nanocomposite science and technology, 1st Ed., Wiley-VCH Verlag, Weinheim, Germany, 2003, P. 2.
2. Y.L. Mi, Y.N. Chan, D. Trau, P.B. Huang and E.Q. Chen, *Polymer*, 47, 5124 (2006).
3. H.J. Bai, H.L. Gou, J.J. Xu and H.Y. Chen, *Langmuir*, 26, 2924 (2010).
4. I. Wong and C.M. Ho, *Microfluid Nanofluid*, 7, 291 (2009).
5. C.E. Hoppe, C. Rodriguez-Abreu, M. Lazzari, M.A. López-Quintela and D. Solans, *Phys. Status Solidi (a)*, 205, 1455 (2008).
6. D.I. Uhlentaut, P. Smith and W. Caseri, *Adv. Mater.*, 18, 1653 (2006).
7. G. Carotenuto, G. La Peruta and L. Nicolais, *Sensors Actuator B*, 114, 1092 (2006).
8. X. Hong and F.J. Kao, *Appl. Optics*, 43 (14), 2868 (2004).
9. T.R. Jensen, M.D. Malinsky, C.L. Haynes and R.P. Van Duyne, *J. Phys. Chem. B*, 104, 10549–10556 (2000).
10. T.R. Jensen, M. L. Duval, K.L. Kelly, A.A. Lazarides, G.C. Schatz and R.P. Van Duyne, *J. Phys. Chem. B*, 103, 9846–9853 (1999).
11. S. Schultz, D.R. Smith, J.J. Mock and D.A. Schultz, *Proc. Natl Acad. Sci.*, 97, 996–1001 (2000).
12. J. Yguerabide and E.E. Yguerabide, *Anal. Biochem.*, 262, 137–156 (1998).
13. J.M. Nam, C.S. Thaxton and C.A. Mirkin, *Science*, 301, 1884–1886 (2003).
14. C.R. Yonzon, D.A. Stuart, X. Zhang, A.D. McFarland, C.L. Haynes and R.P. Van Duyne, *Talanta*, 67, 438–448 (2005).
15. A.J. Haes, L. Chang, W.L. Klein and R.P. Van Duyne, *J. Am. Chem. Soc.*, 127, 2264–2271 (2005).
16. A.B. Dahlin, J.O. Tegenfeldt and F. Hook, *Anal. Biochem.*, 78, 4416–4423, (2006).
17. A.D. McFarland and R.P. Van Duyne, *Nano Lett.*, 3, 1057–1062 (2003).
18. G. Raschke, S. Brogl, A. S. Susha, A. L. Rogach, T. A. Klar and J. Feldmann, *Nano Lett.* 3, 935–938 (2003).
19. R. Elghanian, J.J. Storhoff, R.C. Mucic, R.L. Letsinger and C.A. Mirkin, *Science*, 277, 1078–1081 (1997).
20. D.L. Jeanmaire and R.P. Van Duyne, *J. Electroanal. Chem. Interfacial Electrochem.*, 84, 1–20 (1977).
21. http://www.nanoterra.com/surface_chemistry.asp

22. J.H. Park, Y.T. Lim, O.O. Park, J.K. Kim, J.W. Yu and Y.C. Kim, *Chem. Mater.*, 16, 688 (2004).
23. M.K. Corbierre, N.S. Cameron, M. Sutton, K. Laaziri and R.B. Lennox, *Langmuir*, 21, 6063-6072 (2005).
24. M.K. Corbierre, N.S. Cameron, M. Sutton, S.G.J. Mochrie, L.B. Lurio, A. Rohm and R.B. Lennox, *J. Am. Chem. Soc.*, 123, 10411-10412 (2001).
25. Y.L. Chiang, C.W. Chen, C.H. Wang, C.Y. Hsieh, Y.T. Chen, H.Y. Shih and Y.F. Chena, *Appl. Phys. Lett.*, 96, 041904 (2010).
26. B. Wang, K. Chen, S. Jiang, F. Reincke, W. Tong, D. Wang and C. Gao, *Biomacromolecules*, 7, 1203-1209 (2006).
27. Y. Xia and G.M. Whitesides, *Polym. Mater. Sci. and Eng.*, 77, 596 (1997).
28. V. Santhanam and R.P. Andres, *Nano Lett.*, 4(1), 41-44 (2004).
29. K.S. Giesfeldt, R.M. Connatser, M.A. DeJesus, N.V. Lavrik, P. Dutta and M.J. Sepaniak, *Appl. Spectros.*, 57 (11), 1346 (2003).
30. A. D. Pomogailo and V. N. Kestelman, *Metallopolymer Nanocomposites: Series in Materials Science*, Springer-Verlag, Berlin, Heidelberg, Germany, 2005, 8, P. 1135-222.
31. M.T. Sulak, O. Gokdogan, A. Gulce and H. Gulce, *Biosens. Bioelect.*, 21, 1719 (2006).
32. S. Porel, S. Singhb and T. P. Radhakrishnan, *Chem. Comm.*, 18, 2387-2389 (2005).
33. D.H. Fana, S.W. Yuana and Y.M. Shenb, *Colloid Surf. B*, 75, 608-611 (2010).
34. W.Y. Wua, Z.P. Bianb, W. Wanga and J.J. Zhua, *Sensors Actuators B*, 147, 298-303 (2010).
35. A. Goyal, A. Kumar, P.K. Patra, S. Mahendra, S. Tabatabaei, P.J.J. Alvarez, G. John and P.M. Ajayan, *Macromol. Rapid Comm.*, 30, 1116-1122 (2009).
36. Q. Zhang, J.-J. Xu, Y. Liu and H.Y. Chen, *Lab Chip*, 8, 352-357 (2008).
37. X. Lu, J. Chen, S.E. Skrabalak and Y. Xia, *Proc. IMechE*, 221, 1 (2008).
38. Y. Sun and Y. Xia, *J. Am. Chem. Soc.*, 126, 3892 (2004).
39. X. Lu, H.Y. Tuan, J. Chen, J.Y. Li, B. Korgel and Y. Xia, *J. Am. Chem. Soc.*, 129, 1733 (2007).
40. Q. Zhang, J.Y. Lee, J. Yang, C. Boothroyd and J. Zhang, *Nanotechnology*, 18, 245605 (2007).

41. A. Pearson, A.P. O'Mullane, V. Bansal and S.K. Bhargava, *Chem. Comm.*, 46, 731 (2010).
42. Y.Z. Fu, X.D. Xiu J.H. Liao and J.M. Wang, *J. Disp. Sci. Tech.*, 29, 1291 (2008).
43. S. Cheng, Y. Wei, Q. Feng, K.Y. Qiu, J.-B. Pang, S.A. Jansen, R. Yin and K. Ong, *Chem. Mater.*, 15, 1560-1566 (2003).
44. H.-J. Bai, H.-L. Gou, J.-J. Xu and H.-Y. Chen, *Langmuir*, 26, 2924-2929 (2010).
45. <http://www.nano-cemms.uiuc.edu/media/uploads/content/15/files/4.1.pdf>
46. M.A. DeJesu'S, K.S. Giesfeldt and M.J. Sepaniak, *Appl. Spectro.*, 58, 10 (2004).
47. http://pkcas.dk/205-147-carboxymethyl_dextran.htm
48. http://en.wikipedia.org/wiki/Human_serum_albumin
49. http://en.wikipedia.org/wiki/Scanning_electron_microscope
50. Hitachi S-4700 SEM Training & Reference Guide (2007).
51. http://en.wikipedia.org/wiki/Atomic_force_microscopy
52. Y. Sun, B. T. Mayers and Y. Xia, *Nano Lett.*, 2, 481 (2002).

Chapter 2

**Synthesis, Characterization and Application of Silica –
Silver Nanocomposite**

ABSTRACT

Silver nanoparticles deposited on different substrates are useful in various optoelectronic and biological applications. In this regard, a simple electroless deposition method was employed to prepare a nanocomposite in which Ag nanoparticles have been deposited on SiO₂ spheres. Firstly, monodispersed silica spheres of size 400 – 450 nm were synthesized by well known Stöber's method using aqueous ammonia, ethanol and tetraethylorthosilicate. The surface of silica was activated using different approaches followed by the adsorption of Sn²⁺ ions. The electroless deposition utilizes Sn²⁺ ions, present on the silica spheres, as the reducing agent and ammonical silver nitrate as the silver source. The formation of silica spheres and silver nanoparticles coated silica spheres was evidenced through various characterization techniques such as XRD, FT-IR, FE-SEM, and DRS. From XRD, FE-SEM, and EDXA results, It was proved that there is deposition of silver nanoparticles on the monodispersed silica spheres; no free silver was noticed in the FE-SEM images. The loading level of silver on the silica spheres could be controlled from about 4 to 20 weight % by changing the activation method and the time of deposition. The DRS results showed the presence of a broad band at about 400 – 470 nm that corresponds to the SPR of silver nanoparticles. The silver nanoparticles coated silica spheres were explored for their antimicrobial activity against *Escherichia coli* and *Bacillus subtilis* and inhibitory as well as killing effects were observed against both gram positive and gram negative bacteria.

1.1: Metal-Silica Nanocomposite: General Description

Metal nanoshell particles constitute a special class of nanocomposite materials. They are a class of nanoparticles with tunable resonance to electromagnetic radiation. A metal nanoshell is a spherical nanoparticle consisting of a dielectric core such as polystyrene sphere, silica spheres, glass, sapphire, zinc selenide etc., (1) surrounded by a uniform metallic shell, e.g. silver, titanium and gold. The nanoshells can be chemically attached to a wide variety of materials, including plastics, liquids, aerosols, epoxies, glasses and even fibers. They possess different optical properties as by tailoring the core-shell ratio, the plasmon band could be shifted from UV region to near infrared region. Hence they are being exploited for various applications in different areas as outlined in Figure-1.1. These materials can also be of economic interest because precious materials can be deposited on inexpensive core, so, expensive material is required in lesser amount than usual.

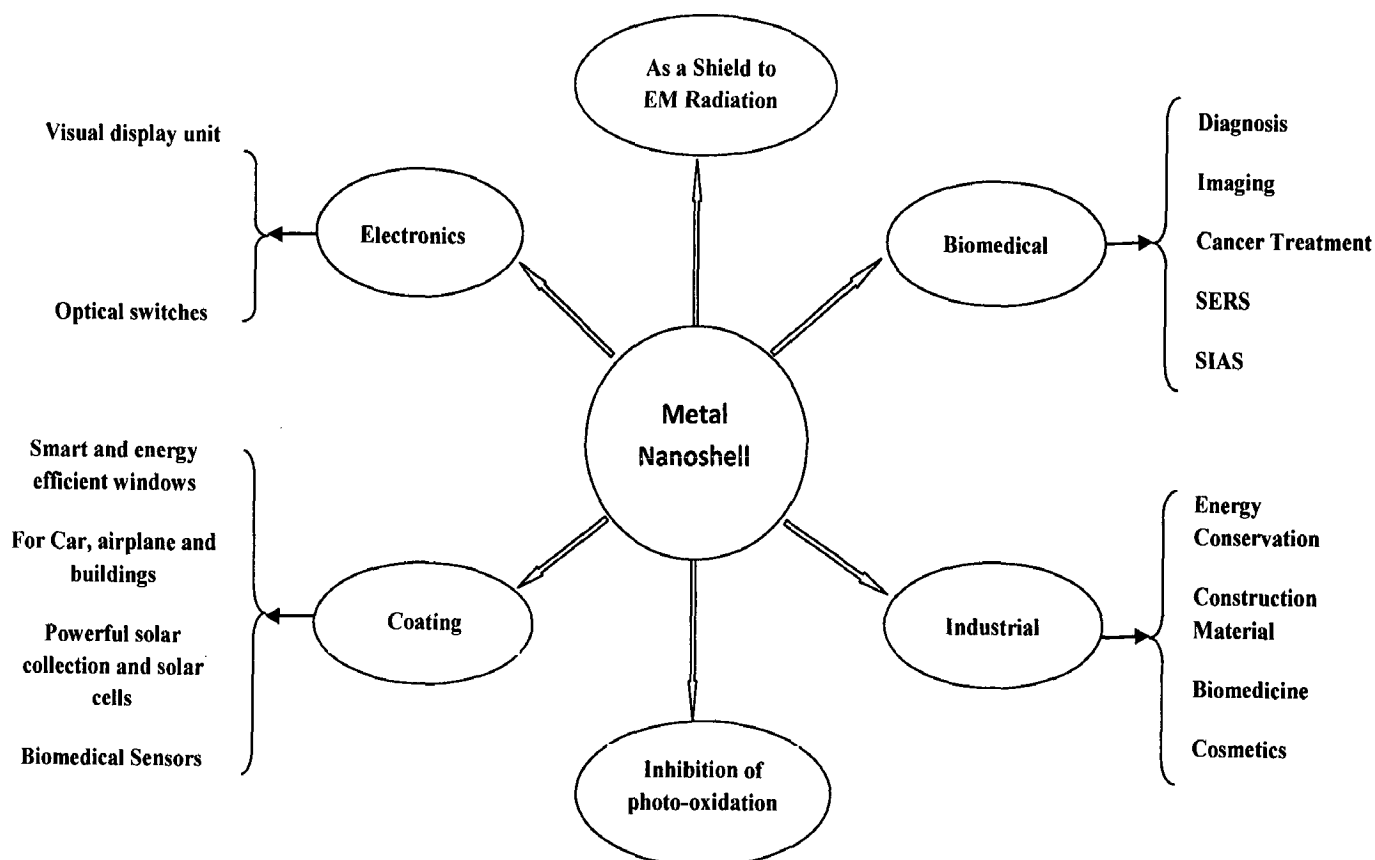


Figure -1.1: Various applications of metal-silica nanocomposites in general (2-4).

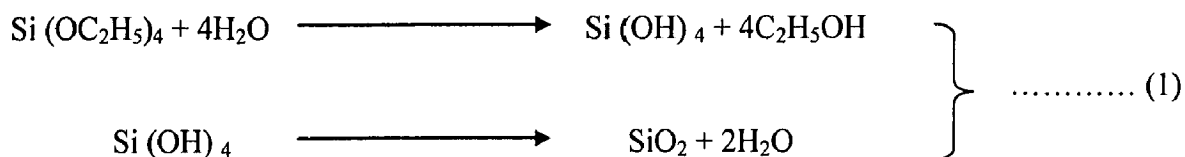
1.2: Silver-Silica Nanocomposite:

Although gold-silica nanocomposite is widely used for various applications, silver nanoparticle-silica nanocomposite is attracting the most attention since silver nanoparticles possess sharper and stronger plasmon resonance at a different location in the electromagnetic spectrum than gold nanoparticles. Also, the relative lower cost of silver compared to gold makes it a favorable choice from an industrial point of view. Silver NPs have great promise for use as materials exhibiting antibacterial (through the release of silver ions), bio-sensing (through surface plasmon resonance) (11-16), and electromagnetic wave shielding (through free electrons) properties.

1.3: Synthesis of Dielectric Silica Core:

Silica (SiO₂) (dielectric constant ~4.5) (5) is a popular material to form core shell particles because of its extraordinary stability against coagulation. Its non-coagulating nature is due to a very low value of Hamaker constant, which defines the Vander Waal forces of attraction among the particles and the medium. It is also chemically inert, optically transparent and does not affect redox reactions at core surfaces (6).

Silica particles with narrow size distribution can be synthesized following the procedure developed by Stöber *et al* (7). This method involves hydrolysis and successive condensation of TEOS (tetraethylorthosilicate (Si (OC₂H₅)₄)) in an alcoholic medium in the presence of ammonium hydroxide (NH₄OH) as the catalyst. The reaction mechanism is explained in equation 1. The first step is hydrolysis, in which ethoxy groups are replaced by OH groups. In the second step, silicon hydroxides undergo polycondensation process to form SiO₂.



By varying the relative ratio of TEOS to solvent and the amount of catalyst, one can synthesize these particles in various sizes ranging from ~ 50 nm to 1 μm. Table-1 summarizes the various methods reported for the synthesis of silica nanoparticles.

Table -1: Various methods for the synthesis of silica nanoparticles of varying size

S. No.	Method	Reagents	Size of silica spheres (nm)	Reference
1	Stöber–Fink–Bohn method	Aqueous ammonia, ethanol, TEOS	223 ± 15	(7)
2	Modified Stöber’s method	Aqueous ammonia, dry ethanol, TEOS	100	(9)
3	Osseo-Asare method	TEOS, cyclohexane, NP-5 (nonyl phenyl ether)	35	(10)

1.4: Methods for the Synthesis of Silver Coated Silica Nanoparticles:

The growth process of nanoscale silver layer on silica spheres mainly includes two steps, i.e. nanoscale nuclei formation and controllable layer growth process. The nucleation-growth mechanism is responsible for the deposition process. Various methods have been reported in the literature to coat silica spheres with silver nanoparticles which could be categorized as one in which the as prepared silver nanoparticles is coated on silica spheres, and second is where, silver ions are attached to silica spheres followed by reduction of ions on the surface itself. They can be classified as follows:

- a) Seed mediated growth techniques
 - (i) Electroless deposition
 - (ii) Sonochemical deposition
- b) Microwave Irradiation Method
- c) Chemical reduction
- d) Surface functionalization
- e) Physical adsorption
- f) Sol-gel method/modified Stöber’s method
- g) Reverse micelle method

The literature methods are briefly summarized in the tables given below-

a) Seed Mediated Growth Techniques

One of the promising approaches to form metal coatings involves the activation of the template particle surface (silica spheres in our case) by using “seeds” of a metal to facilitate further metal deposition. The seeds are formed on silica spheres surface using one of following methods:

(i) Electroless Deposition Method

S. No.	Metal Precursor	Sensitizing Mixture	Reducing agents	Size of silver nanoparticles formed on silica surface (nm)	Reference
1.	Ammonical AgNO ₃	SnCl ₂ , Sn powder, HCl, 2% NaOH	Sn ²⁺ (for seed) HCHO (for shell)	22.0-60.0	(17)
2.	Ammonical AgNO ₃	SnCl ₂ , CF ₃ COOH, HCL	Sn ²⁺ (for seed) HCHO (for shell)	~ 5.0	(18-20)

(ii) Sonochemical Deposition Method

S. No.	Metal Precursor	Solvent/ Atmosphere	Stabilizer	Irradiation Power	Size of silver nanoparticles formed on silica surface (nm)	Reference
1.	Aqueous AgNO ₃	DMF	PVP	800W/cm ²	15-60	(21)
2.	Ammonical AgNO ₃	D.I. Water and Ar/N ₂	-	40W/cm ²	4-5	(22)

b) Microwave Irradiation Method

S. No.	Metal Precursor	Solvent	Irradiation Power	Size of silver nanoparticles (nm)	Reference
1.	Aqueous AgNO ₃	PEG or EG	900W/cm ²	20.0	(23)

c) Chemical Reduction Method

S. No.	Metal Precursor	Reducing Species	Size of silver nanoparticles formed on silica surface (nm)	Reference
1.	Ammonical AgNO ₃	Glucose	7.0-22.0	(24)
2.	AgNO ₃	Formaldehyde	20.0	(25)

d) Surface Functionalization Method

S. No.	Metal Precursor	Functionalizing agent	Reducing agent	Size of silver nanoparticles formed on silica surface (nm)	Reference
1.	AgNO ₃	APTMS	NaBH ₄ , Sodium citrate	Variable	(26)
2.	AgNO ₃	MPTMS	Sodium Citrate	2.9-9.0	(27)

e) Physical Adsorption Method

In this method, the as prepared Ag nanoparticles are deposited on the surface of silica spheres by the principle of physical adsorption simply by mixing the as prepared Ag nanoparticles with the silica spheres

S. No.	Metal Precursor	Reduction Method	Reducing Agent	Protective Agent	Size of silver nanoparticles formed on silica surface (nm)	Reference
1.	Ag-Oleate	Thermal Decomposition	-	-	8±1.3	(28)
2.	As prepared Ag nanoparticles	Chemical Reduction	Trisodium Citrate	PVP	~10.0	(29)

f) Sol-Gel Method / Modified Stöber's Method

S. No.	Metal Precursor	Solvent	Reducing Agent	Size of silver nanoparticles formed on silica surface (nm)	Reference
1.	AgNO ₃	Ammonical Water, 2-Propanol, TEOS	NaBH ₄	15.0-60.0	(30)

g) Reverse Micelle Method

S. No.	Metal Precursor	Solvent/ Micelles	Reducing Agent	Size of silver nanoparticles formed on silica surface (nm)	Reference
1.	AgNO ₃	NP-5/AgNO ₃ /Cyclohexane NP-5/Water/Cyclohexane	Glucose	3.0	(31)

Other than the above mentioned methods for the fabrication of silver nanoparticles coated silica nanocomposite, thin films could also be fabricated. These techniques are summarized below:

S. No.	Metal Precursor	Substrate	Reducing Agent	Size of silver nanoparticles formed on silica surface (nm)	Fabrication method	Reference
1.	As prepared silver nanoparticles	Colloidal silica coated silicon wafer	-	10.0	Physical Adsorption	(32)
2.	AgNO ₃	PDMS	Glucose	30-40	Micro contact Printing & Chemical Reduction	(33)
3	AgNO ₃	Colloidal silica coated silicon wafer	Glucose	20.0	Chemical Reduction	(42)

1.5: Application of Silver nanoparticles Coated Silica Spheres:

Core shell particles with highly controlled optoelectronic and chemical properties are used in several applications. It is possible to modify these particles to enhance their integration with bimolecular components for their biotechnological applications such as biomedical imaging and therapeutics. Metal nanoparticles coated silica spheres, specifically silver nanoparticles coated silica spheres, have potential applications in various fields, such as-

- a) Medicine
- b) Biosensor
- c) Textiles
- d) Photonics
- e) Catalysis
- f) Food and healthcare
- g) Water treatment
- h) EM wave shielding
- i) Inhibition of photo oxidation in conducting polymers

The current and future applications of silver nanoparticles in above mentioned fields are discussed below by considering representative examples.

(a) Medicine

For biomedical applications, mostly silica core and gold or silver shells have been used because they offer highly favorable optical and chemical properties. It is possible to attach biomolecules to the core shell assembly and form an immunoassay to detect analytes, cancer cells, tumors, antibodies and microorganisms. These nanoparticles offer a sensitive, reliable and rapid detection method of biomolecules.

• Application in Optically Triggered Drug Delivery

Thermally responsive hydrogels and membranes have been extensively evaluated as platforms for the pulsatile delivery of drugs. One of the characteristics of temperature-responsive hydrogels is the presence of a lower critical solution temperature (LCST), a temperature at which the hydrogel material will undergo a dramatic phase change. One of the examples of such a

polymer is N-isopropylacrylamide (NIPAAm). In order to have controlled and targeted release of a drug, composites hydrogels have been designed and the composites are fabricated by mixing nanoshells into the monomer mixture. After polymerization, the nanoshells get physically entrapped in the hydrogel matrix and undergo a pronounced collapse in response to near infrared light; the nanoshells absorb the light, generating heat within the composite to exceed the LCST of the copolymer (43-44).

- **Photothermal Ablation**

Nanoshells can be designed to strongly absorb near infrared light and thus to generate localized heating, potentially enabling nanoshell-mediated thermal ablation therapies for applications such as cancer treatment. Due to the lack of absorption of near infrared light by tissue components, use of this type of light source, with nanoshells at the desired tissue locations, should minimize collateral tissue damage. *In vitro* studies with nanoshells bound to breast carcinoma cells have demonstrated effective destruction of the cancerous cells upon exposure to near infrared light, with cell damage limited to the laser treatment spot (43-44).

- **Molecular Imaging**

Optical methods for diagnosis and treatment in medicine and biology are attractive due to their potential for non-invasive and minimally-invasive applications. Nanoshells could be designed to preferentially scatter rather than absorb light, so that nanoshells can serve as strong optical contrast agents for a variety of biomedical optical imaging applications. Recently, SiO₂@Au nanoshells have been used for imaging HER2, a clinically relevant cancer biomarker, *in vivo* (43). Same potential application could be expected for silver nanoshell along with the benefit of reduced cost.

- **Wound Dressing**

In the late 1970s, Robert O. Becker discovered that silver ions promote bone growth and kill surrounding bacteria. Silver kills some 650 different disease causing microorganisms. Silver based topical dressing has been widely used as a treatment for infections in burns, open wounds and chronic ulcers. The silver nanoparticles and Ag⁺ carriers such as silica nanoparticles can be

beneficial in delayed diabetic wound healing as diabetic wounds are affected by many secondary infections. The nanoparticles can help the diabetic patients in early wound healing with minimal scars.

(b) Sensors

• As SERS Substrate

It is generally agreed that an important contribution to the SERS enhancement comes from the electromagnetic (EM) enhancement mechanism, in which plasmon excitation in the particle creates an enhanced electric field near the particle, which in turn leads to enhanced Raman excitation and emission. This phenomenon is specifically shown by metal nanoparticles. SiO₂/Ag composite spheres have been observed as excellent SERS substrates. Hence, they provide an effective approach toward the detection of proteins under biologically relevant conditions through functionalization of SiO₂ surfaces to control the interactions between the SERS substrate and the selected analytes.

- Ag/SiO₂ composite has been shown to increase Raman signals for 4-aminobenzenethiol (4-ABT) which otherwise was absent. Moreover, the Raman peaks of 4-ABT also appeared in the SERS spectra even at low concentration (41).
- The enhancement ability of the Ag nanoparticles coated silica colloidal crystals film (ANSCC) was estimated to be about 5 times larger than the Ag foil film and about 3.5 times larger than the Ag mirror film (42).
- The silica coated colloidal crystal (SCCC) substrate provides the strongest Raman enhancement for the detection of *p*-toluenethiol with the smallest background signal. The intensity derived from the SCCC substrate was about 40 times larger than that from the flat silver film and about three times larger than that from the oxidation-reduction cycle (ORC)-treated substrate (32).

• In Instantaneous Whole Blood Immunoassay

A new immunoassay technique has been developed utilizing antibody-conjugated, near-infrared resonant nanoshells. This assay can be performed in whole blood and provides results

within several minutes. When antibody conjugated particles are exposed to a multivalent analyte, multiple particles will bind to the analyte, forming particle dimers and higher order assemblies of the particles. The aggregation of nanoshells gives rise to additional optical resonances at longer wavelengths for the aggregate structure. This appears in the optical signal as a net shift in the nanoshell resonance to longer wavelengths in the near infrared extinction spectrum, allowing detection of analyte in blood samples. The performance of the nanoshell-based immunoassay has been evaluated in saline, serum, and blood samples for a variety of analytes (43).

- **Detection of Metal Ions**

Silver nanoshells can also be used for the detection of toxic ions such as Cd, Hg and Pb present in water. The extinction spectrum of silver nanoshells changes when it is mixed with a solution containing these ions (44).

(c) Textiles

The antimicrobial properties of silver are well known. The coating solutions of $\text{SiO}_2@Ag$ can be easily applied onto textiles by dip-coating. As compared to free silver, the antimicrobial properties of the textile fabrics treated with $\text{SiO}_2@Ag$ are even present after several times of washing under household conditions. Silica spheres act as Ag metal carriers and effective matrix, causing good dispersion of silver. The encouraging bacteriostatic properties of textiles doped with SiO_2/Ag powder has opened a way for their various practical applications, for example in sport and recreational textiles or in textiles used in hospitals.

- Crystalline silver deposited SiO_2 coated in textile samples have been shown to have a high antimicrobial effect against the bacteria *E.coli* even under household washing condition. This is because the presence of SiO_2 particles causes a certain improvement of adhesion due to film formation, and hence the improvement in antimicrobial effect (38).
- A study of antimicrobial activity of three forms of silver incorporated in textiles has revealed that among three kinds of Ag doped textiles only those doped with SiO_2/Ag

spheres are bacteriostatically active. Both *E. coli* and *S. aureus* were shown to be sensitive (40).

(d) Photonics

Photonic crystals are three-dimensional periodic dielectric structures, with lattice constants of the order of the desired electromagnetic wavelength of operation. The free-EM wave dispersion in such crystals is greatly modified due to the presence of periodicity and refractive-index contrast. Under favorable circumstances, a photonic band gap (PBG) in the dispersion relation can open up in which light cannot propagate in any direction. Such a structure is believed to have a deep impact on a wide range of photonic applications. It has been found that spherical-silver nanoparticles of radii of about 160 nm are plausible building blocks for self assembled photonic crystals operating at optical frequencies. The difficulty of fabricating such particles can be bypassed by using silver-coated silica spheres, with the added advantage that the frequency of the PBG can be tuned simply by changing the size of the silica core. Mono-dispersed metal coated spheres are ideal to build photonic crystals with large dielectric contrast, which has been demonstrated to have complete photonic band gap (CPBG) even in the optical wavelengths. Because of their low bulk absorption, metal like silver and gold are the most suitable for the creation for photonic crystals with a band gap in the visible range (45).

(e) In Catalysis

Metal nanoparticles are efficient catalysts because of their high surface area to volume ratio. They have been demonstrated to possess high catalytic activities for hydrogenation, hydroformylation, carbonylation, and so forth. But nanosized metal particles in the solution are active and prone to coalesce due to vander Waals forces and high surface energy unless they are protected. Hence their catalytic efficiency is reduced. On the other hand, supported metal particles on silica spheres effectively avoids flocculation of nanosized colloidal metal particles during a catalytic process in the solution, which allows one to carry out the successful catalytic reduction.

- Recently, Ag nanoparticles supported on silica spheres have been reported for the efficient reduction of dyes such as methylene blue, eosin, and rose bengal by NaBH_4 , which otherwise is not observed to a good extent in the absence of silver nanoparticles. Moreover, the rate of the reduction for dyes gradually increased with the increase in the concentration of silver particles on silica. The catalytic process can be explained by an electrochemical mechanism, where silver nanoparticles-supported silica spheres serve as an electron relay for an oxidant and a reductant, and electron transfer occurs via the supported metal particles (35).
- Catalytic activity of Ag/SiO_2 composites have been demonstrated for the reduction of different kinds of dyes such as reactive Rhodamine B (basic dye) and Brilliant Red K-2BP (reactive dye) (41).

(f) Food and Healthcare

The antimicrobial effect of silver additives is broadly used in various injection-molded plastic products used for food packaging, and in coating-based applications, including air ducts, counter tops, and food preparation areas. Some important advantages of silver-based antimicrobials are their excellent thermal stability and their health and environmental safety characteristics. The emergence of gentle (non-thermal) process conditions for the preservation and shelf life extension of foods makes packaging and packages an integral part of retaining food safety criteria. Antimicrobial packaging is a form of active packaging now days. Silver additives based on silver salts or metallic silver such as silver coated on silica may be readily incorporated into thermoplastic polymers, such as polyethylene, polypropylene, polystyrene, or nylon. The bactericidal efficacy of silver-containing polymers is based on the release of silver ions (Ag^+) through interaction with a liquid watery phase.

- The silver-silica nanocomposite-containing polystyrene demonstrated that materials functionalized with the silver nanocomposite have excellent antimicrobial properties. It has shown significant antibacterial activity against both *E. coli* and *S. aureus* (37).
- Ag-SiO_2 nanocomposite thin film showed a strong bactericidal activity against *E. coli* and *S. aureus* bacteria with the relative rate of reduction of the viable bacteria of 1.05 and

0.73 h⁻¹, respectively. In fact, whole of the *E. coli* and *S. aureus* bacteria (about 10⁵cfu/ml) were killed after 5 and 7 h contact with the antibacterial film. These films could be use to coat food packaging material (36).

(g) Water Treatment

Water related infections belong to the one of the main health problems. The most dangerous water pathogenic pollutants, *Escherichia coli* and *Staphylococcus aureus*, are resistant to biodegradation. Silver nanoparticles (NPs) or silver ions have long been known to have strong inhibitory and bactericidal effects in solutions and composites with silica films and particles (SiO₂@Ag) with developed surface area. In case of SiO₂@Ag application, the specific surface area of silica is of great importance for effective adsorption of the species desirable.

- Composite systems containing strongly bound and homogeneously distributed Ag NPs on silica surface serve as potential wide-spectrum effective antimicrobial materials for water cleaning (39).

(h) EMI Shielding

Electromagnetic interference (EMI) is the electromagnetic wave radiation emitted by an electrical device as a by-product of its normal operation. The emitted EM waves might cause serious damage to the human body. Metals are most common materials for EMI shielding. They function mainly by reflection due to the free electrons in them. Ag/silica composite microspheres exhibit superior electromagnetic shielding effectiveness relative to that of the pure silica microspheres. This is because of the electromagnetic wave shielding properties of silver through free electrons.

- The Ag-coated silica microspheres were shown to exhibit electromagnetic shielding effectiveness of 32.5 dB at 761 MHz (27).

(i) Inhibition of Photo Oxidation in Conducting Polymers

The incorporation of nanoshells into the semiconductor films has shown the reduction in photo oxidation of semiconductor polymer film on exposure to oxygen, with no reduction in the photoluminescence. Semiconductor polymer-based devices such as light emitting diodes, photodiodes, flat panel displays, solar cells, lasers, and transistors are not getting much commercial attention because of the rapid rate of photo-oxidation of the semiconducting polymer material itself and hence lowering of their performance and life time. Light emission in semiconducting polymers occurs by radiative recombination of the singlet exciton. In the case in which intersystem crossing occurs and a triplet exciton is formed, it can de-excite non-radiatively through energy transfer and formation of singlet oxygen. This highly reactive species chemically modifies the polymer chains, producing trap states that quench the light-emission pathways in the polymer. This problem could be overcome by incorporation of triplet-exciton resonant nanoshells into the conducting polymer. It has been observed that the rate of photo-oxidation can be slowed tenfold in P3OT and by fivefold in MEH-PPV by the incorporation of nanoshells into the material (46).

1.6: Aim and Scope of the Present Work:

From the literature survey, it's clear that silver-silica nanocomposites possess a variety of industrial applications in almost every area. So, scientific attention is towards developing a new, easy synthetic method for their synthesis. In the present project, attempts have been made to synthesize silver nanoparticles coated silica spheres using a simple, easy and cost effective approach of electroless reduction. Firstly, silver seed is formed on silica spheres by reduction of silver ions on Sn²⁺ decorated silica surface, which then were used to grow uniform layer of silver in further growth step. The silver nanoparticles coated silica spheres were characterized by Fourier transform infrared spectroscopy (FT-IR), X-ray diffraction (XRD), field emission scanning electron microscopy (FE-SEM), energy dispersive X-ray analysis (EDXA) and diffuse reflectance spectroscopy (DRS). The effect of silica sphere activation method and the deposition time on the coating of silver nanoparticles on silica spheres was also studied. The silver nanoparticles coated silica spheres were studied further for their antimicrobial activity against both *E. coli* and *B. subtilis*, a gram negative and a gram positive bacterium, respectively.

2.1: Materials Used

The materials and the chemicals that were used for the synthesis of silver nanoparticles coated silica spheres are given in Table 2. All the chemicals were used as received, without further purification. All glassware used for the solution synthesis were first rinsed with chromic acid solution, then thoroughly with Millipore deionized water, and dried in oven before use.

Table - 2: Chemicals used for the synthesis of silver coated silica spheres

S. No.	Chemicals	Grade	Assay	Company
1	Tetraethylorthosilicate	A.R	98%	Sigma Aldrich
2	Ammonia solution (25%)	L.R	25%	RFCL Limited
3	Ethanol	A.R	99.99%	Jigansu Hauxi International Trade Co. Ltd.
4	NaOH	A.R	98%	RFCL Limited
5	SnCl ₂	A.R	99%	HIMEDIA [®]
6	Sn powder	A.R	99%	HIMEDIA [®]
7	HCl	L.R	35-38%	THOMAS BAKER Chem. Pvt. Ltd.
8	Silver nitrate	A.R	99.9%	SISCO Research Laboratories Pvt. Ltd.
9	Formaldehyde	L.R	37-41%	S D fine Chem. Limited
10	D.I	-	-	Millipore

2.2: Sample Preparation:

2.2.1: Sample A- Silica spheres

Silica spheres of size 300-400 nm were synthesized using well known Stober's method (8). By varying the ratio of TEOS and ammonia solution, the particle size could be varied. To obtain monodispersed silica nanoparticles of size 400-500 nm, about 88 ml of ethanol was added to a RB flask followed by addition of 11.9 ml of ammonia solution (23%) under vigorous stirring. Then, 3.6 ml of TEOS was added during and then the stirring continued at a medium speed for 15 h. The solution containing silica nanoparticles was centrifuged at 3000 rpm for 30 min followed by redispersion of the precipitate in ethanol/water (50:50) mixture to remove unreacted components. The samples were dried overnight in an oven.

2.2.2: Sample B- Ag nanoparticles coated silica spheres

Ag nanoparticles coated silica spheres were synthesized by using a simple electroless reduction method (17). About 500 mg of silica spheres were activated by different approaches as described in Table 3. The spheres were then added to a mixed solution (50 ml) containing SnCl_2 (0.053 mol l^{-1}), HCl (0.01 mol l^{-1}), and Sn powder (20 mg). After rinsing for 4– 6 times with deionized water and drying in oven, the colloids were transferred into a 50 ml silver solution containing 0.27 mol l^{-1} ammonical silver nitrate. After some time (2h to 4h), the above solution was rinsed again with deionized water and added into a mixture of 6 ml ethanolic solution of formaldehyde (0.025 mol l^{-1}), 6 ml aqueous ammonical silver nitrate (0.05 mol l^{-1}) and 30 ml ethanol. The contents were added to an air tight RB flask, and oxygen was removed from the solution by bubbling N_2 gas for 20 min. The solution was stirred for 24h under N_2 environment. Different batches of the samples were prepared with variation in the activation method of silica spheres and the deposition time, as described in Table 3.

Table-3: Various conditions for the optimization of silver coating on silica nanospheres

S. No.	Sample	Activation Method	Deposition Time (h)
1.	B-1	No Activation	3
2.	B-2	2% NaOH	2
3.	B-3	2% NaOH	3
4.	B-4	2% NaOH	4
5.	B-5	Calcination at 450 °C	3
6.	B-6	Calcination at 750 °C	3

2.2.3: Antimicrobial activity of silver nanoparticle coated silica spheres

The antimicrobial activity of the nanocomposites was studied against the *Escherichia coli* and *Bacillus subtilis*, a gram negative and a gram positive bacterium, respectively. The minimal inhibitory concentration (MIC) of the nanocomposite was determined by preparing twofold serial dilutions of the additives in an appropriate growth medium (Luria-Bertani Media). The wells were then inoculated with $\sim 10^7$ CFU/ml from overnight cultures of the bacteria and incubated on a shaker (180 rpm) for 18 h. Optical density values were recorded before incubation and after incubation with samples along with silica spheres as a control.

2.3: Characterization of Samples:

Silica spheres and silver coated silica spheres were characterized by various techniques in order to determine the distribution, size, morphology, chemical composition and optical properties of silver nanoparticles present on the silica surface. Various techniques used are described below briefly:-

2.3.1: Field Emission - Scanning Electron Microscopy

FE-SEM analyses were made to observe the morphology and particle size of the silica and silver nanoparticles. The instrument used was QUANTA 200 FEG marketed by FEI Netherlands. In this instrument, a high voltage (20kV) electron beam produced by field emission gun (FEG) interacts with the sample resulting in the emission of secondary electrons, which are detected by a secondary electron detector. The number of electrons that reach the detector at each point on the sample depends on the topology of the sample and the atomic weight of the atoms at the surface, and these variations in signal strength leads to image formation (47, 48). For SEM imaging, the samples were prepared by drying a drop of sample on glass substrate followed by coating with a thin layer of gold.

2.3.2: Energy Dispersive X-Ray Analysis (EDXA)

EDXA is an integrated part of FE-SEM used to get qualitative as well as quantitative information about the chemical nature of structures on surface of the specimen. For EDXA analysis of specimen, a high energy beam of electron is used to get X-rays emitted from the element. An EDXA spectrum plot not only identifies the elements corresponding to each of its peak, but also the type of X-rays to which it corresponds.

2.3.3: Powder X-ray Diffraction (PXRD)

XRD is a widely used technique for the determination of crystallinity, crystal structure and lattice constants of the nanoparticles. Powder XRD data was recorded at room temperature on a Bruker AXS D-8 Advanced powder X-ray diffractometer. The X-ray radiation source (Cu K α , $\lambda = 0.154$ nm) was operated at 40 kV applied voltage and 30 mA current. The scan speed was 1°/min and the 2 θ ranged from 5° to 75°. The mean crystallite size was calculated using Debye-Scherrer formula (8).

$$D = k \lambda / \beta \cos\theta$$

Where,

k = constant (shape factor, = 0.9 assuming that the particles are spherical)

λ = X-ray wavelength (0.154 nm)

β = Full width at half maximum (FWHM in radians)

θ = Bragg's angle

D = Mean crystallite size (nm)

2.3.4: Infrared Spectroscopy (FT-IR)

FT-IR spectroscopy was used to characterize the silica nanoparticles. The IR spectra were recorded using a Nicolet Nexus FT-IR spectrometer in the range of 400-4000 cm^{-1} . The samples were prepared by adding a pinch of sample to KBr (1:100), followed by formation of a pellet using a hydraulic press.

2.3.5: Diffuse Reflectance Spectroscopy (DRS)

Diffuse reflectance spectroscopy is used mainly for powder solid samples. Since light can't penetrate opaque (solid) samples, it is reflected on the surface of the samples. If incident light is reflected symmetrically with respect to the normal line, then is called "specular reflection," while incident light scattered in different directions is called "diffuse reflection." An integrated microsphere is used that allows the measurement of only diffuse light and not the specular light when angle of incidence is 0° . The spectra were recorded using UV-2450 UV-vis spectrophotometer marketed by SHIMADZU. Samples were prepared by diluting the sample with BaSO_4 (30mg: 4g) and forming a pellet. The spectra were recorded in wavelength range from 200-800 nm. The reflectance spectra were converted into absorption spectra using Kubelka-Munk function.

3.1: FT-IR Analysis

FT-IR gives information about the chemical groups present that are characteristic of a particular compound. In order to confirm the synthesis of silica nanoparticles, FT-IR measurements were carried out by the KBr pellet method. Figure 3.1 shows the FT-IR spectrum of pure silica nanoparticles and the assignments of the bands are given in Table 4.

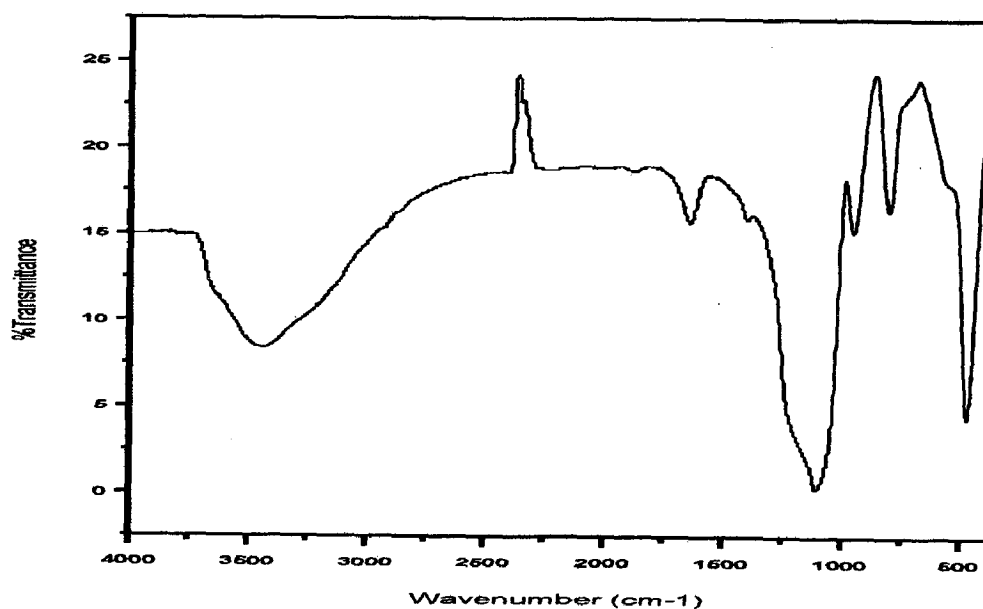


Figure –3.1 FT-IR spectra of silica nanoparticles synthesized by Stöber's method (7).

The broad feature between 3352 and 3477 cm^{-1} corresponds to the stretching of O-H groups present on the silica sphere surface (48). The bands observed at about 1102 cm^{-1} , 800 cm^{-1} and 475 cm^{-1} , correspond to the asymmetric stretching, the symmetric stretching and the flexural vibration modes of the Si–O–Si bridge of the siloxane link, respectively (49,50). The band at 957 cm^{-1} is attributed to the stretching vibration of Si–OH bonds (51).

Table 4: Assignments of the bands in the infrared spectrum of pure silica Nanoparticles synthesized by Stöber's method (7).

S. No.	Band position (cm ⁻¹)	Assignment of peaks	Reference
1	3352–3477	O–H stretch	(48)
2	1643	O-H stretch	(48)
3	1102	Asymmetric stretching vibration of Si-O-Si	(49, 50)
4	957	Stretching vibration of Si–OH bonds	(51)
5	800	Symmetric stretching vibration of Si-O-Si	(49, 50)
6	471	Flexural vibration modes of the Si–O–Si	(49, 50)

3.2: Powder XRD Analysis:

The structures of as prepared silica spheres and silver nanoparticles coated silica spheres were investigated by powder X-ray diffraction (XRD) analysis.

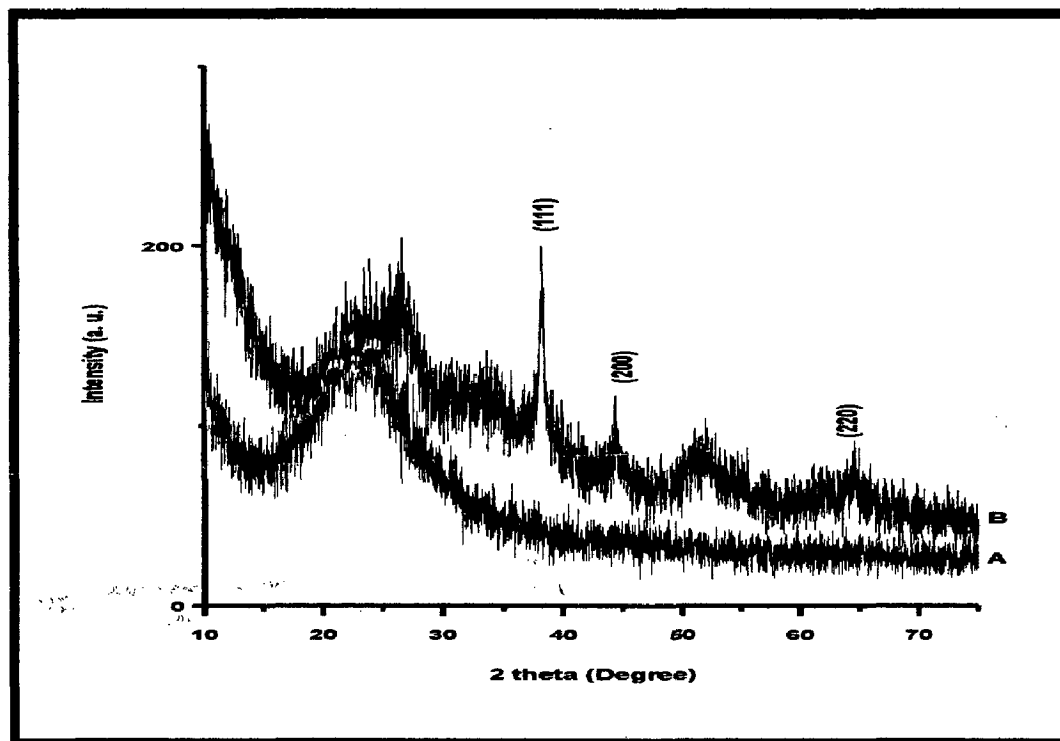


Figure –3.2 Powder XRD patterns of (a) silica spheres and (b) silver nanoparticles coated silica spheres (sample B-1)

The amorphous nature of silica spheres was confirmed by the XRD analysis. The silica spheres are non crystalline in nature, but produce a single broad diffraction peak in powder diffraction as shown by spectra A (Red) in Figure 3.2. In the XRD pattern of sample B (black) in Figure 3.2, three distinct diffraction peaks are observed at 2θ values of 38.1° , 44.3° , and 64.4° , corresponding to the (111), (200) and (220) crystalline planes, respectively of the cubic Ag (JCPDS No. 4-0783). The mean crystallite size was calculated by Debye-Scherrer equation using the FWHM of the (111) reflections. The calculated crystallite size for different silver nanoparticles coated on silica spheres with the variation in the activation method and the deposition methods are summarized in Table 5.

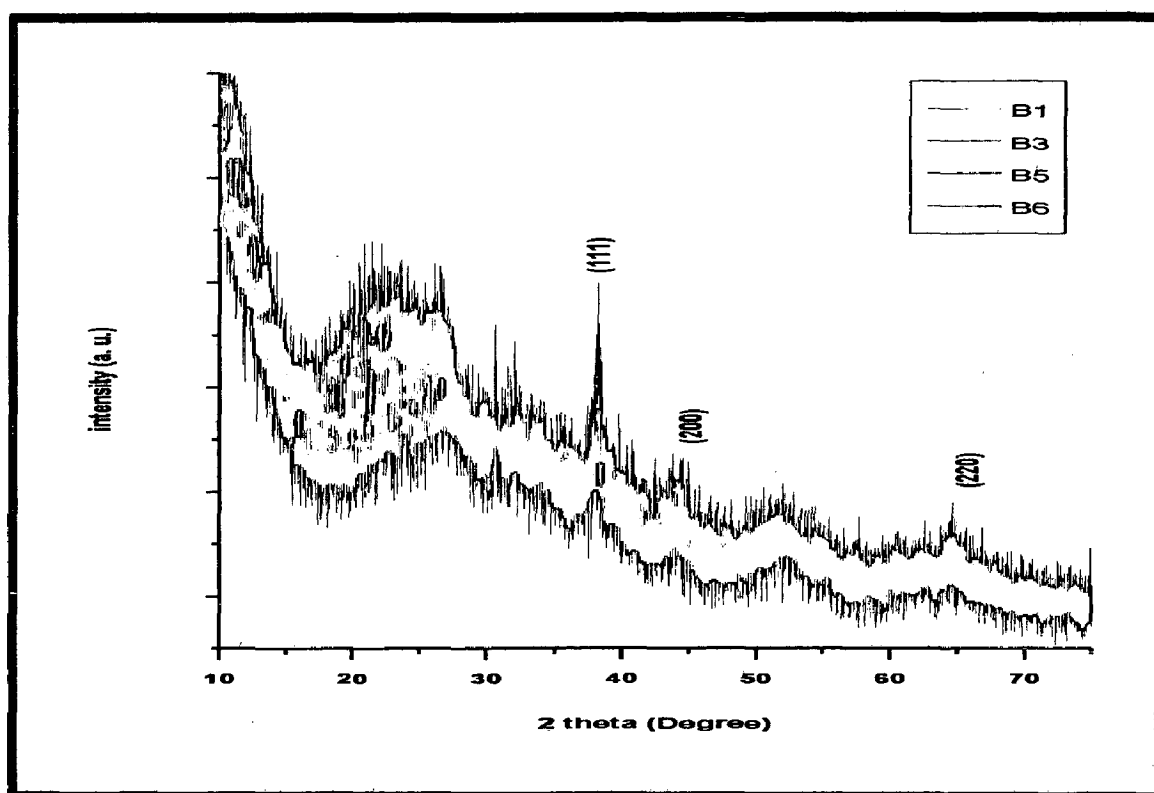


Figure 3.3: Powder XRD patterns for silver nanoparticles coated silica spheres fabricated with variation in activation method of silica spheres (B-1, B-3, B-5, and B-6)

Table 5: Crystallite size calculation for the silver nanoparticles coated on silica spheres activated by different methods

S. No.	Sample	Activation Method	Incubation Time (h)	FWHM (β)		Crystallite size (nm)
				(Degree)	(Radians)	
1.	B-1	No Activation	3	0.2487	4.336×10^{-3}	34.2
2.	B-2	2% NaOH	2	0.51	8.90×10^{-3}	16.6
3.	B-3		3	0.369	6.445×10^{-3}	23.0
4.	B-4		4	0.337	5.8817×10^{-3}	25.2
5.	B-5	Calcination at 450 °C	3	0.2576	4.4959×10^{-3}	33.0
6.	B-6	Calcination at 750 °C	3	0.3374	5.88×10^{-3}	25.1

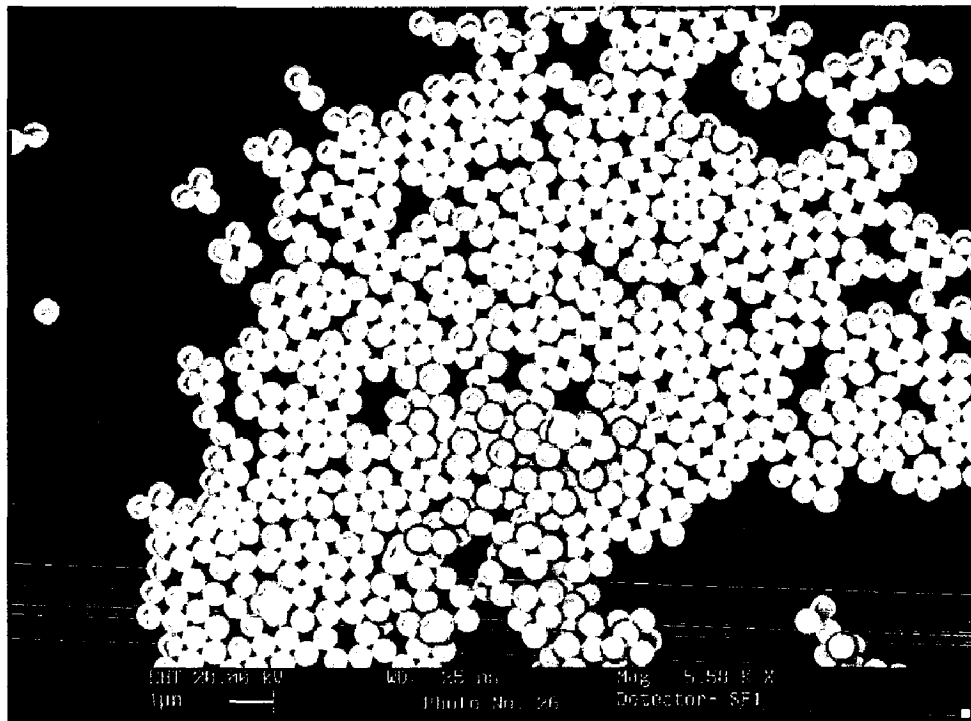
It can be concluded that the size of silver nanoparticles formed on silica spheres varies with variation in activation method and the deposition time and is in the range of 16.0 – 35 nm.

3.3: FE-SEM Images and EDXA Analysis:

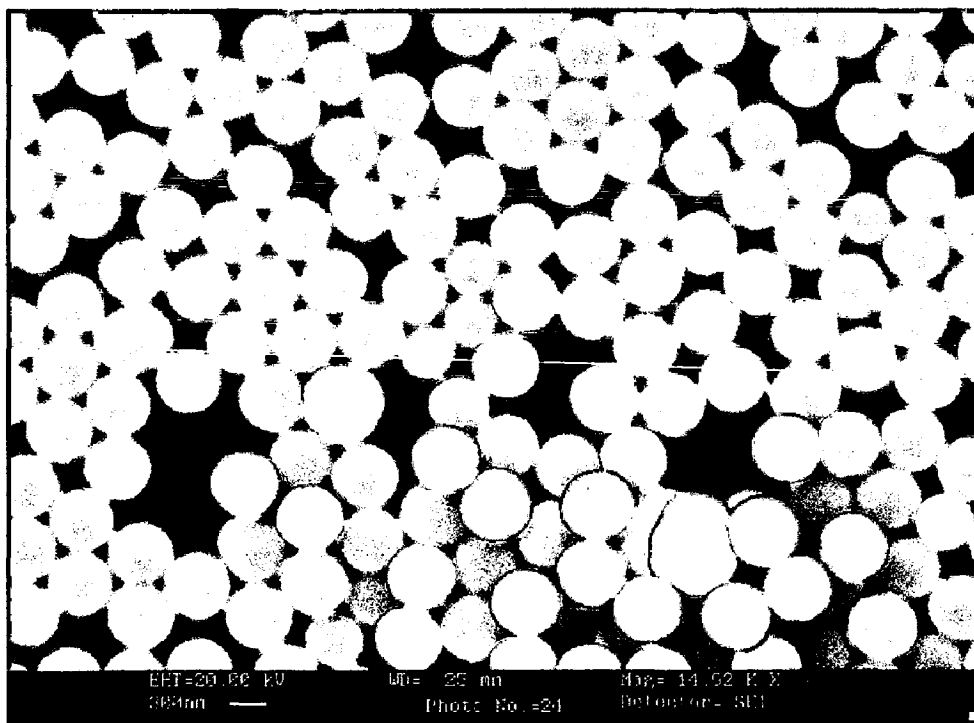
FE-SEM images and EDXA data were obtained for all the samples and they are shown in the Figures 3.2 to 3.4. FE-SEM images of the silica spheres were recorded before calcinations and after calcination at different temperatures as shown in Figures 3.2 and 3.3. For the as prepared samples, it can be seen that the silica spheres are monodispersed and spherical in morphology and looks agglomerated after calcination at 750°C temperature. The morphology remains unchanged after deposition of silver nanoparticles on silica spheres. EDXA analysis indicates the presence of silver on silica spheres. The weight % of silver for different samples varies accordingly with variation in the activation method and the time of deposition

3.3.1: As prepared sample A:-

FE-SEM images:



(a)



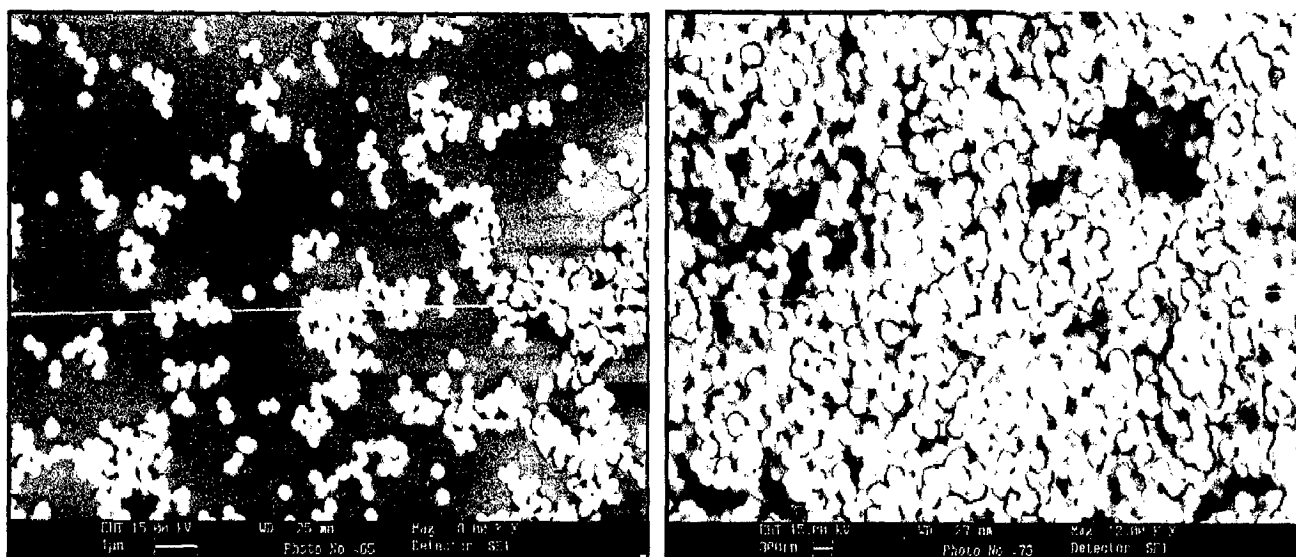
(b)

Figure-3.2: FE-SEM images of silica nanoparticles in different magnifications at (a) lower magnification and (b) higher magnification.

Monodispersed silica spheres that were obtained by Stöber's method are shown in Figure 3.2. The size of spheres is in range of 400-450 nm. A very good assembly is observed because of the monodispersity in size.

3.3.2: Sample A after Calcination:

FE-SEM images:



(a)

(b)

Figure 3.3: FE-SEM images of silica nanoparticles after calcination at (a) 450 °C and (b) 750 °C

It is clear from Figure 3.3 (a) that calcination at 450 °C doesn't cause any change in the morphology of silica spheres but when calcined at 750 °C, agglomeration increases as observed in Figure 3.3(b). This could be explained by the fact that calcination at higher temperature leads to the removal of most of the -OH groups present on the surface of silica.

3.3.3: As prepared sample B:

Silica spheres were coated by silver nanoparticles using electroless deposition method (17). The weight percent of silver on silica spheres was controlled by variation in the activation method of the silica spheres and the deposition time of silver nanoparticles on silica spheres. FE-SEM and EDXA data of all the samples mentioned in tables are presented below. A summary of silver wt % on the surface of silica sphere is given in Table 6.

3.3.3.1: Sample B-1

FE-SEM image:

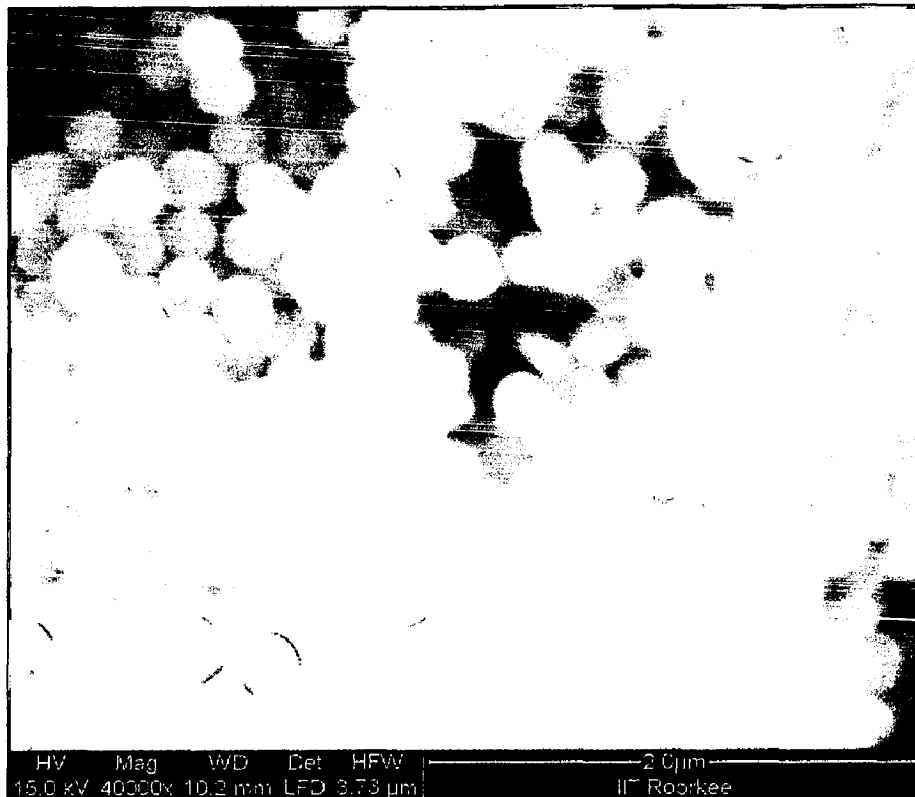
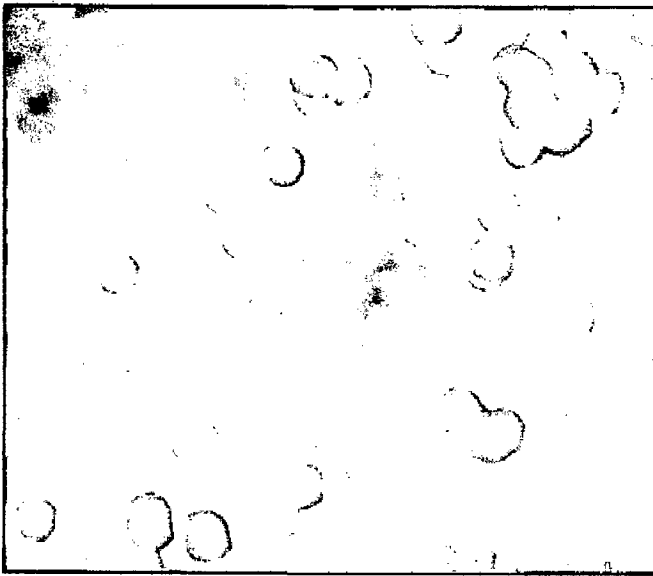


Figure3.4 (a) FE-SEM image for sample B-1

EDXA data:



<i>Element</i>	<i>Wt%</i>	<i>At%</i>
<i>OK</i>	40.93	60.60
<i>SiK</i>	42.37	35.73
<i>AgL</i>	16.70	03.67
<i>Matrix</i>	Correction	ZAF

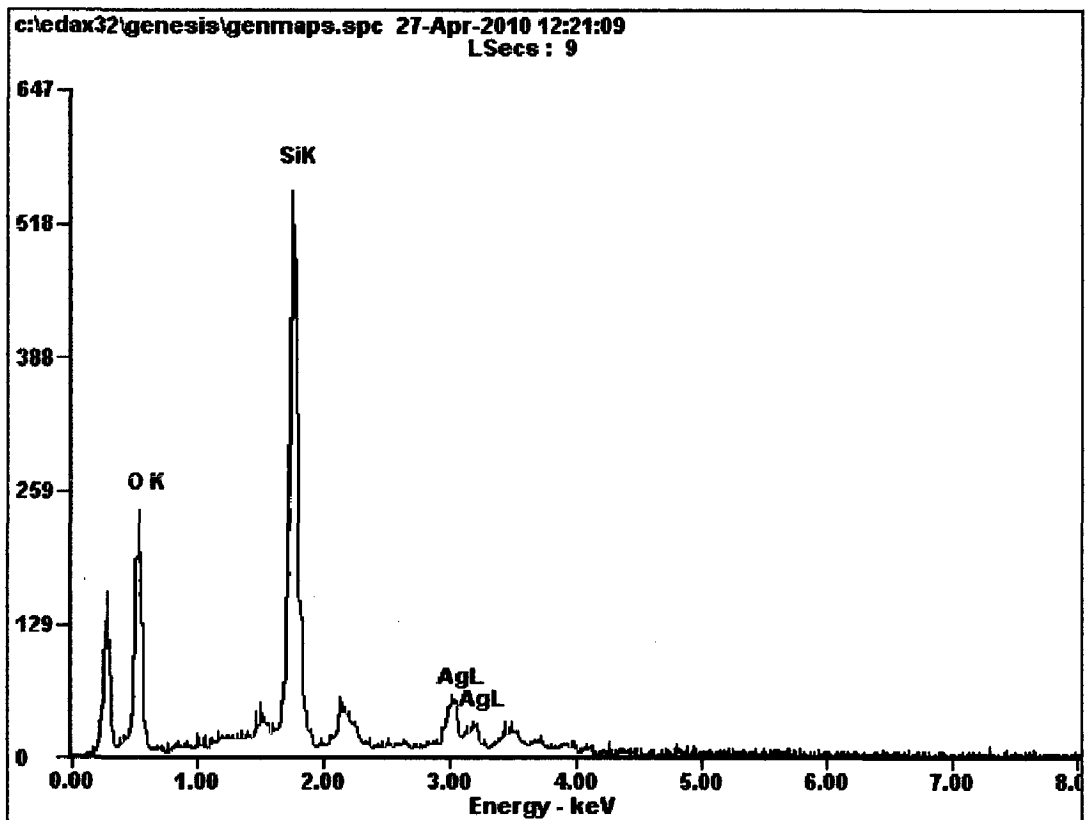


Figure 3.4 (b): EDXA plot for sample B-1

3.3.3.2: Sample B-3

FE-SEM image:

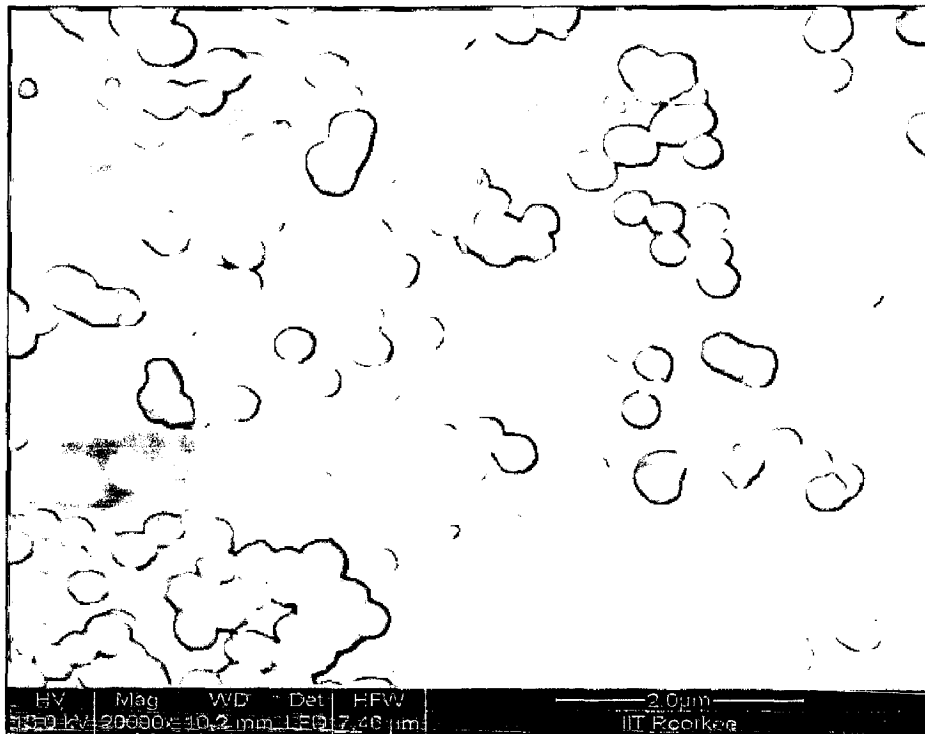
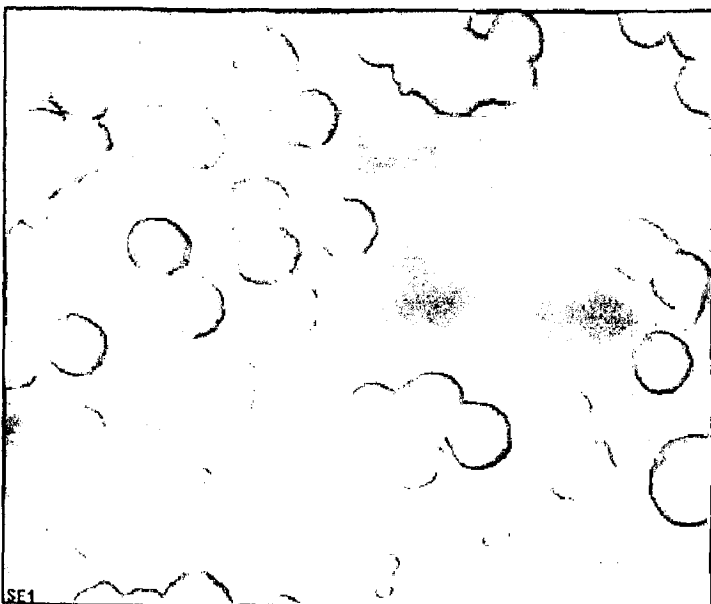


Figure 3.4 (c) FE-SEM image for sample B-3

EDXA data:



<i>Element</i>	<i>Wt%</i>	<i>At%</i>
<i>OK</i>	54.70	74.08
<i>SiK</i>	29.47	22.74
<i>AgL</i>	15.83	03.18
<i>Matrix</i>	Correction	ZAF

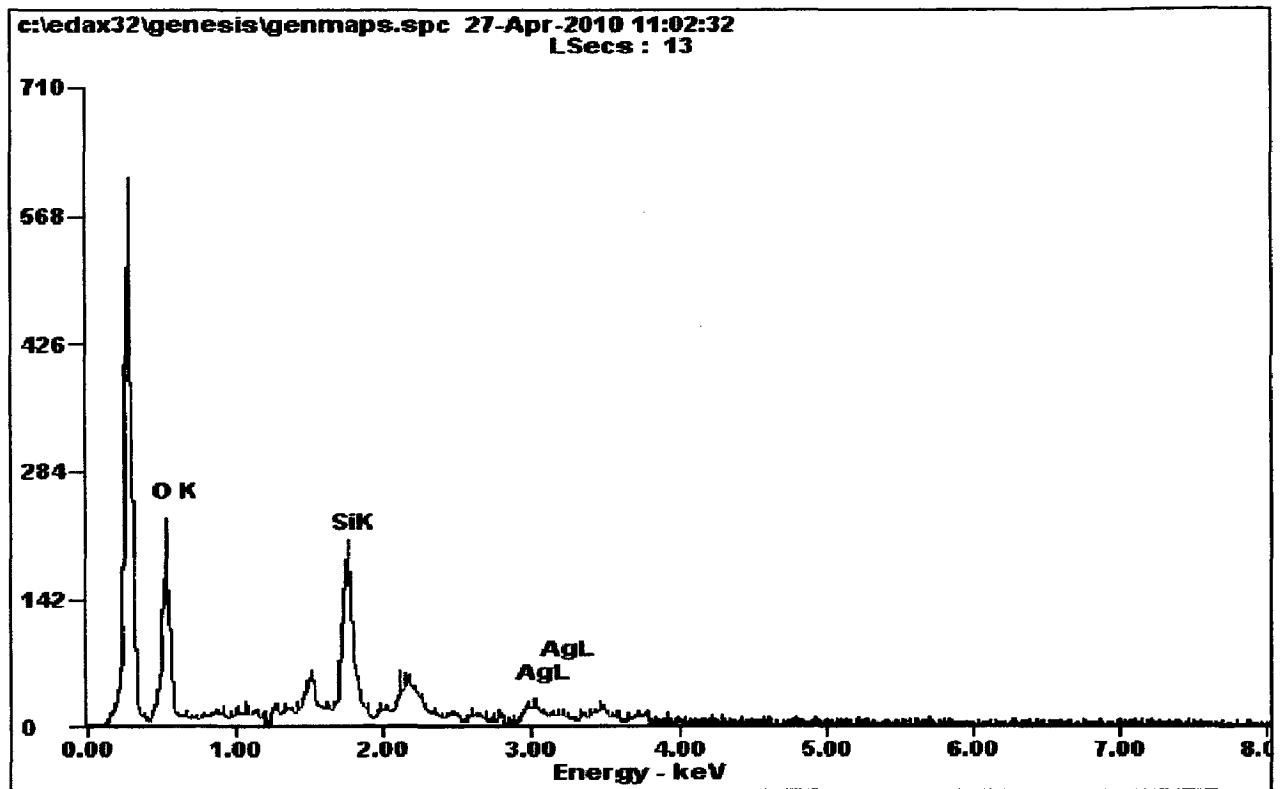


Figure 3.4 (d): EDXA plot for sample B-3

3.3.3.3: Sample B-5:

FE-SEM image:

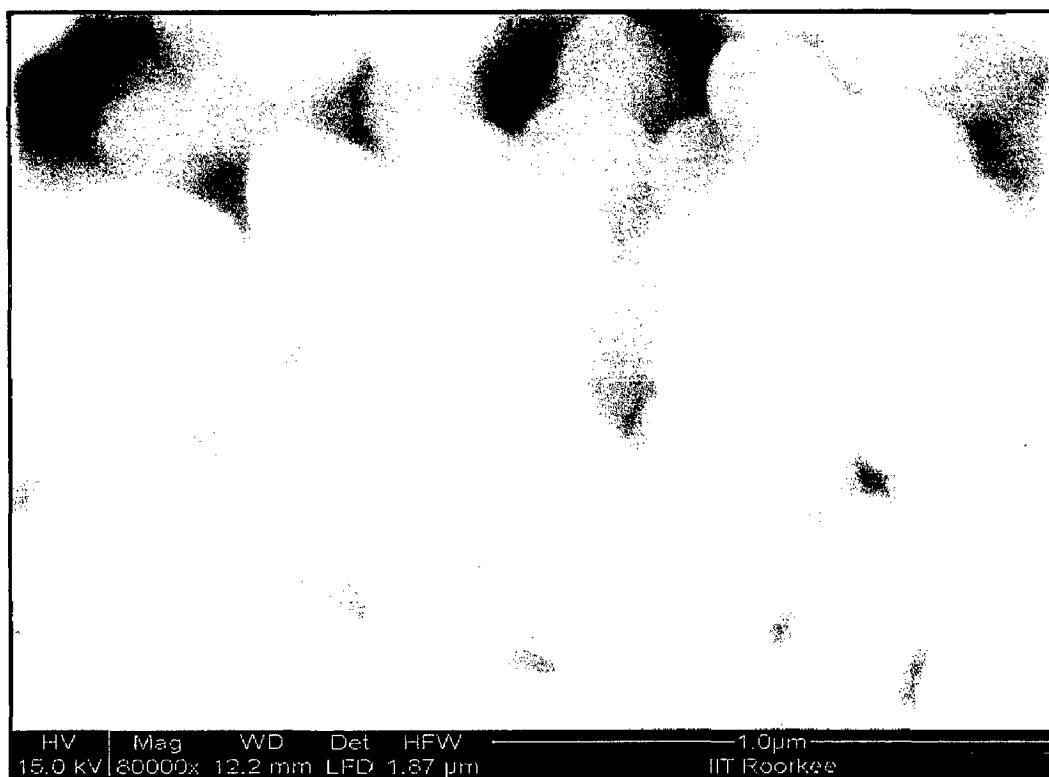
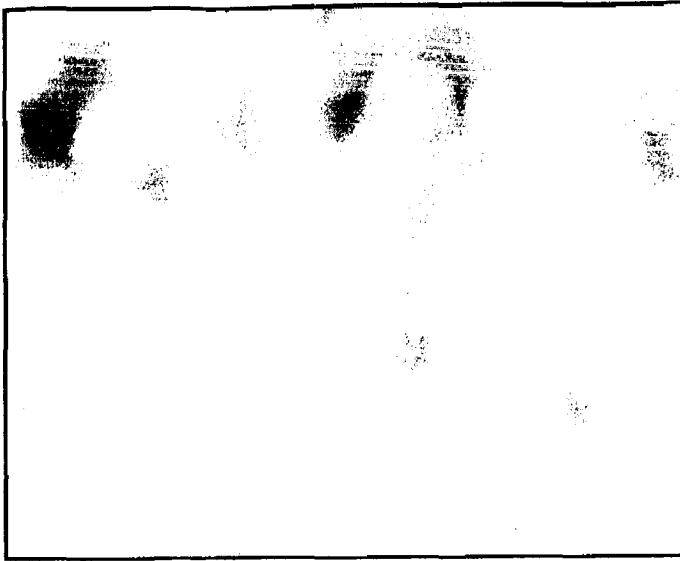


Figure 3.4 (e): FE-SEM image for sample B-5



<i>Element</i>	<i>WT%</i>	<i>At%</i>
<i>CK</i>	11.89	20.91
<i>OK</i>	35.05	46.29
<i>SiK</i>	40.25	30.29
<i>AgL</i>	12.81	02.51
<i>Matrix</i>	Correction	ZAF

EDXA data:

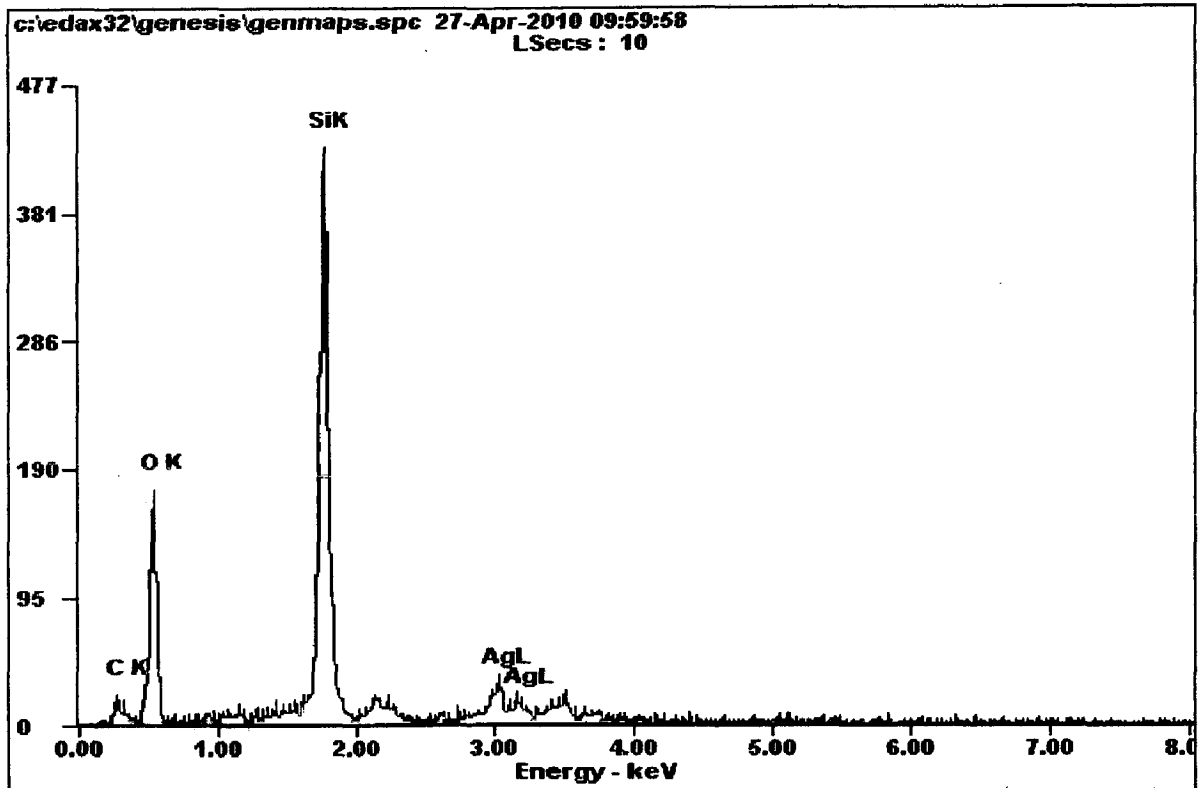


Figure 3.4 (f): EDXA plot for sample B-5

3.3.3.4: Sample B-6:

FE-SEM image:

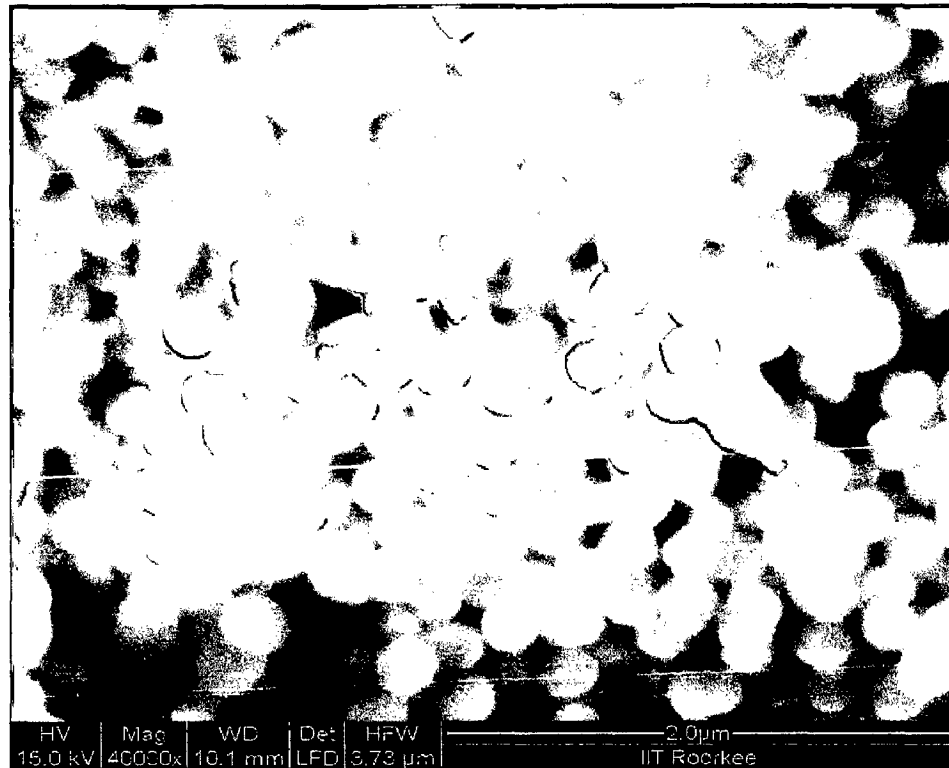


Figure 3.4 (g): FE-SEM image for sample B-6



<i>Element</i>	<i>Wt%</i>	<i>At%</i>
<i>OK</i>	38.85	54.41
<i>SiK</i>	55.74	44.47
<i>AgL</i>	05.41	01.12
<i>Matrix</i>	Correction	ZAF

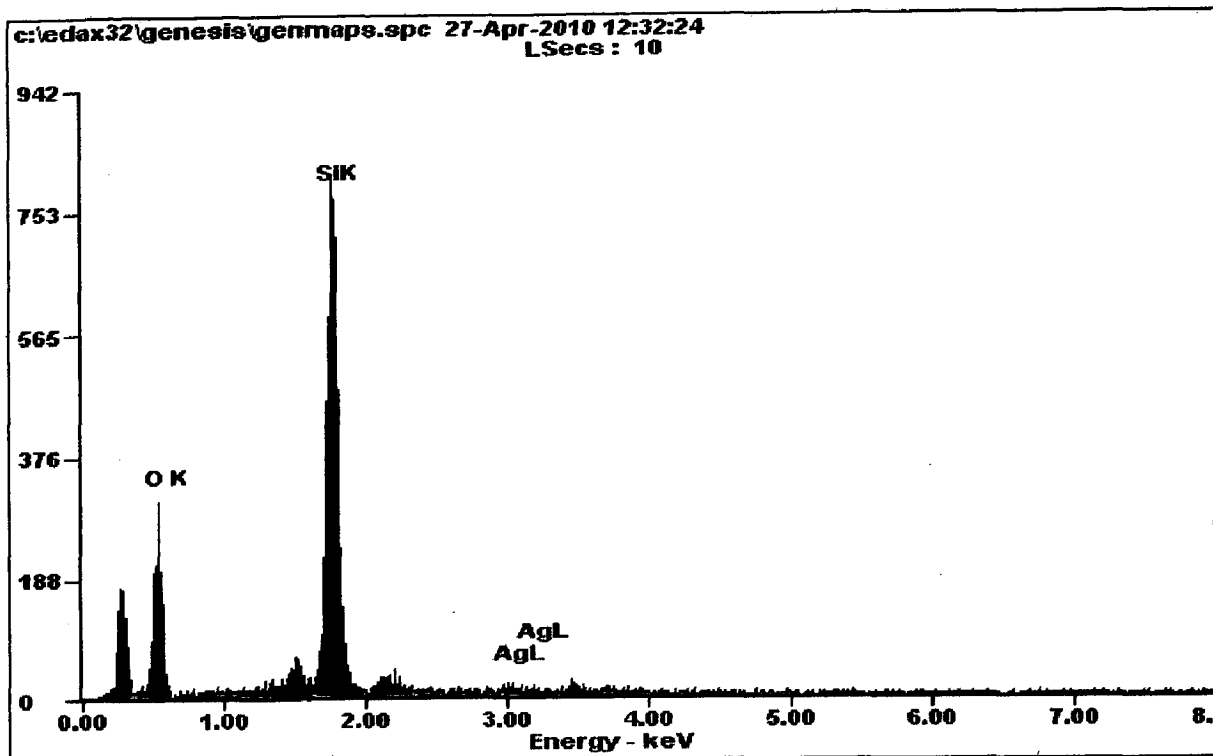


Figure 3.4 (h): EDXA plot for sample B-6

3.3.1 (A): Analysis of sample B

EDXA data has shown that the variation in activation method leads to the variation in weight percent of silver nanoparticles on silica spheres. The EDXA data could be summarized as below in Table 6:

Table -6: Variation of silver weight percent with variation in the activation method and the deposition time

S. No.	Sample Notation	Activation Method	Incubation Time (h)	Amount of Silver present (wt %)
1.	B-1	No Activation	3	14-17
2.	B-2	2% NaOH	2	8-13
3.	B-3		3	12-16
4.	B-4		4	18-20
5.	B-5	Calcination at 450 °C	3	10-13
6.	B-6	Calcination at 750 °C	3	4-6

It is clear from Table 6 that activation of silica spheres affects directly the amount of silver deposited on silica spheres. This is because the activation method affects the no. of activated OH groups present on the surface of silica spheres. In the earlier reported method of activation the use of 2% NaOH, dissolves the uppermost layer of silica spheres for activation and also it causes loss of most of the spheres because of its etching effect. This reduces the yield of the end product. But, in the present study, it was possible to have deposition of silver even without NaOH activation as shown in SEM images (Figures 3.4 (a) and 3.4 (b)). The calcination at high temperature ($\sim 750^{\circ}\text{C}$) reduces the number of $-\text{OH}$ group on surface, and hence the silver deposition as shown in Figure 3.4(h). Also, the influence of deposition time on silver weight percent was deduced. With increase in deposition time, the silver weight percent as well as the size of silver nanoparticle increases. This could be explained by the fact that with increase in deposition time, the size of seed particles on silica spheres increase which is further used to grow uniform layer of silver nanoparticles around silica spheres.

3.4: Diffuse Reflectance Spectroscopy

Diffuse reflectance spectra were recorded for all the samples to characterize their optical properties. The optical properties were investigated as a function of the activation method and the time of deposition. The reflectance spectra were converted into absorbance spectra via Kubelka-Munk function.

3.4.1: Influence of activation method

Activation method affects the no. of $-\text{OH}$ groups and hence the presence of silver on silica spheres. Silica nanoparticles doesn't show surface plasmon resonance phenomenon, and they don't absorb in the UV-Visible range. Silver nanoparticles coated silica spheres show surface plasmon at about 300 nm, the characteristic band of silver nanoparticles which is a function of size, dielectric constant, shape and aggregation level.

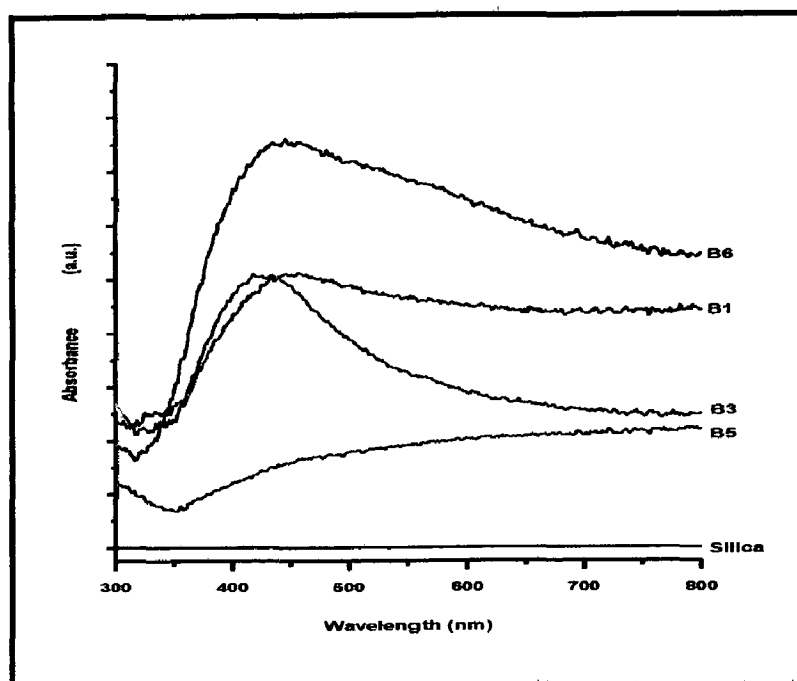


Figure 3.4 (a): Absorption spectra of silver nanoparticles coated silica spheres synthesized by variation in activation method

The analysis of Figure 3.4(a) reveals that silica spheres show no absorption (black line). This is because the dielectric function of the silica has no imaginary part and is almost constant in the present wavelength range (300–800 nm). However, the absorption spectrum of the silver coated silica spheres corresponds to LSPR band of silver nanoparticles. The extinction band is broadened greatly and almost covers the wavelength range from 320 to 800 nm. The dipole–dipole interactions between the neighboring silver particles and the Mie scattering of the silver shell as a whole may serve as the main reason of the large band broadening and shift effect. The ratio of silica core radius to silver shell thickness affects the band position greatly. This ratio directly depends on the activation methods. Several other factors, such as nanoparticle size, shape, and aggregation state, may cause these features of band width, position etc. Also, as shown by EDXA analysis, the weight % of Ag on silica is low (e.g. sample B-6), and hence for low Ag, the Ag surface plasmon band may be screened by the strong scattering from the silica spheres.

3.4.2: Effect of deposition time:-

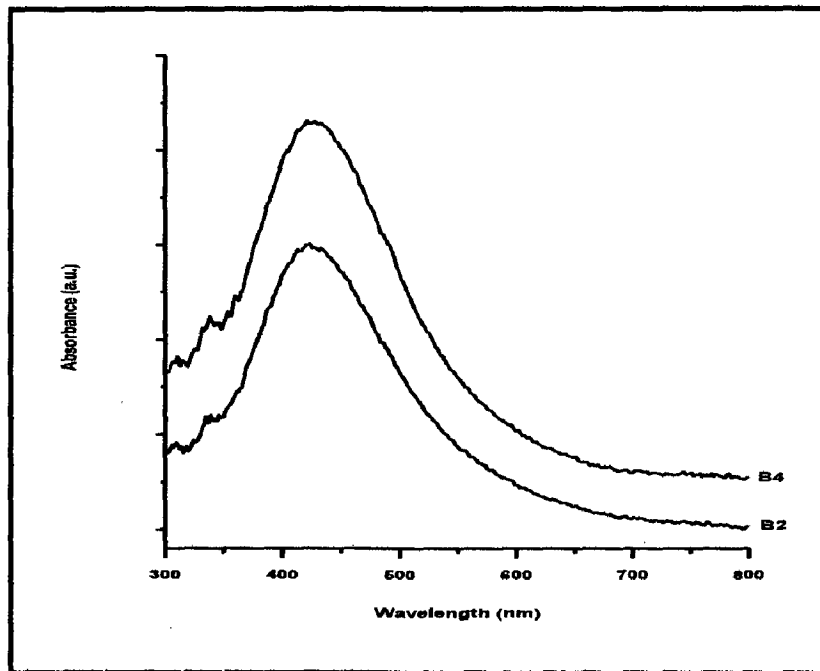


Figure 3.4 (b) Effect of deposition time of silver nanoparticles on silica spheres

It is clear from Figure 3.5 (b) that with increase in deposition time, the intensity of Ag LSPR band increases because of increase in weight % of silver on silica. Also, the band appears sharper comparatively; this could be explained by the fact that with increase in weight % of Ag nanoparticles on silica surface, the scattering effect of silica spheres could be shielded out.

3.6: Antibacterial Study:

The antibacterial activity of silver nanoparticles coated silica spheres was studied against gram positive bacteria, *Bacillus subtilis*, and gram negative bacteria, *Escherichia coli DH5a*. The initial culture containing $\sim 10^8$ bacterial cell/ml was incubated with different dilutions of the silver nanoparticles coated silica spheres. The silica spheres were used as control. The results observed for different samples are given below in Table-7.

Table 7: Minimal inhibitory concentration (MIC) of silver nanoparticles coated silica sphere samples against *E.coliDH5a* and *Bacillus subtilis*.

S.No.	Sample	Minimal Inhibitory Concentration ($\mu\text{g/ml}$)	
		<i>E. coli DH5a</i>	<i>Bacillus subtilis</i>
1	B-1	62.5	62.5
2	B-2	15.625	7.8
3	B-3	31.25	62.25
4	B-4	7.8	15.625
5	B-5	15.625	31.25
6	B-6	250	250

It can be revealed from Table 7 that silver nanoparticles coated silica spheres kills both gram positive and gram negative bacterium but silica spheres themselves do not kill the bacteria, which was confirmed by using them as a control. Also, with the variation of weight percent of silver present on the silica sphere surface, the amount of silver nanoparticles coated silica composites (minimal inhibitory concentration) for complete inhibition of bacterial growth varies. As evidenced from the Table 7 that MIC for sample B-6 is high because of small weight percent of silver nanoparticles present on silica spheres and that of sample B-4 is the lowest, having highest wt % of silver. The mechanism of inhibition of growth by silver nanoparticles is not very clear but it is proposed that the silver ions that they interact with disulfide or sulfhydryl groups of enzymes, causing structural changes that lead to disruption of metabolic processes followed by cell death. The inhibitory action of silver nanoparticles is also based on the release of Ag. In addition to the increased surface area and associated increased potential for the release of Ag, when dispersed in liquid suspensions, silver nanoparticles may accumulate in the bacterial cytoplasmic membrane, causing a significant increase in permeability and cell death. Recently, it has been suggested that the antimicrobial mechanism of silver nanoparticles may also be related to membrane damage due to free radicals that are derived from the surface of the nanoparticles. This bactericidal activity also appears to be dependent on the size and shape of the silver nanoparticles (37).

Silver nanoparticles coated silica spheres were synthesized by using a simple, easy, and cost effective method based on principle of electroless reduction. The synthesized nanocomposites were studied for their antimicrobial activity against both gram positive and gram negative bacterium. Electroless reduction, in the absence of external reducing and capping agents, leads to the coating of silver nanoparticles on Sn^{2+} decorated silica spheres. The nanocomposites so fabricated were characterized by infrared spectroscopy (FT-IR), X-ray diffraction (XRD), field emission scanning electron microscopy (FE-SEM), energy dispersive X-ray analysis (EDXA) and diffuse reflectance spectroscopy (DRS). The effect of activation methods of silica spheres and deposition time were investigated. It was found that a good wt % of silver could be deposited on silica spheres even in the absence of activation of spheres by NaOH, which generally leads to activation as well etching of top layer of silica spheres. With increase in deposition time, the wt % of silver increase along with increase in size of silver nanoparticles on silica spheres. Antimicrobial studies revealed that the silver nanoparticles coated silica spheres posses bacteriostatic activity even when they are coated on SiO_2 spheres. This opens up new opportunities to disperse these nanocomposites in textiles and polymers for commercial application, with the reduction of amount of expensive silver to be needed for particular effect. Silica nanoparticles act as carrier as well as the substrate for silver nanoparticles, hence increasing the loading level and reducing the cost.

1. <http://en.wikipedia.org/wiki/Nanoshell>
2. <http://www.i-sis.org.uk/nanoshells.php>
3. <http://www.sciencedaily.com/releases/1998/09/980910074738.htm>
4. [http://composite.about.com/Chameleon Nanoshells - Composite Materials.mht](http://composite.about.com/Chameleon+Nanoshells+-+Composite+Materials.mht)
5. D.R. Lide (Ed.), CRC Handbook of Chemistry and Physics, 74th Ed., CRC Press, Boca Raton, FL, 1993, P. 15-25.
6. S. Kalele, S.W. Gosavi, J. Urban, and S.K. Kulkarni, *Current Science*, 91, 1038-52 (2006).
7. W. Stöber, A. Fink and E. Bohn, *J. Colloid Interface Sci.*, 26, 62–69 (1968).
8. B.D. Cullity and S.R. Stock, *Elements of X-Ray Diffraction*, 3rd Ed., Prentice-Hall Inc., New Jersey, 2001, P. 167-171.
9. S. L. Westcott, S. J. Oldenburg, T.R. Lee, and N. J. Halas, *Langmuir*, 14, 5396–5401(1998).
10. F.J. Arriagaka and K. Osseo-Asare, *J. Colloid Interface Sci.*, 211, 210 (1999).
11. F.H. Scholes, A. Bendavid, F.L. Glenn, M. Critchley, T.J. Davis and B.A. Sexton, *J. Raman Spectros.*, 39, 673–678 (2008).
12. N. Masuda, M. Kawashita and T. Kokubo, *J. Biomed. Mater. Res. B: Appl. Biomater.*, 83B, 114–120 (2007).
13. M. Kawashita, S. Toda, H-M. Kim, T. Kokubo and N. Masuda, *J. Biomed. Mater. Res. A*, 66, 266–274 (2003).
14. F.X. Liu, Y. Xiao and Y. S. Li, *J. Raman Spectros.*, 32, 73–77 (2001).
15. S. Thomás, S.K. Nair, E.M.A. Jamal, S.H. Al-Harthi, M.R. Varma and M.R. Anantharaman, *Nanotechnology*, 19, 075710-17(2008).
16. H.J. Zhai, D.W. Sun, H.S. Wang, *J. Nanosci. Nanotechnol.* 6, 1968-72 (2006).
17. Y. Kobayashi, V. Salgueiríao-Maceira and L.M. Liz-Marz'an, *Chem. Mater.*, 13, 1630-33 (2001).
18. F. Chen and R.L. Johnston, *Plasmonics*, 4, 147–152 (2009).
19. M. Zhu, G. Qian, Z. Hong, Z. Wang, X. Fan and M. Wang, *J. Phys. Chem. Solids*, 66, 748–752 (2005).

20. Z. Chen, Z.L. Wang, P. Zhan, J.H. Zhang, W.Y. Zhang, H.T. Wang and N.B. Ming, *Langmuir*, 20, 3042-3046 (2004).
21. X. Ye, Y. Zhou, J. Chen and Y. Sun, *Appl. Surf. Sci.*, 253, 6264–6267 (2007).
22. V.G. Pol, D.N. Srivastava, O. Palchik, V. Palchik, M.A. Slifkin, A.M. Weiss and A. Gedanken, *Langmuir*, 18, 3352-3357 (2002).
23. T. Tuval and A. Gedanken, *Nanotechnology*, 18, 255601-08 (2007)
24. Z. Chen, T. Gang, K. Zhang, J. Zhang, X. Chen, Z. Sun and B. Yang, *Colloids Surf., A*, 272, 151–156 (2006).
25. Y. Zhang, M. Ma, N. Gu, L. Xu and K.J. Chen, *Chinese Chem. Lett.*, 15(8), 1005-1008 (2004).
26. Z. Jiang and C.Y. Liu, *J. Phys. Chem. B*, 107, 12411-12415 (2003).
27. C.K. Huang, C.Y. Chen, J.L. Han, C.C. Chen, M.D. Jiang, J.S. Hsu, C.H. Chan and K.H. Hsieh, *J. Nanopart. Res.*, 12, 199–207 (2010).
28. Y.H. Kim, D.K. Lee and Y.S. Kang, *Colloids Surf., A*, 257–258, 273–276 (2005).
29. J.C. Flores, V. Torres, M. Popa, D. Crespo and J. M. Calderón-Moreno, *Colloids Surf., A*, 330, 86–90 (2008).
30. S. Shibata, K. Aoki, T. Yano and M. Yamane, *J. Sol-Gel Sci. Tech.*, 11, 279–287 (1998).
31. D.B. Zhang, H.M. Cheng and J.M. Ma, *J. Mater. Sci. Lett.*, 20, 439–440 (2001).
32. S. Kubo, Zhong-Ze Gu, D.A. Tryk, Y. Ohko, O. Sato and A. Fujishima, *Langmuir*, 18, 5043-5046 (2002).
33. Z. Chen, T. Gang, X. Yan, X. Li, J. Zhang, Y. Wang, X. Chen, Z. Sun, K. Zhang, B. Zhao and B. Yang, *Adv. Mater.*, 18, 924–929 (2006).
34. Z. Chen, T. Gang, Y. Wang, X. Chen, C. Guan, J. Zhang, Z. Sun, K. Zhang, B. Zhao and B. Yang, *Colloid Surf., A*, 277, 37–43 (2006).
35. Z-J. Jiang, C-Y. Liu, L-W. Sun, *J. Phys. Chem. B*, 109, 1730-1735 (2005).
36. O. Akhavan, E. Ghaderi, *Current Appl. Phys.*, 9, 1381–1385 (2009).
37. S. Egger, R.P. Lehmann, M.J. Height, M.J. Loessner and M. Schuppler, *Appl. Environ. Micro.*, 2973–2976 (2009).
38. B. Mahltig, E. Gutmann, M. Reibold, D.C. Meyer and H. Bottcher, *J. Sol-Gel Sci. and Tech.* 51, 204–214 (2009).

39. I. Mukhal, A. Eremenko, G. Korchak and A. Michienkova, *J. Water Resour. Prot.*, 2, 131-136 (2010).
40. M. Jasiorski, A. Leszkiewicz, S. Brzezinski, G. Bugla-Ploskon'ska, G. Malinowska, B. Borak, I. Karbownik, A. Baszczuk, W. Streck and W. Doroszkiewicz, *J. Sol-Gel Sci. and Technol.*, 51, 330-334 (2009).
41. Z. Deng, M. Chen and L. Wu, *J. Phys. Chem. C*, 111, 11692-11698 (2007).
42. Z. Chen, T. Gang, Y. Wang, X. Chen, C. Guan, J. Zhang, Z. Sun, K. Zhang, B. Zhao and B. Yang, *Colloids Surf., A*, 277, 37-43 (2006).
43. L.R. Hirsch, J. Jackson, A. Lee, N.J. Halas, and J.L. West, *Anal. Chem.*, 75, 2377-2381 (2003).
44. M. Zhu, G. Qian, Z. Wang and M. Wang, *Mater. Chem. Phys.*, 100, 333-336 (2006).
45. N. J. Halas, *Optical Properties of Nanoshell*, *Optics and Photonics News*, August 2002.
46. http://en.wikipedia.org/wiki/Scanning_electron_microscope
47. Hitachi S-4700 SEM Training & Reference Guide, (2007).
48. C.J. Brinker and G.W. Scherer, *Sol-Gel Science: The Physics and Chemistry of Sol-Gel Processing*, Academic Press, New York, San Diego, CA, 1990, P. 581-585
49. C.T. Kirk, *Phys. Rev. B*, 38, 1255 (1988).
50. A. Patra, E. Sominska, S. Ramesh, Y. Koltypin, Z. Zhong, H. Minti, R. Reisfeld and A. Gedanken, *J. Phys. Chem. B*, 103, 3361 (1999).
51. S.A. Kalele, S.S. Ashtaputre, N.Y. Hebalkar, S.W. Gosavi, D.N. Deobagkar, D.D. Deobagkar and S.K. Kulkarni, *Chem Phys. Letter*, DOI 10.1002/sml.200500286.

PUBLICATIONS

1. P. Devi, A.Y. Mahmoud, S. Badilescu, M. Packirisamy, P. Jeevanandam and Vo-Van Troung, BIOTECHNO Conference, 2010, Cancun, Mexico.
2. <http://doi.ieeeecomputersociety.org/10.1109/BioSciencesWorld.2010.28>.
3. P. Devi, S. Badilescu, M. Packirisamy and P. Jeevanandam, Revised Manuscript submitted entitled "Synthesis of Gold-Poly (dimethylsiloxane) Nanocomposite through a Polymer- Mediated Silver/Gold Galvanic Replacement Reaction", Gold Bulletin, 2010.
4. P. Devi and P. Jeevanandam, National Seminar on Nanomaterials for Devices: Characterization and Applications, 2010, Pune.